## General Disclaimer

## One or more of the Following Statements may affect this Document

- This document has been reproduced from the best copy furnished by the organizational source. It is being released in the interest of making available as much information as possible.

- This document may contain data, which exceeds the sheet parameters. It was furnished in this condition by the organizational source and is the best copy available.

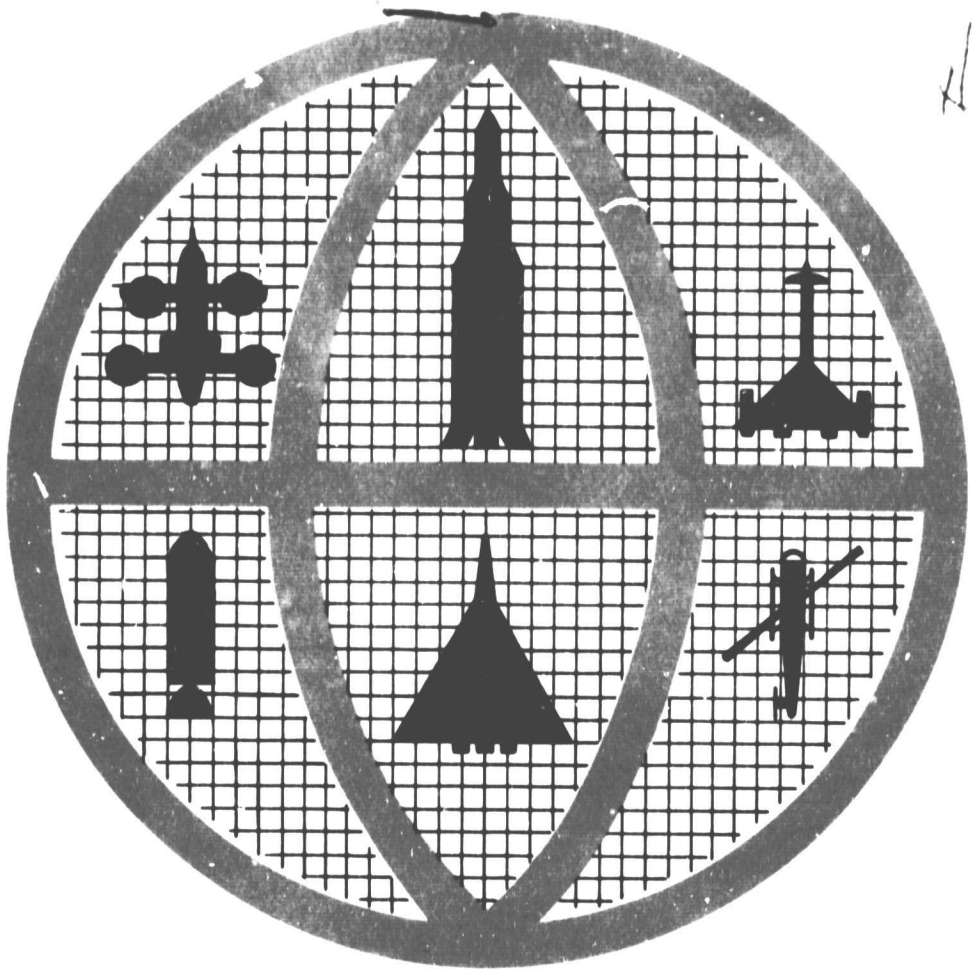
- This document may contain tone-on-tone or color graphs, charts and/or pictures, which have been reproduced in black and white.

- This document is paginated as submitted by the original source.

- Portions of this document are not fully legible due to the historical nature of some of the material. However, it is the best reproduction available from the original submission.

Produced by the NASA Center for Aerospace Information (CASI)

N69-31365
(ACCESSION NUMBER) (THRU) 1
111 (PAGES) (CODE)
CR-102220 (NASA CR OR TMX OR AD NUMBER) 15 (CATEGORY)
FACILITY FORM 602



FINAL REPORT

# INNER LOOP INTEGRATOR FEASIBILITY STUDY

FOR

NATIONAL AERONAUTICS AND SPACE ADMINISTRATION

GEORGE C. MARSHALL SPACE FLIGHT CENTER

Contract NAS8-20730

July 15, 1968

MAR 1969
RECEIVED
NASA STI FACILITY
INPUT BRANCH

HYDRAULIC RESEARCH
AND MANUFACTURING COMPANY

a textron company

SQ 25797

HR 73900000

# FINAL REPORT

# INNER LOOP INTEGRATOR FEASIBILITY STUDY

FOR

NATIONAL AERONAUTICS AND SPACE ADMINISTRATION
GEORGE C. MARSHALL SPACE FLIGHT CENTER

Contract NAS8-20730

July 15, 1968

By

Hydraulic Research and Manufacturing Company
2835 North Naomi Street, Burbank, California

Prepared: _____
S. M. Goldstein
Project Engineer

Approved: _____
J. C. Rombach
Head, Engineering Analysis

Approved: _____
D. L. Jennings, Manager
Research and Development

Report Number HR 73900000

CONTENTS

1.0 INTRODUCTION. . . . . 1

2.0 CONCEPTUAL FEASIBILITY STUDY. . . . . 2

2.1 Linear Analysis . . . . . 2

2.2 Computer Simulation - Hydraulic Fluid MIL-H-5606. . . . . 18

2.3 Pneumatic Investigation of Inner Loop Integrator . . . . . 23

2.4 Electrical Implementation Tests . . . . . 35

2.5 Feasibility Study Results . . . . . 37

3.0 DESIGN AND FABRICATION. . . . . 68

3.1 Initial Design Concepts . . . . . 68

3.2 Implementation. . . . . 68

3.3 Assembly and Subsequent Modifications . . . . . 71

3.4 Mechanization, Comments and Recommendations . . . . . 73

4.0 ASSEMBLY AND TEST PROCEDURES. . . . . 75

4.1 Assembly and No-Load Test Procedures. . . . . 75

4.2 Tests with Inertia Loads. . . . . 76

4.3 Load Force Tests. . . . . 79

5.0 DISCUSSION OF RESULTS . . . . . 84

5.1 Subassembly and No-Load Tests . . . . . 84

5.2 Simulated Load Tests. . . . . 88

6.0 CONCLUSIONS AND RECOMMENDATIONS . . . . . .103

FIGURES


1. Inner Loop Integrator Conceptual Schematic. . . . . 3
2. Inner Loop Integrator $\frac{X_5}{E_c}$ Gain Requirements and Predicted Response. . . . . 4
3. Inner Loop Integrator $\frac{X_5}{E_c}$ Phase Lag and Phase Lag Requirements. . . . . 5
4. Inner Loop Integrator System Block Diagram. . . . . 7
5. Inner Loop Integrator, Reduced Block Diagram. . . . 8
6. Free Integrator Reduced Block Diagram with Restriction of Zero Steady-State Position Error . . 10
7. Inner Loop Integrator $\frac{X_5}{F/k_s}$ Load Force Response 1052350 Actuator Sizing . . . . . 15
8. Hydraulic Computer Schematic. . . . . 24
9. Pneumatic Inner Loop Integrator Schematic . . . . . 25
10. Pneumatic Computer Program. . . . . 34
11. Electrical Implementation Cost Schematic. . . . . 36
12. Hydraulic Simulation. . . . . 42
13. Engine Position Frequency Response for Integrally Compensated Actuator (Hydraulic) . . . . 43
14. Engine Position Phase Shift for Integrally Compensated Actuator (Hydraulic). . . . . 44
15. 20,000-lb Load Force Step Response with Force Applied to Retract Direction for Integrally Compensated Actuator (Hydraulic). . . . . 45
16. $\frac{A_a P_\ell}{F}$ Load Force Frequency Response for Integrally Compensated Actuator (Hydraulic) . . . . 46
17. $\frac{X_e}{F/k_s}$ Load Force Frequency Response for Integrally Compensated Actuator (Hydraulic) . . . . 47
18. Engine Position Frequency Response for Integral and Lead Compensation (Hydraulic) . . . . . 48
19. Engine Position Phase Shift for Integral and Lead Compensation (Hydraulic) . . . . . 49

FIGURES (CONTINUED)


20. 20,000-lb Load Force Step Response Force Applied to Retract Direction for Integral and Lead Compensation (Hydraulic) . . . . . 50

21. $\frac{A_a P_c}{F}$ Load Force Frequency Response for Integral and Lead Compensation (Hydraulic). . . . 51

22. $\frac{X_e}{F/k_s}$ Load Force Frequency Response for Integral and Lead Compensation (Hydraulic). . . . 52

23. Pneumatic Simulation Step Response Curves . . . . 53

24. Engine Position Frequency Response for Integral Compensation (Pneumatic). . . . . 54

25. Engine Position Phase Shift for Integral Compensation (Pneumatic). . . . . 55

26. 20,000-lb Load Force Step Response for Integral Compensation (Pneumatic) . . . . . 56

27. $\frac{A_a P_\ell}{F}$ Load Force Frequency Response for Integral Compensation (Pneumatic) . . . . . 57

28. $\frac{X_e}{F/k_s}$ Load Force Frequency Response for Integral Compensation (Pneumatic) . . . . . 58

29. Engine Position Frequency Response for Integral and Lead Compensation (Pneumatic). . . 59

30. Engine Position Phase Shift for Integral and Lead Compensation (Pneumatic) . . . . . 60

31. 20,000-lb Load Force Step Response for Integral and Lead Compensation (Pneumatic). . . . 61

32. $\frac{A_a P_\ell}{F}$ Load Force Frequency Response for Integral and Lead Compensation (Pneumatic). . . . 62

33. $\frac{X_e}{F/k_s}$ Load Force Frequency Response for Integral and Lead Compensation (Pneumatic) . . . . . 63

34. Step Response of Inner Loop Integrator from Electrical Implementation Test. . . . . 64

FIGURES (CONTINUED)

35. Engine Position Frequency Response from Electrical Implementation Test. . . . . 65
36. Engine Position Phase Shift from Electrical Implementation Test. . . . . 66
37. Static Sensitivity from Electrical Implementation Test . . . . . 67
38. Inner Loop Integrator Test Schematic. . . . . 77
39. S1-C Actuator P/N 301100 S/N 057 on Load Simulator. . . . . 81
40. Inner Loop Integrator and S-1C Actuators in Relation to Simulator Inertia Beam Bearing . . 82
41. Inner Loop Integrator Actuator on Load Simulator . . . . . 83
42. First-Stage Flow Gain . . . . . 85
43. First-Stage Blocked Port Pressure Gain. . . . . 86
44. Inner Loop Integrator - P/N 31000020 No-Load Hysteresis. . . . . 87
45. Inner Loop Integrator P/N 31000020 Load Simulator Static Sensitivity Without Load Spring Rate Compensation. . . . . 91
46. Inner Loop Integrator P/N 31000020 Load Simulator Static Sensitivity With Load Spring Rate Compensation. . . . . 92
47. Inner Loop Integrator P/N 3 00020 Amplitude Frequency Response Without Load Spring Rate Compensation . . . . . 93
48. Inner Loop Integrator P/N 31000020 Frequency Response Without Load Spring Rate Compensation . . . . . 94
49. Inner Loop Integrator P/N 31000020 Amplitude Frequency Response with Load Spring Rate Compensation. . . . . 95

FIGURES (CONCLUDED)

50. Inner Loop Integrator P/N 31000020 Frequency Response with Load Spring Rate Compensation . . . . . 96
51. Inner Loop Integrator P/N 31000020 Engine Step Response with Load Spring Rate Compensation . . . . . 97
52. Inner Loop Integrator P/N 31000020 $\frac{AP_L}{F}$ Load Force Frequency Response without Load Spring Rate Compensation . . . . . 98
53. $\frac{AP_L}{F}$ Load Force Frequency Response with Load Spring Rate Compensation . . . . . 99
54. Inner Loop Integrator P/N 31000020 $\frac{X_5}{F/k_s}$ Amplitude Frequency Response with Load Spring Rate Compensation. . . . . 100
55. Amplitude Response Comparison . . . . . 101
56. Step Response Comparison. . . . . 102

## 1.0 INTRODUCTION

This program was undertaken to demonstrate feasibility of a concept for making a hydromechanical actuator exhibit infinite static stiffness. The effort was particularly applied to a flight-type actuator configuration embodying the sizing and performance requirements of HR&M servoactuator P/N 1052350.

Initially, an analytical study of the concept operating on MIL-H-5606 oil was accomplished by linear analysis techniques. The results obtained were verified by a nonlinear computer simulation. Conceptual feasibility was concluded with a hybrid evaluation test series in which the proposed modifications to P/N 1052350 were simulated by an analog computer. Performance tests were conducted using an inertial load on the HR&M S1-C load simulator. Finally, pneumatic system performance using 2000 psi ambient temperature nitrogen gas was investigated by analog simulation.

Layout and detail design drawings required to modify P/N 1052350 to an inner loop integrator configuration were prepared. Fabrication was accomplished in accordance with the detail designs. Required modifications which became apparent as a result of assembly and test problems were completed.

A test program using a simulated inertial load was conducted in order to determine correlations with feasibility study results.

## 2.0 CONCEPTUAL FEASIBILITY STUDY

A 3-section analytical study was undertaken to demonstrate feasibility of the inner loop integrator concept. Initial performance investigations were accomplished by means of a linear analysis and sizing study. Nonlinear analog models were then prepared to verify results of the linear analysis, and to compare actuator performance using hydraulic and pneumatic power sources. Finally a hybrid test program was undertaken in which planned modifications to HR&M P/N 1052350 were simulated, and load force and response tests were conducted.

### 2.1 Linear Analysis

Linear analysis of the Inner Loop Integrator configuration shown in Fig. 1 was undertaken to determine sizing feasibility, and investigate conformance of the modified actuator P/N 1052350 to the gain and phase envelopes of Fig. 2 and 3. These envelopes have been taken as the S-II stage dynamic requirements under an inertia load of 110 $\frac{\text{lb-sec}^2}{\text{in.}}$.

Referring to the conceptual schematic of Fig. 1, the following system equations are written.

$$A_2 P_\ell = k_s (X_4 - X_5) \quad \text{where } k_s = \frac{1}{k_V} + \frac{1}{k_E} \qquad \ldots(2.1.1)$$

$$A_2 P_\ell + F = MS^2 X_5 + BSX_5 \qquad \ldots(2.1.2)$$

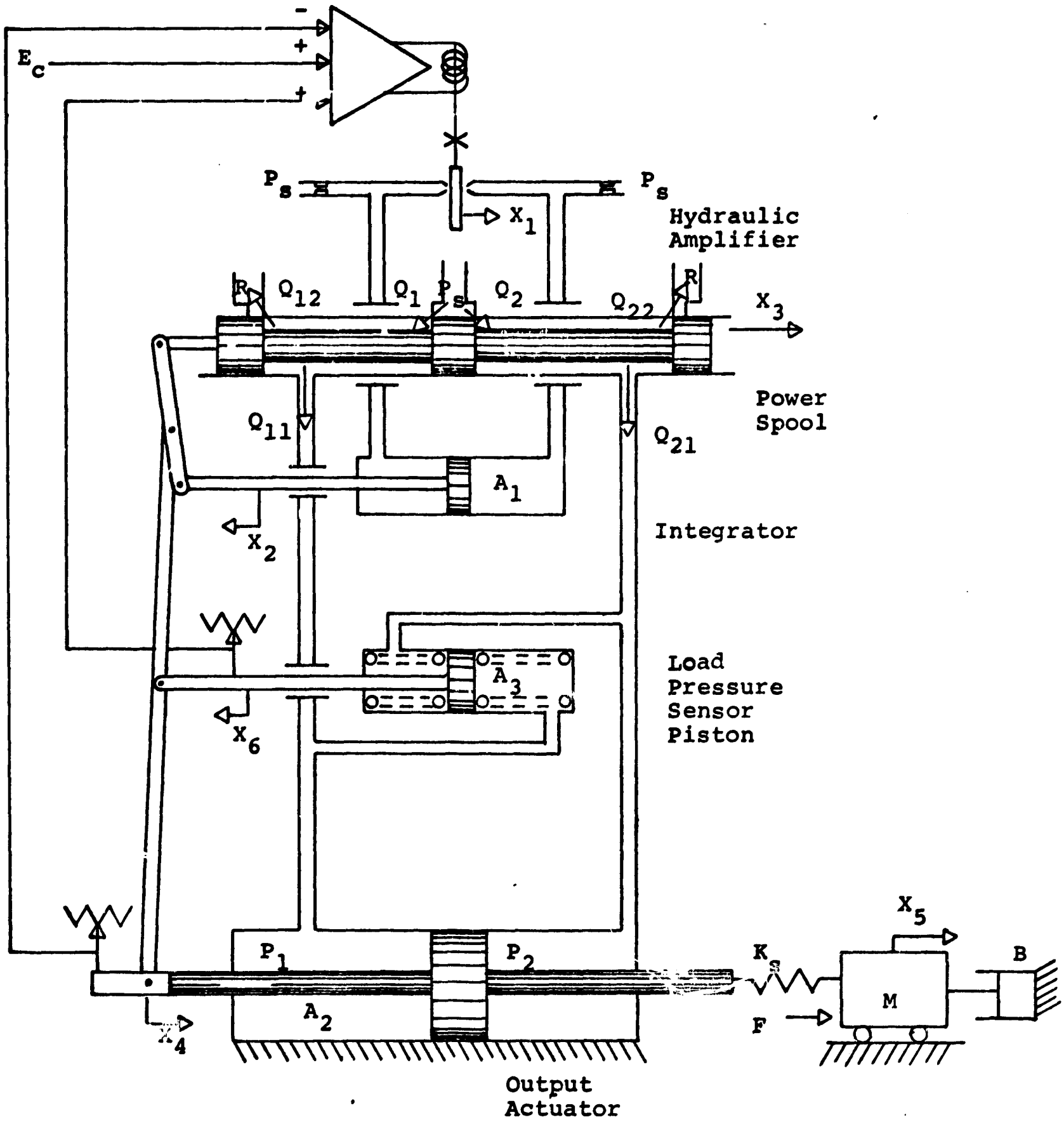



Figure 1. Inner Loop Integrator Conceptual Schematic

K&E SI OGAR C 537
3 CYCLES X 60 DIVISIONS MADE IN U.S.A.
KEUFFEL & ESSER CO.

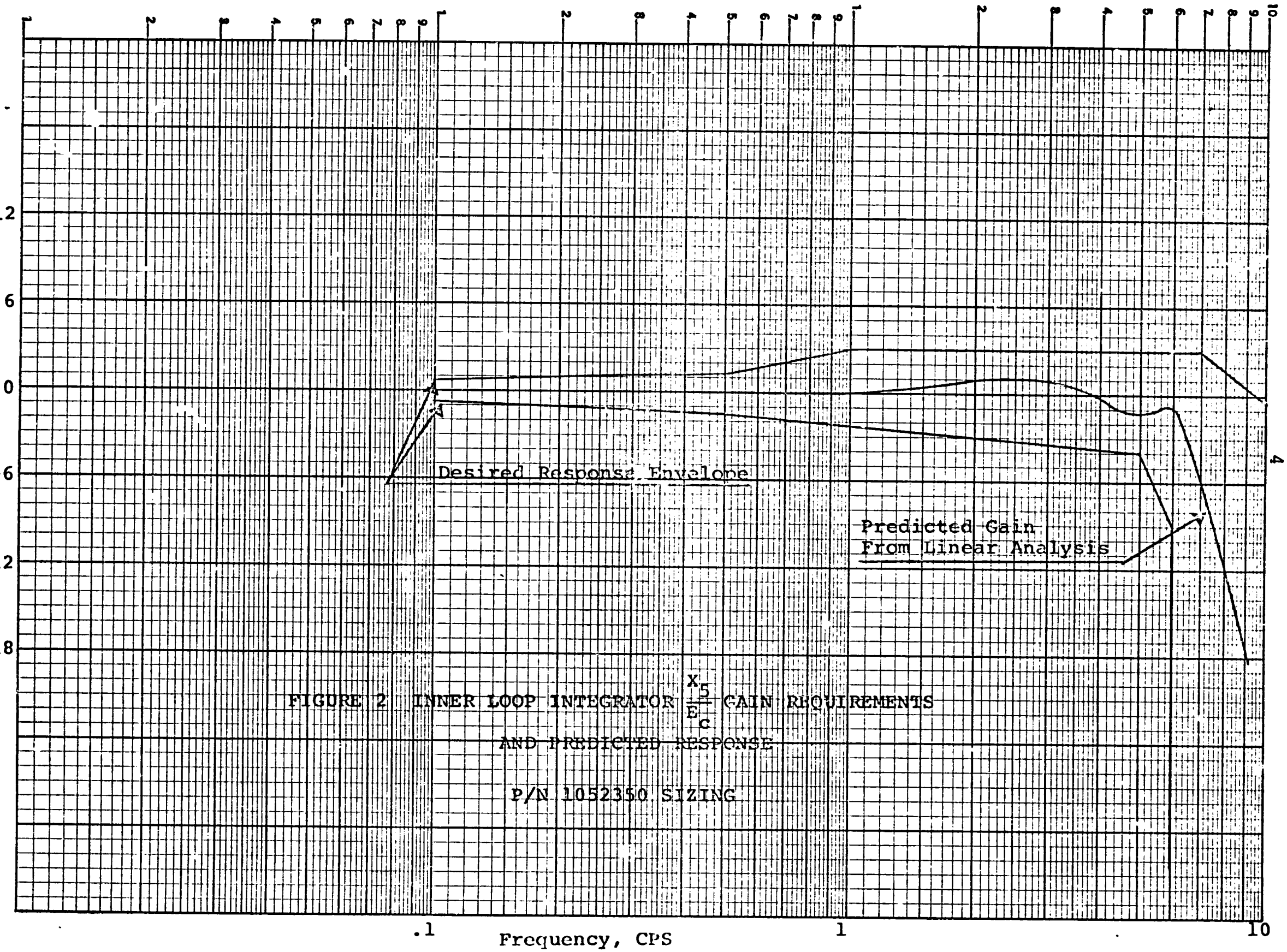



FIGURE 2 INNER LOOP INTEGRATOR $\frac{X_5}{E_c}$ GAIN REQUIREMENTS AND PREDICTED RESPONSE

P/N 1052350 SIZING

HR 7390000

K+E LOGARITHMIC 5 53
3 CYCLES X 60 DIVISIONS MADE IN U.S.A.
KEUFFEL & ESSER CO.

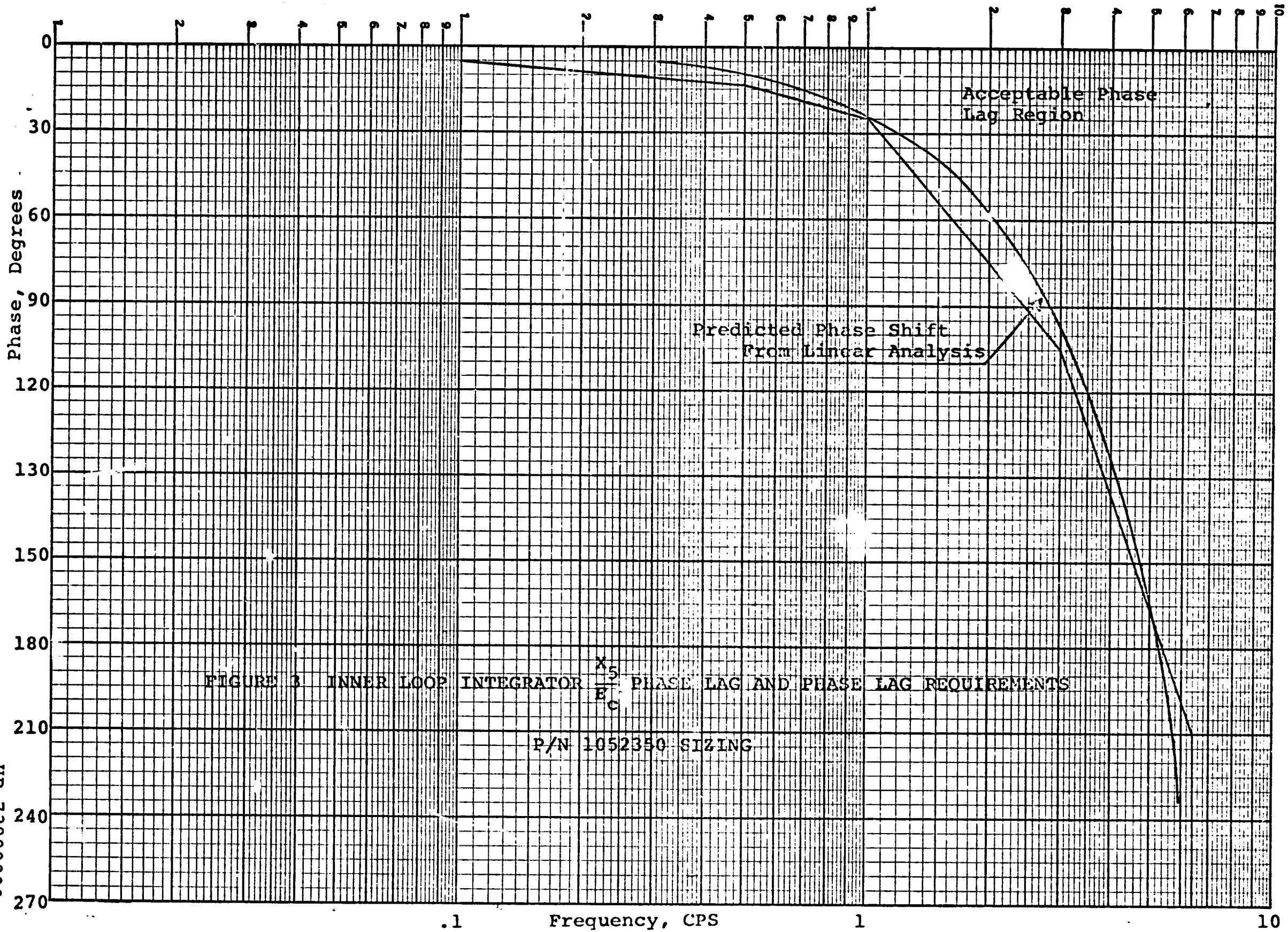



FIGURE 3 INNER LOOP INTEGRATOR $\frac{X_5}{E_c}$ PHASE LAG AND PHASE LAG REQUIREMENTS

P/N 1052350 SIZING



HR 73900000

$$Q = \frac{\partial Q}{\partial X_3} X_3 - \frac{\partial Q}{\partial P_\ell} P_\ell = \frac{A_2^2}{k_H} P_\ell S + A_2 X_4 S \qquad \ldots(2.1.3)$$

$$X_3 = K_3 X_2 - K_8 X_6 - K_5 X_4 \qquad \ldots(2.1.4)$$

$$X_6 = K_7 P_\ell \qquad \ldots(2.1.5)$$

$$X_2 = \frac{K_2}{A_1 S} i_e \qquad \ldots(2.1.6)$$

$$i_e = K_1 (E_c - K_6 X_4 + K_9 X_6) \qquad \ldots(2.1.7)$$

This set of seven equations is used to form the inner loop integrator system block diagram shown in Fig. 4. By standard block diagram manipulations, this can be reduced to the configuration of Fig. 5.

From Fig. 5, the following load force transfer function can be written.

$$\frac{X_5(s)}{F(s)} = \left\{ \left[ \frac{-K_7 K_9}{A_2} + \frac{S}{A_2} \left( \frac{\frac{\partial Q}{\partial P_\ell} + K_4 K_7 K_8 + \frac{A_2^2}{K_h} S}{\frac{K_1 K_2 K_3 K_4}{A_1} G_2(S)} \right) \right] \right. \qquad \ldots(2.1.8)$$

$$\left. + \frac{1}{k_s} \right\} \frac{\frac{K_1 K_2 K_3 K_4}{A_1 A_2 S \left( \tau_1 S^3 + \tau_2 S^2 + \tau_3 S + \frac{K_4 K_5}{A_2} \right) + \frac{K_6 S^2}{\omega_s^2} + \frac{K_6 2\zeta_2}{\omega_s} S + K_6 \frac{-K_7 K_9 M}{A_2} S^2 - \frac{K_7 K_9 B}{A_2} S}}{\frac{S^2}{\omega_s^2} + \frac{2\zeta_s}{\omega_s} S + 1}$$

REPRODUCIBILITY OF THE ORIGINAL PAGE IS POOR.

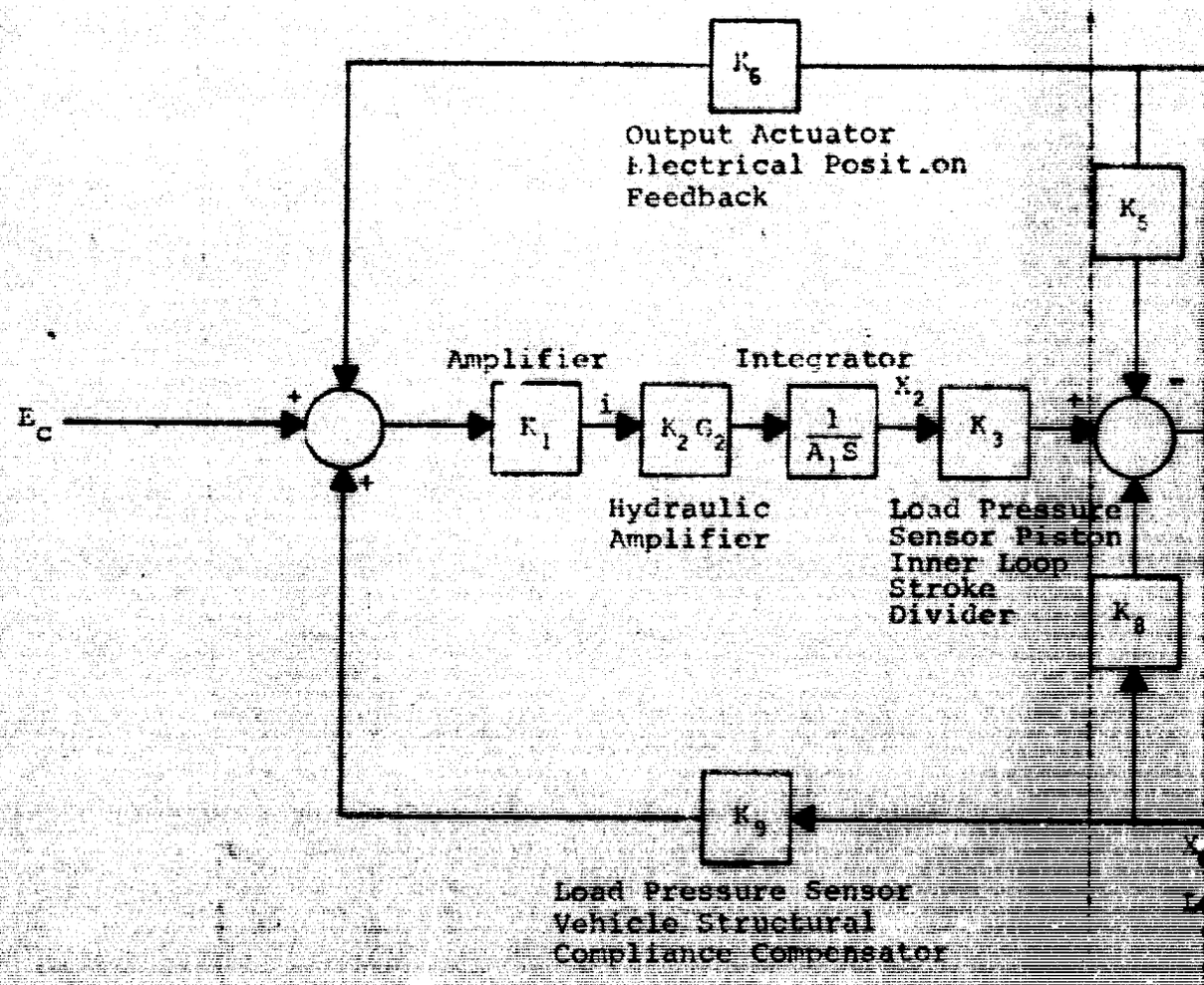
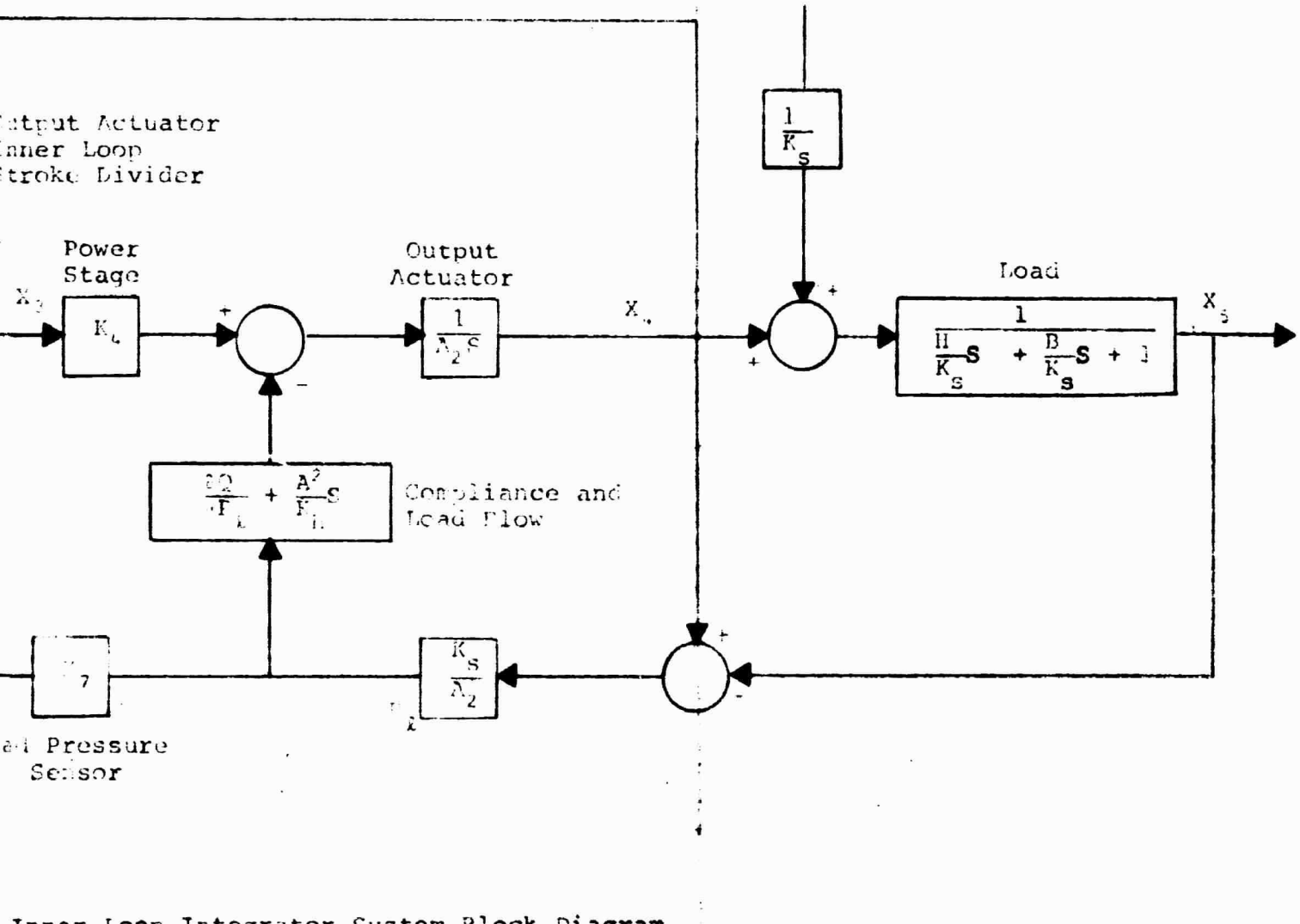



Figure 4.

REPRODUCIBILITY OF THE ORIGINAL PAGE IS POOR.

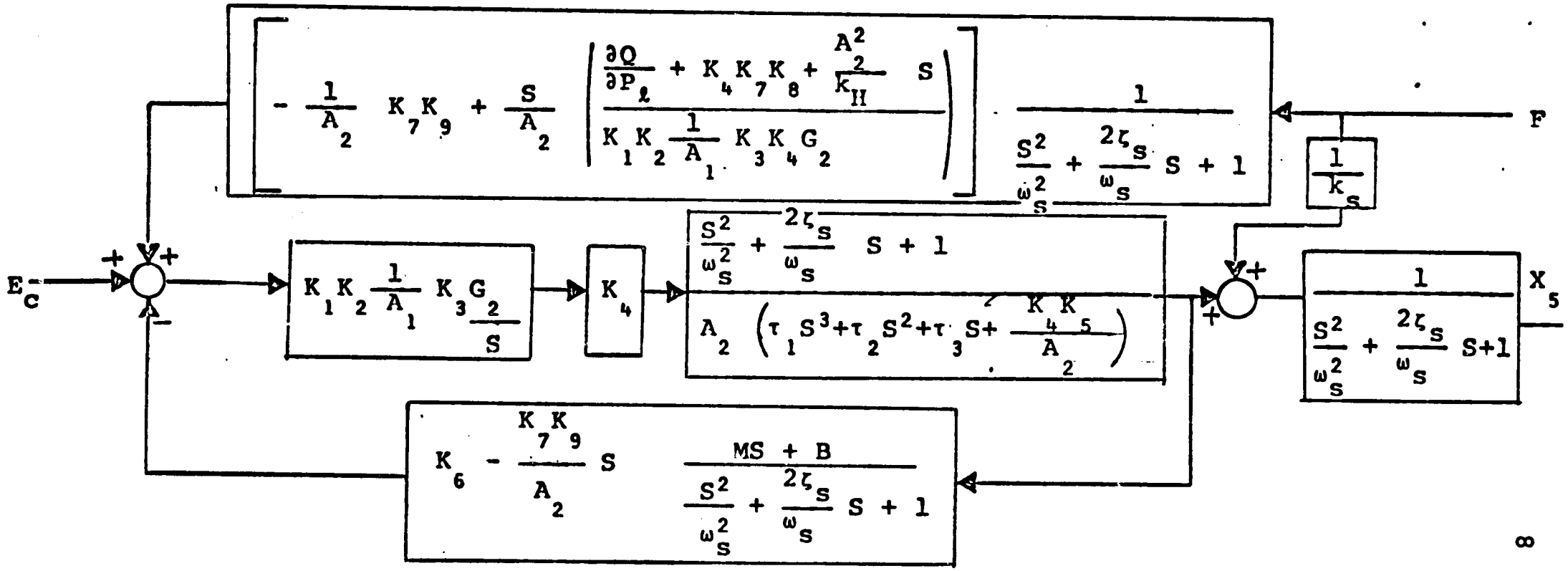





Inner Loop Integrator System Block Diagram

Foldout frame

1-B






where: $\frac{1}{\omega_s^2} = \frac{M}{k_s}$

$$\frac{1}{\omega_a^2} = \frac{1}{\omega_s^2} + \frac{M}{k_h}$$

$$\tau_1 = \frac{1}{\omega_a^2} \qquad \tau_2 = \frac{2\zeta_a}{\omega_a} + \frac{K_4 K_5}{A_2 \omega_s^2} + \frac{M}{A_2^2} \left( \frac{\partial Q}{\partial P_\ell} + K_7 K_8 K_9 \right)$$

$$\tau_3 = 1 + \frac{K_4 K_5}{A_2} \frac{2\zeta_s}{\omega_s} + \frac{B}{A_2^2} \left( \frac{\partial Q}{\partial P_\ell} + K_7 K_8 K_9 \right)$$

Figure 5. Inner Loop Integrator - Reduced Block Diagram

HR 73900000

The conditions necessary to achieve zero steady-state error with force input can be determined by applying the Final Value Theorem to equation 2.1.8.

$$X_5(t)_{t\to\infty} = SX_5(S)_{S\to 0} \qquad \ldots(2.1.9)$$

using a load force step input, $F(S) = \frac{F}{S}$, and applying equation 2.1.9, equation 2.1.8 reduces to

$$F\left(\frac{1}{k_s} - \frac{K_7K_9}{A_2K_6}\right) = X_5(\infty) \equiv 0 \qquad \ldots(2.1.10)$$

since $F \neq 0$;

$$\frac{1}{k_s} - \frac{K_7K_9}{A_2K_6} = 0 \qquad \ldots(2.1.11)$$

To impose the restrictions of zero steady-state error with load force, equation 2.1.11 is substituted into the block diagram of Fig. 5. Subsequent block diagram manipulation yields Fig. 6.

Sizing calculations are performed by referring to Fig. 6, letting $F = 0$ and writing the transfer function:

$$\frac{X_5}{E_c} = \frac{1}{K_6}\left[\frac{1}{\frac{K_4K_5}{A_2K_aG_2}S\left(\frac{A_2\tau_1S^3}{K_5K_4} + \frac{A_2\tau_2S^2}{K_5K_4} + \frac{A_2\tau_3S}{K_5K_4} + 1\right) + 1}\right] \qquad \ldots(2.1.12)$$

where: $K_a = \dfrac{K_1K_2K_3K_4K_6}{A_1A_2}$.

Assume $G_2 = 1$, $B = 0$ $\quad \frac{\partial Q}{\partial P_\ell}$ is negligible, $\approx 0$.

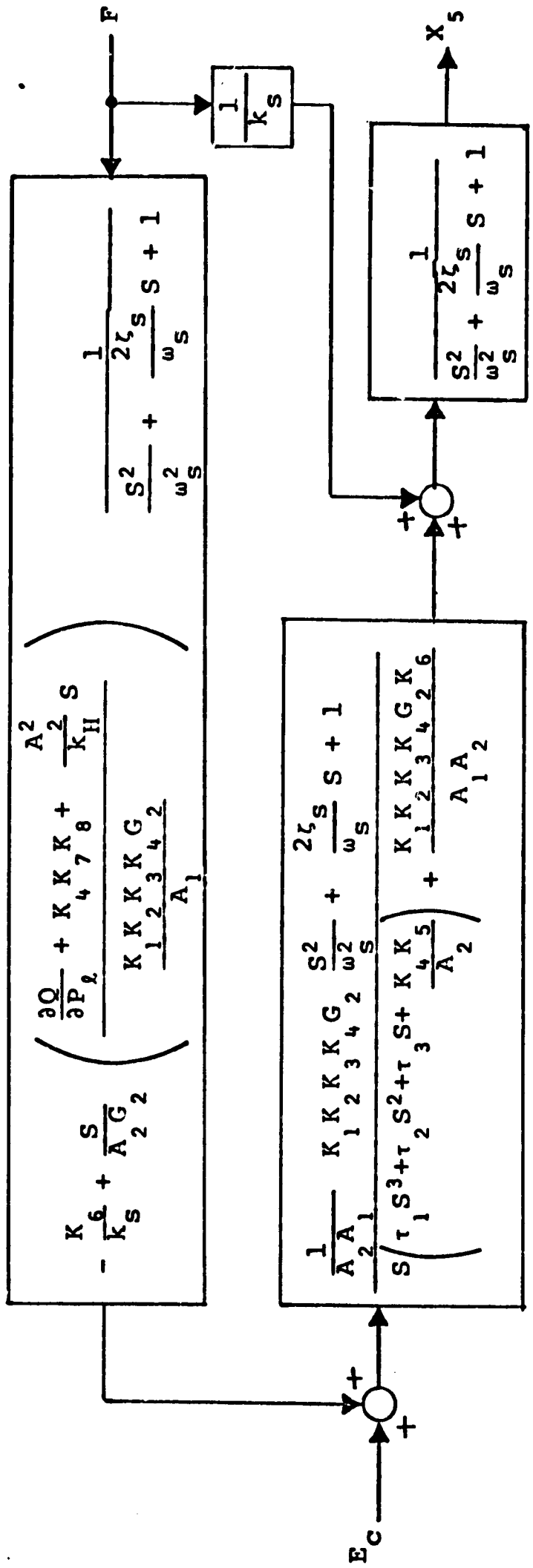



Figure 6. Free Integrator Reduced Block Diagram with Restriction of Zero Steady-State Position Error

Equation 2.1.12 becomes:

$$\frac{X_5}{E_c} = \frac{1}{K_6}\left[\frac{1}{\frac{SK_4K_5}{K_aA_2}\left(\frac{A_2\tau_1' S^3}{K_5K_4} + \frac{A_2\tau_2' S^2}{K_5K_4} + \frac{A_2\tau_3' S}{K_5K_4} + 1\right) + 1}\right] \quad \ldots(2.1.13)$$

where: $\tau_1' = \frac{1}{\omega_a^2}$

$$\tau_2' = \frac{K_4K_5}{A_2\omega_s^2} + \frac{M}{A_2^2K_4K_7K_8}$$

$$\tau_3' = 1.$$

Preliminary sizing calculations were accomplished by assuming that the 4th-order equation of 2.1.13 could be approximated by two 2nd-order lags, and by using the values below.

$M = 110 \ \frac{\text{lb-sec}^2}{\text{in.}}$

$k_s = 275{,}000$ lb/in.

$k_H = \frac{4\beta A_2^2}{L} = 1.62 \times 10^6$ lb/in. where it was assumed $\beta = 8.7 \times 10^4$ lb/in$^2$ to account for actuator compliance and entrained air.

$\omega_s^2 = 2500$ rad$^2$/sec$^2$

Gain and phase response curves of Fig. 3 and 4 respectively were obtained from a pair of 2nd-order lags defined by $\omega_1 = 3.2$ cps, $\zeta_1 = 0.6$ and $\omega_2 = 5.4$ cps, $\zeta_2 = 0.15$.

Therefore, the desired transfer function becomes:

$$(5)\quad \frac{X_5}{E_c} = \frac{1}{K_6}\left[\frac{1}{\left(\frac{S^2}{(19.5)^2} + \frac{1.2}{19.5}S + 1\right)\left(\frac{S^2}{(33.8)^2} + \frac{.3}{33.8}S + 1\right)}\right] \qquad \ldots(2.1.14)$$

Equating coefficients between equations 2.1.13 and 2.1.14, the following gain restrictions are obtained.

$$(6)\quad K_a = 216 \qquad \ldots(2.1.15)$$

$$\frac{K_a A_2}{K_4 K_5} = 15.5$$

$$\frac{K_4 K_5}{A_2} = 13.9$$

$$\frac{K_4 K_7 K_8}{A_2} = .00132$$

Working within these restrictions, the following component and linkage gains can be physically realized.

No-load actuator rate = 5.2 in./sec @ 3500 psi supply.

Main piston area, $A_2$ = 14 in.$^2$

$Q_{max}$ = 73 cis

Assume $X_{3max}$ = 0.030 in.

Then $K_4 = \frac{\partial Q}{\partial X_3} = \frac{73}{0.030} = 2.4 \times 10^3$ cis/in.

Assume 0.3-in. deflection of the load pressure sensor piston at $P_\ell$ = 3000 psi.

Then $K_7 = \frac{0.3}{3000} = 10^{-4}$ in./psi

From equation 2.1.15,

$$K_8 = \frac{0.00132 \times A_2}{K_4 K_7} = \frac{0.00132 \times 14}{2.4 \times 10^3 \times 10^{-4}} = 0.077$$

$$K_5 = \frac{13.9 \times 14}{2.4 \times 10^3} = 0.081$$

$$K_6 = 1.96\ K_9$$

$$\frac{K_1 K_2 K_3 K_6}{A_1} = \frac{216 \times 14}{2.4 \times 10^3} = 1.26$$

To determine response under force input, the transfer function is determined from Fig. 6 after making the following assumptions.

$$E_c = 0,\ G_2 = 1,\ B \approx 0,\ \frac{\partial Q}{\partial P_\ell} = 0$$

$$\frac{X_5}{F}_{\overline{K_s}} = \frac{\frac{S}{K_b}\left[\frac{\tau_1' S^3}{K_c} \quad \frac{\tau_2' S^2}{K_c} + \left(\frac{\tau_3'}{K_c} + \frac{K_8 K_b k_s}{A_2^2 K_a}\right)\right]}{\left[\frac{S}{K_b}\left(\frac{\tau_1}{K_c} S^3 + \frac{\tau_2}{K_c} S^2 + \frac{\tau_3}{K_c} S+1\right)+1\right]}$$

$$\frac{S+ 1+ \frac{k_s K_d K_b}{A_2 K_a}}{\left(\frac{S^2}{\omega_s^2} + \frac{2\zeta_s}{\omega_s} S + 1\right)} \qquad \ldots(2.1.16)$$

$$K_b = \frac{K_a A_2}{K_4 K_5}$$

$$K_c = \frac{K_5 K_4}{A_2}$$

$$K_d = \frac{K_7 K_8 K_4}{A_2}$$

Substituting the gain restrictions of equations 2.1.15 into equation 2.1.16, the load force transfer function becomes:

$$\frac{X_5}{FK_{13}} = \frac{0.077\, S\left(\frac{S}{15.8} + 1\right)\left(\frac{S^2}{(47)^2} + \frac{0.38}{0.47} S + 1\right)}{\left(\frac{S^2}{(19.5)^2} + \frac{1.2}{19.5} S + 1\right)\left(\frac{S^2}{(33.8)^2} + \frac{0.3}{33.8} S+1\right)\left(\frac{S^2}{(50)^2} + \frac{0.1}{50} S+1\right)} \qquad \ldots(2.1.17)$$

The Bode plot of equation 2.1.17 is shown in Fig. 7.

KEUFFEL & ESSER CO.
3 CYCLES X 60 DIVISIONS

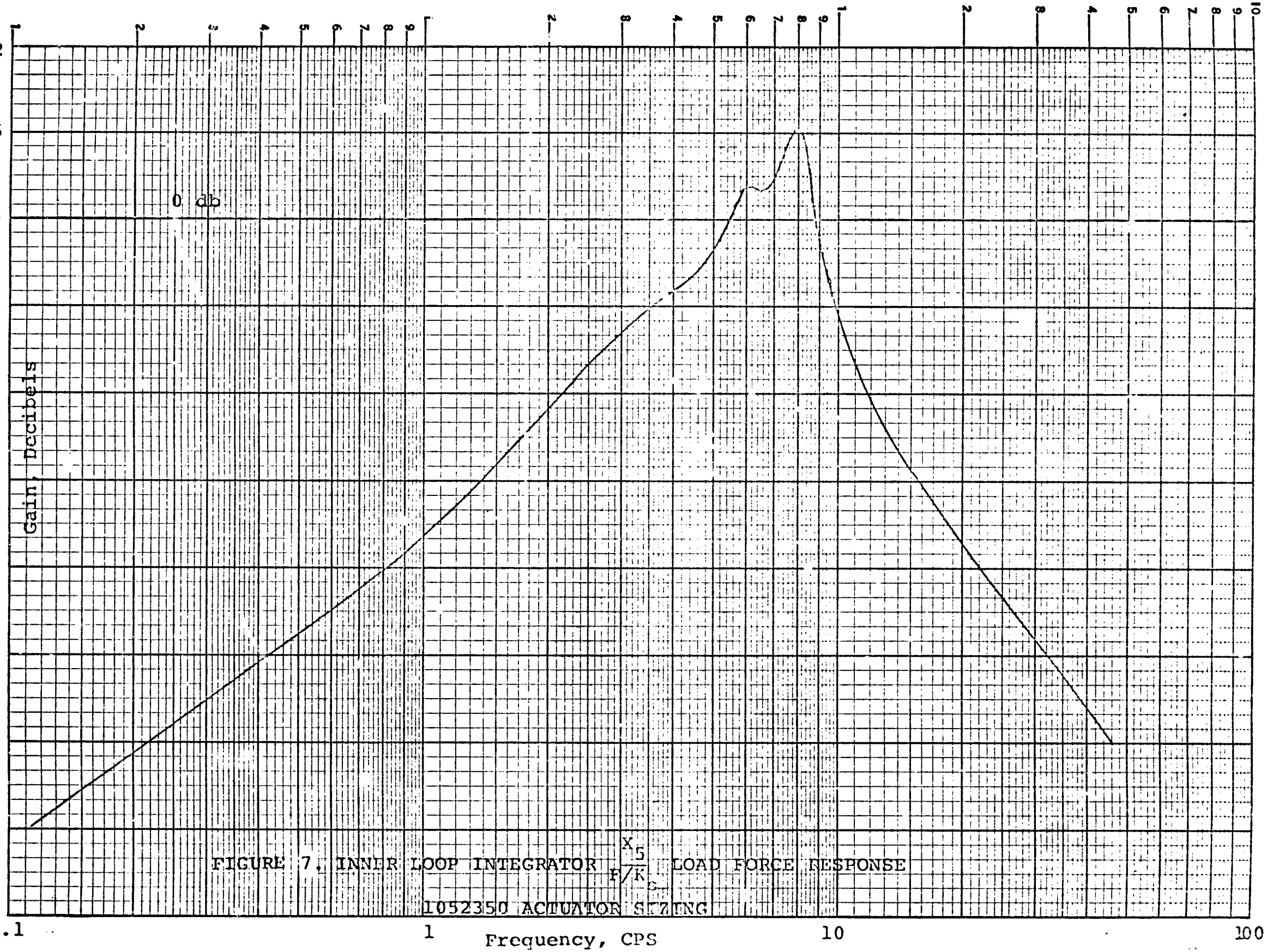



FIGURE 7. INNER LOOP INTEGRATOR $X_s/F/K_s$ LOAD FORCE RESPONSE

1052350 ACTUATOR SIZING



HR 7390000

## DEFINITIONS

| SYMBOL | DEFINITION | UNITS |
|---|---|---|
| $A_1$ | Integrator Piston Area | sq. in. |
| $A_2$ | Main Actuator Piston Area | sq. in. |
| $A_3$ | Pneumatic Load Pressure Piston Area | sq. in. |
| B | Engine Damping Coefficient | $\frac{\text{lb-sec}}{\text{in.}}$ |
| b | Slot Width | in. |
| $E_c$ | Input Command | volt |
| F | Load Force | pound |
| $G_2$ | Hydraulic Amplifier Dynamics | |
| $i_e$ | Error Current | Milliamp |
| $k_E$ | Engine Spring Rate | lb/in. |
| $k_H$ | Actuator Spring Rate | lb/in. |
| $k_s$ | Total Structural Spring Rate | lb/in. |
| $k_v$ | Vehicle Structural Spring Rate | lb/in. |
| $K_1$ | Summing Amp. Gain | ma/v |
| $K_2$ | Hydraulic Amp. Gain | cis/ma |
| $K_3$ | Integrator Output - Power Stage Value Displacement Gain | in./in. |
| $K_4$ | Power Stage Flow Gain with Load $\frac{\partial Q}{\partial X_3}$ | cis/in. |
| $K_5$ | Output Actuator Inner Loop Stroke Divider Gain | in./in. |
| $K_6$ | Output Actuator Outer Loop Gain | v/in. |
| $K_7$ | Load Pressure Sensor Position Gain | in./psi |
| $K_8$ | Load Pressure Sensor Piston Inner Loop Stroke Divider Gain | in./in. |
| $K_9$ | Load Pressure Sensor Piston Outer Loop Gain | v/in. |
| L | Output Actuator Stroke | inch |
| M | Engine Reflected Mass | $\frac{\text{lb-sec}^2}{\text{in.}}$ |
| $P_1$ | Hydraulic Actuator Extend Pressure | psi |
| $P_2$ | Hydraulic Actuator Retract Pressure | psi |
| $P_3$ | Pneumatic Actuator Extend Pressure | psi |

| SYMBOL | DEFINITION | UNITS |
|---|---|---|
| $P_4$ | Pneumatic Actuator Retract Pressure | psi |
| $P_\ell$ | Actuator Load Pressure | psi |
| $P_R$ | Actuator Return Pressure | psi |
| $P_S$ | Actuator Supply Pressure | psi |
| $Q_1$ | Hydraulic Extend Flow | cis |
| $Q_2$ | Hydraulic Retract Flow | cis |
| $Q_{12}$ | Return Flow from Extend Volume | cis |
| $Q_{22}$ | Return Flow from Retract Volume | cis |
| $S$ | Laplace Operator | $sec^{-1}$ |
| $V_1$ | Actuator Extend Volume | $in^3$ |
| $V_2$ | Actuator Retract Volume | $in^3$ |
| $V_T = V_1+V_2$ | Total Volume | $in^3$ |
| $\dot{W}_7$ | Pneumatic Extend Flow | lbs/sec |
| $\dot{W}_8$ | Pneumatic Extend Flow | lbs/sec |
| $\dot{W}_9$ | Pneumatic Return Flow from Extend Volume | lbs/sec |
| $\dot{W}_{10}$ | Pneumatic Return Flow from Retract Volume | lbs/sec |
| $\rho$ | Gaseous Nitrogen Density | $lbs/ft^3$ |
| $X_1$ | Hydraulic Amplifier Flapper Displacement Relative to Actuator Body | inch |
| $X_2$ | Integrator Piston Displacement Relative to Actuator Body | inch |
| $X_3$ | Power Spool Displacement Relative to Actuator Body | inch |
| $X_4$ | Output Actuator Displacement Relative to Actuator Body | inch |
| $X_5$ | Engine Position Relative to Vehicle Reference | inch |
| $\frac{\partial Q}{\partial P_\ell}$ | Power Stage Flow Gain with $X_3$ Held Constant | $\frac{cis}{psi}$ |
| $\beta$ | Hydraulic Oil Bulk Modulus | $\frac{lb.}{in^2}$ |
| $\zeta_s$ | Reflected Load Damping Ratio $\frac{B\omega_s}{2k_s}$ | |
| $\omega_s$ | Reflected Load Resonant Frequency $\left(\frac{k_s}{M}\right)^{1/2}$ | $\frac{rad}{sec}$ |

## 2.2 Computer Simulation- Hydraulic Fluid MIL-H-5606

Further refinement of the analysis of section 2.1 was accomplished by development of a nonlinear computer simulation of the system of Fig. 1. The system equations presented in 2.2.1 through 2.2.11 were used to generate an analytical model of the inner loop integrator which allowed the following.

1. Verification of the loop-sizing results of section 2.1
2. Determination of nominal component and linkage sizes for design purposes
3. Investigation of power spool leakage effect.
4. Consideration of additional servo loop compensation techniques
5. Accurate simulation of compressibility effects due to fluid bulk modulus
6. Accurate description of power spool flow characteristics

## SYSTEM EQUATIONS

$$Q_2 = (C_{10}bX_3 + C_{11}A_{Leak}) \frac{2g}{\rho} (P_s - P_2)^{1/2} \quad \ldots(2.2.1)$$

$$C_{10} = \begin{cases} 0.63, & X_3 < 0 \\ 0, & X_3 \geq 0 \end{cases}$$

$$\dot{P}_2 = \frac{\beta}{\frac{V_t}{2} - A_2X_4} [Q_2 - Q_{22} + A_2\dot{X}_4] \quad \ldots(2.2.2)$$

$$Q_{22} = (C_{12}bX_3 + C_{11}A_{Leak}) (\frac{2g}{\rho} P_2)^{1/2} \quad \ldots(2.2.3)$$

$$C_{12} = \begin{cases} 0.63, & X_3 > 0 \\ 0, & X_3 \leq 0 \end{cases}$$

$$Q_1 = (C_{12}bX_3 + C_{11}A_{Leak}) [\frac{2g}{\rho} (P_s - P_1)]^{1/2} \quad \ldots(2.2.4)$$

$$\dot{P}_1 = \frac{\beta}{\frac{V_t}{2} + A_2X_4} [Q_1 - Q_{12} - A_2\dot{X}_4] \quad \ldots(2.2.5)$$

$$Q_{12} = (-C_{10}bX_3 + C_{11}A_{Leak}) [\frac{2g}{\rho} P_1]^{1/2} \quad \ldots(2.2.6)$$

$$A_2(P_1 - P_2) = k_s(X_4 - X_5) = (MS^2 + BS) X_5 - F \quad \ldots(2.2.7)$$

$$X_3 = K_3X_2 - K_8X_6 - K_5X_4 \quad \ldots(2.2.8)$$

$$X_2 = \frac{1}{A_1S} Q_{ha} \quad \ldots(2.2.9)$$

$$X_6 = K_7(P_1 - P_2) \quad \ldots(2.2.10)$$

$$Q_{ha} = K_1K_2[E_c - K_6X_4 + K_9X_6] \quad \ldots(2.2.11)$$

The simulation equations 2.2.12 through 2.2.22 are developed by substitution of the appropriate constants in the system equations.

## SIMULATION EQUATIONS

$$Q_2 = \begin{cases} [-100\ X_3 + 0.03]\ (P_3 - P_2)^{1/2} & X_3 < 0 \\ 0.03\ (P_s - P_2)^{1/2} & X_3 \geq 0 \end{cases} \quad \ldots(2.2.12)$$

$$\dot{P}_2 = \frac{2 \times 10^5}{46.2 - 28\ X_4} [Q_2 - Q_{22} + 14\ \dot{X}_4] \quad \ldots(2.2.13)$$

$$Q_{22} = \begin{cases} (100\ X_3 + 0.03)\ P_2^{1/2} & X_3 > 0 \\ 0.03\ P_2^{1/2} & X_3 \leq 0 \end{cases} \quad \ldots(2.2.14)$$

$$Q_1 = \begin{cases} (100\ X_3 + 0.03)\ (P_s - P_1)^{1/2} & X_3 > 0 \\ 0.03\ (P_s - P_1)^{1/2} & X_3 \leq 0 \end{cases} \quad \ldots(2.2.15)$$

$$\dot{P}_1 = \frac{2 \times 10^5}{46.2 + 28\ X_4} [Q_1 - Q_{12} - 14\ \dot{X}_4] \quad \ldots(2.2.16)$$

$$Q_{12} = \begin{cases} [-100\ X_3 + 0.03]\ P_1^{1/2} & X_3 < 0 \\ 0.03\ P_1^{1/2} & X_3 \geq 0 \end{cases} \quad \ldots(2.2.17)$$

$$14(P_1 - P_2) = 2.75 \times 10^5\ (X_4 - X_5) = (110S^2 + 0.05S)\ X_5 - F \quad \ldots(2.2.18)$$

$$X_3 = K_3\ X_2 - 0.077\ X_6 - 0.081\ X_4 \quad \ldots(2.2.19)$$

$$X_2 = \frac{(10 \rightarrow 1)}{S}\ Q_{HA} \quad \ldots(2.2.20)$$

$$X_6 = 10^{-4}\ (P_1 - P_2) \quad \ldots(2.2.21)$$

$$Q_{HA} = K_1\ K_2\ [E_c - K_6\ X_4 + K_9\ X_6] \quad \ldots(2.2.22)$$

SCALED EQUATIONS

$$[.1Q_2] = ([-100\ X_3] + 0.03)$$

$$\left\{10\,[\frac{Ps}{500}] - 10\,[\frac{P_2}{500}]\right\}^{1/2} \frac{7.06}{10}\ ,\quad X_3<0$$

$$= 0.03\left\{10\,[\frac{Ps}{500}] - 10\right.$$

$$\left.[\frac{P_2}{500}]\right\}^{1/2} \frac{7.06}{10}\ ,\qquad X_3\geq 0 \quad \ldots(2.2.23)$$

$$[\frac{\mathring{P}_2}{500}] = 40 \times \frac{10}{4.62-0.56[sX_4]}$$

$$\left\{[.1Q_2]-[.1Q_{22}] + 0.28[5\mathring{X}_4]\right\} \qquad \ldots(2.2.24)$$

$$[.1Q_{22}] = ([100X_3] + 0.03)(10[\frac{P_2}{500}])^{1/2}$$

$$\frac{7.06}{10}\ ,\qquad X_3>0$$

$$= 0.03(10[\frac{P_2}{500}])^{1/2}\ \frac{7.06}{10}\ ,\qquad X_3\leq 0 \quad \ldots(2.2.25)$$

$$[.1Q_1] = ([100X_3] + 0.03)\left\{10[\frac{P_s}{500}]-10\right.$$

$$\left.[\frac{P_1}{500}]\right\}^{1/2} \frac{7.06}{10}\ ,\qquad X_3>0$$

$$= 0.03(10[\frac{P_s}{500}]-10[\frac{P_1}{500}])^{1/2}$$

$$\frac{7.06}{10}\ ,\qquad X_3\leq 0 \quad \ldots(2.2.26)$$

$$\left[\frac{\overset{\circ}{P}_1}{500}\right] = 40 \times \frac{10}{4.62+0.56[5X_4]} \left\{[.1Q_1]-[.1Q_{12}]+ 0.28[5\overset{\circ}{X}_4]\right\} \quad \ldots(2.2.27)$$

$$[.1Q_{12}] = \begin{cases} ([-100X_3]+ 0.03)(10[\frac{P_1}{500}])^{1/2} & \\ \frac{7.06}{10} & X_3<0 \\ = 0.03(10[\frac{P_1}{500}])^{1/2} \frac{7.06}{10} & X_3\geq 0 \end{cases} \quad \ldots(2.2.28)$$

$$[\ddot{X}_5] = 9.1\ [0.001F] + 63.7 \left\{[\frac{P_1}{500}] - \frac{P_2}{500} - 4.9[\overset{\circ}{X}_5]\right\}$$

$$[X_4] = \frac{1.02}{40}\ [\frac{P_1}{500}] + [\overset{\circ}{X}_5] \quad \ldots(2.2.29)$$

$$[100X_3] = 100K_3[X_2]-0.77[10X_6]- 8.1\ [X_4] \quad \ldots(2.2.30)$$

$$[10X_2] = (\frac{1}{A_1})\ \frac{[10\ G_{HA}]}{S} \quad \ldots(2.2.31)$$

$$[10X_6] = 0.5\ [\frac{P_2}{500}] \quad \ldots(2.2.32)$$

$$[10Q_{HA}] = 10\ (E_c - K_6[X_4] + \frac{K_9}{10}\ [10X_6] \quad \ldots(2.2.33)$$

The amplitude-scaled equations of 2.2.23 through 2.2.33 provide the basis for the computer diagram of Fig. 8. Gains shown by the diagram reflect a time scaling which allows the simulation to function 10 times slower than real time.

## 2.3 Pneumatic Investigation of Inner Loop Integrator

The basic system considered is shown in Fig. 9. Since this investigation is intended to consider feasibility of the inner loop integrator concept on a high-mass, low-load damping actuator system, a conventional flapper-nozzle configuration first stage has been used without justification. Analysis of the system is based on the following assumptions.

1. Perfect gas laws are applicable.

2. Adiabatic conditions apply for compressibility effects.

3. Line dynamics are neglected.

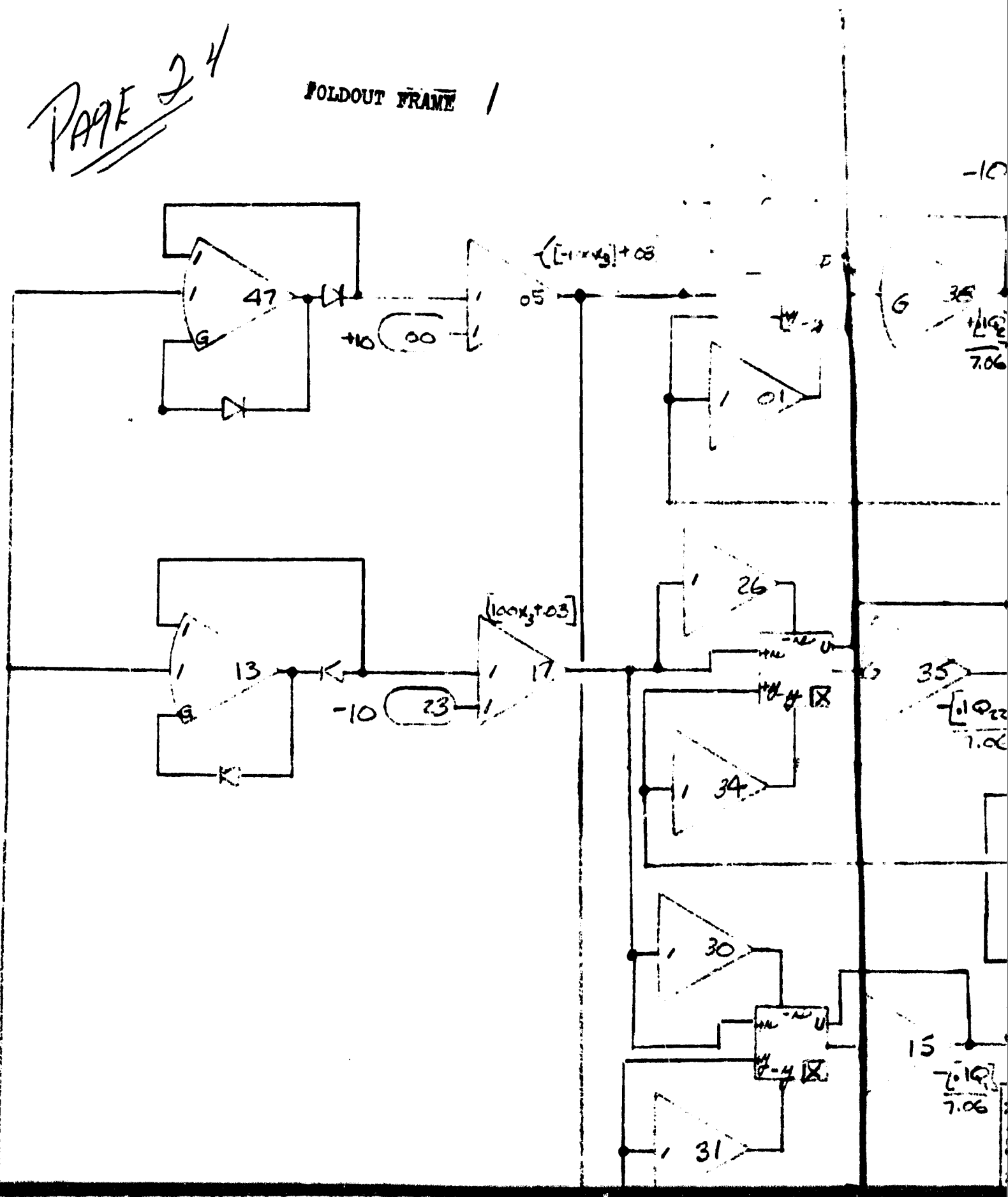
4. Chamber pressures are uniform.

5. Linkage dynamics are neglected.

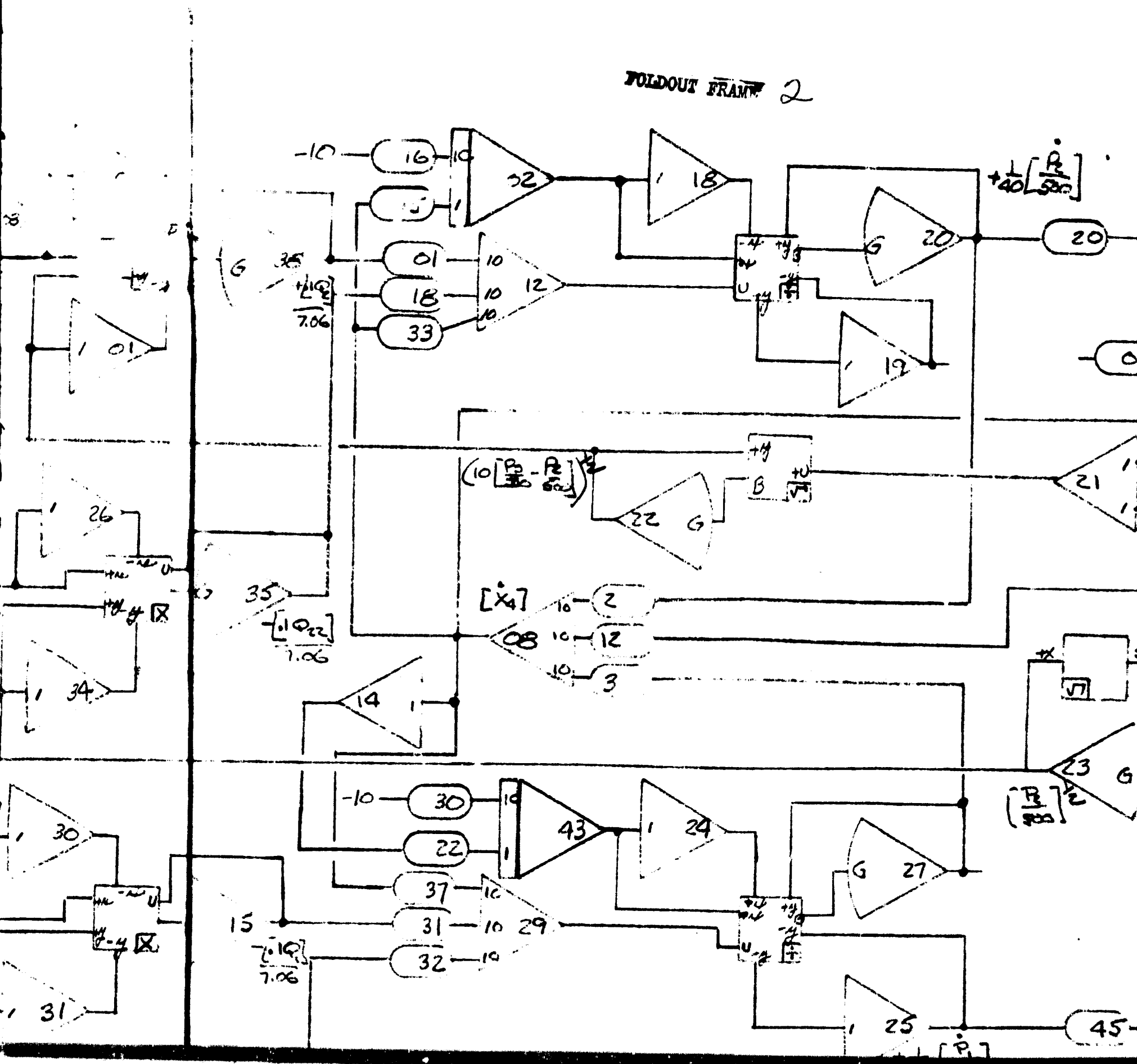
For an analytical description of the power actuator, consider the continuity equation as applied to the volume on each side of the piston.

PAGE 24

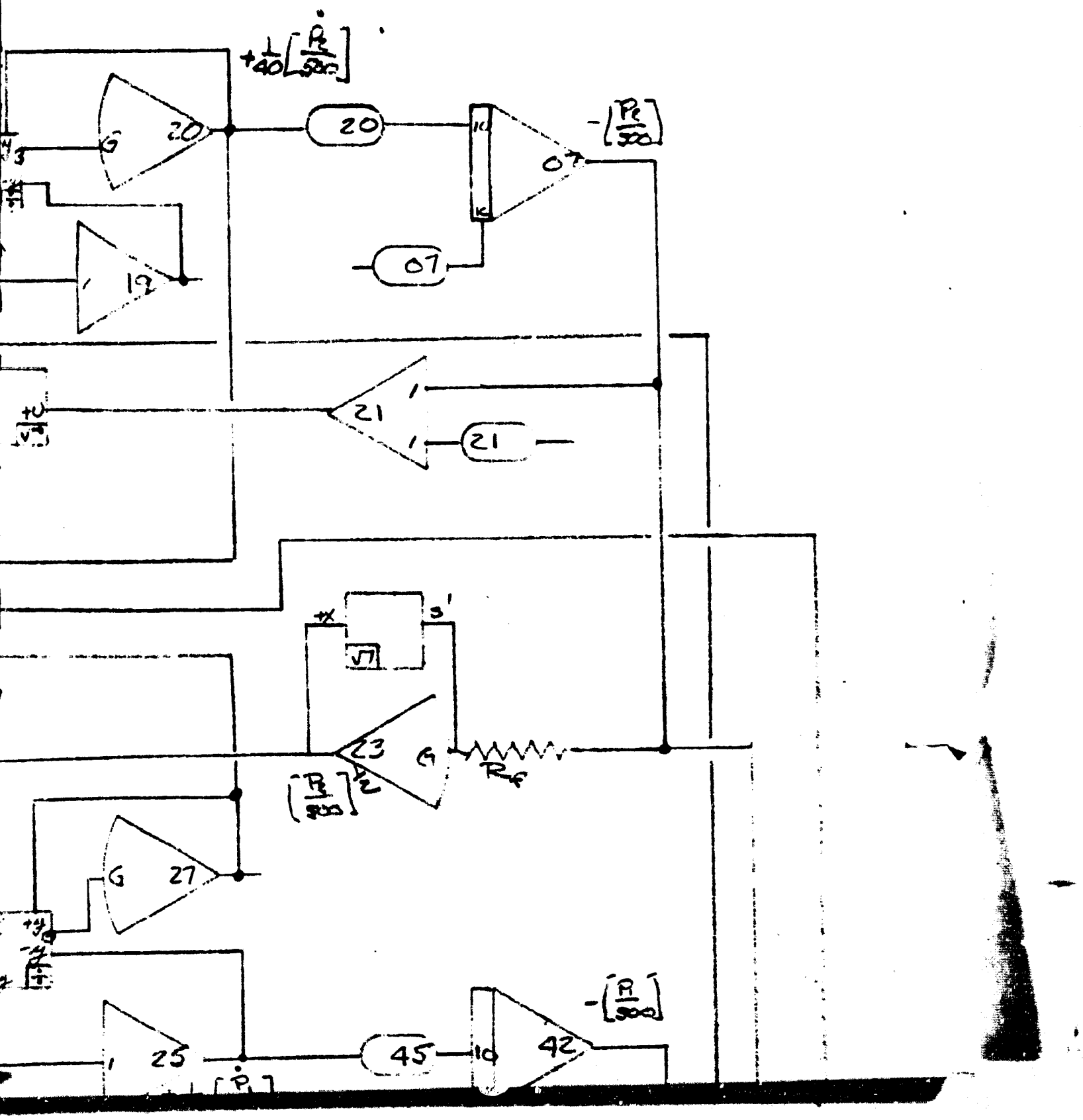
FOLDOUT FRAME 1

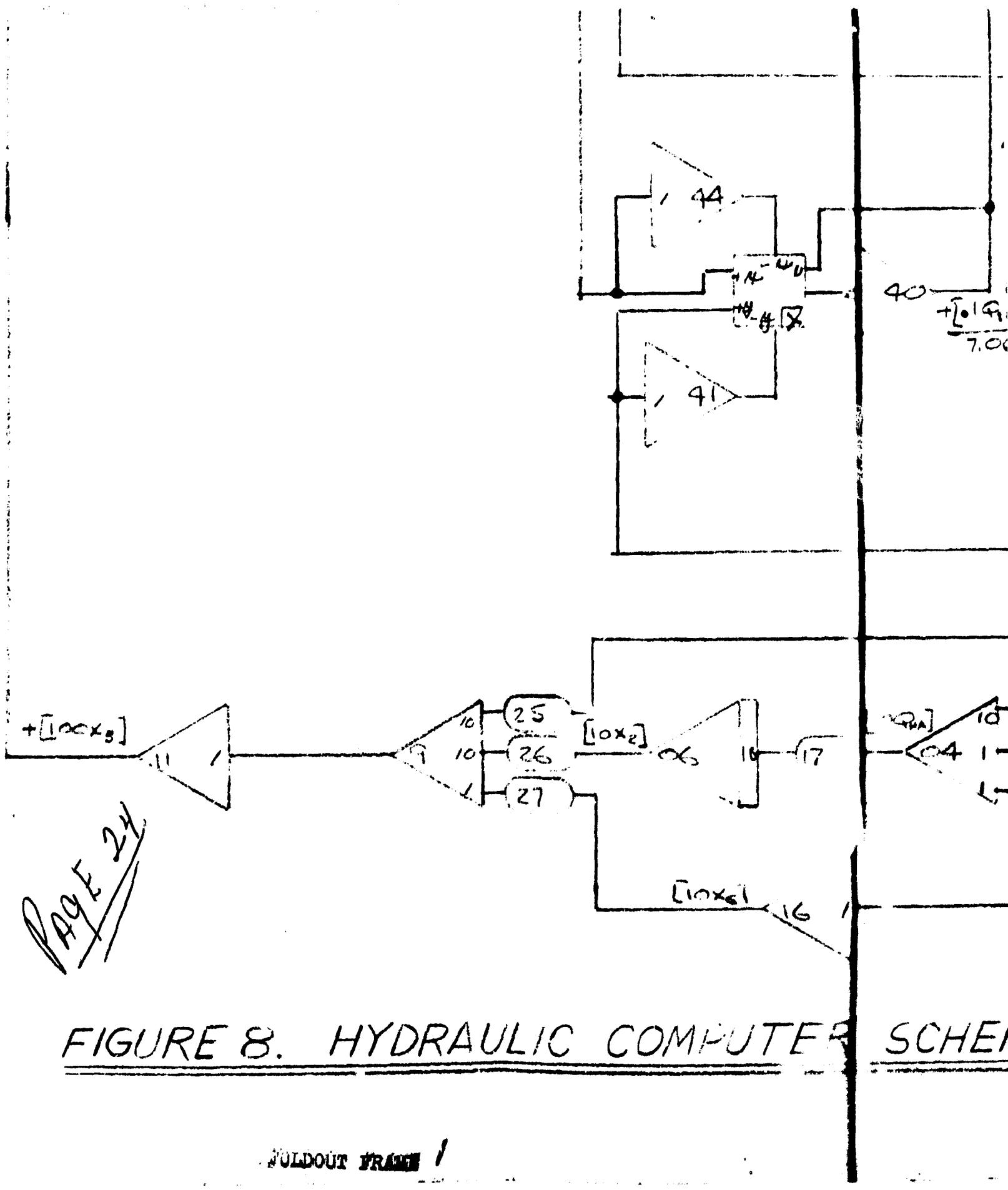


FOLDOUT FRAME 2



FOLDOUT FRAME 3

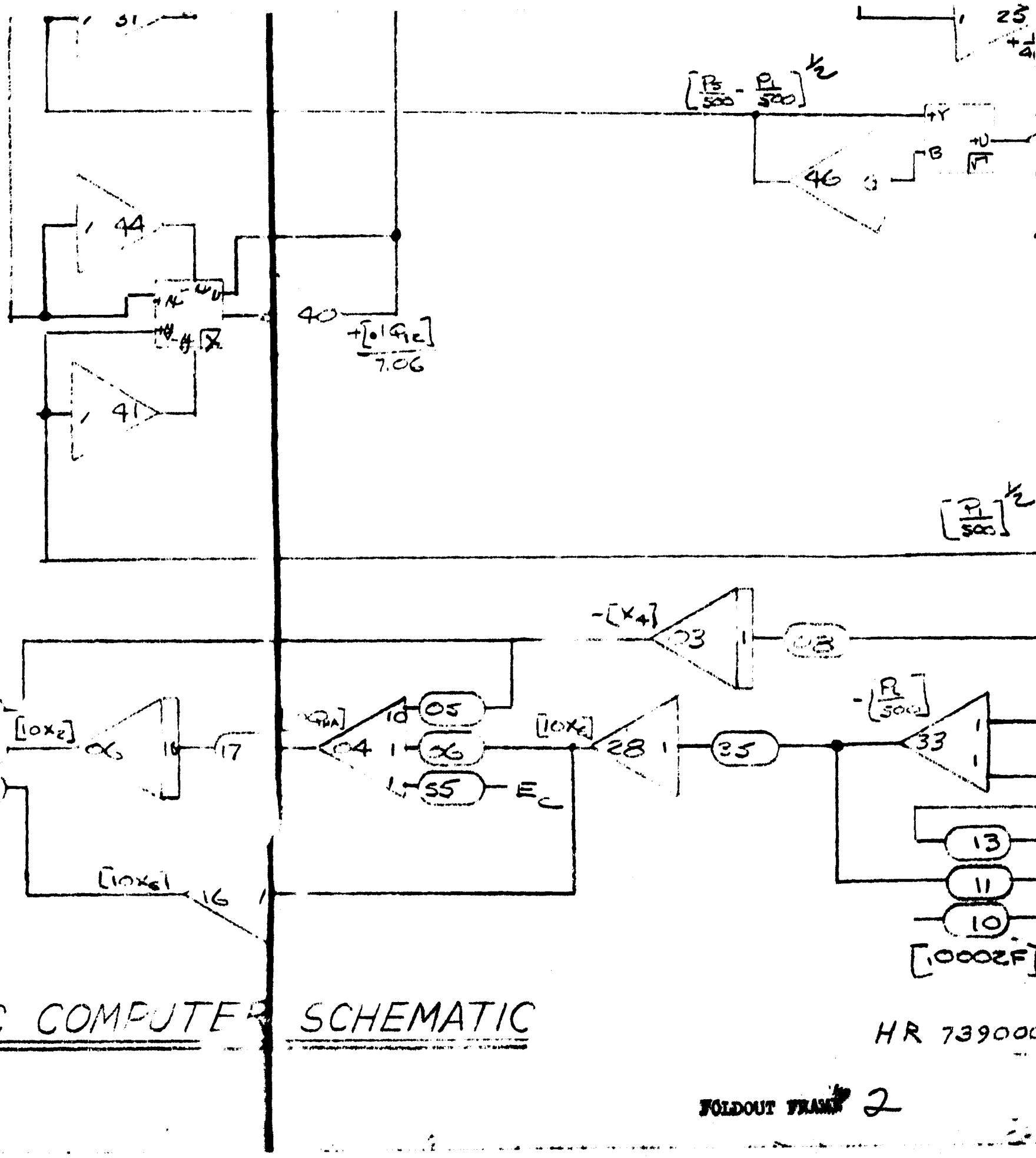





PAGE 24

FIGURE 8. HYDRAULIC COMPUTER SCHE

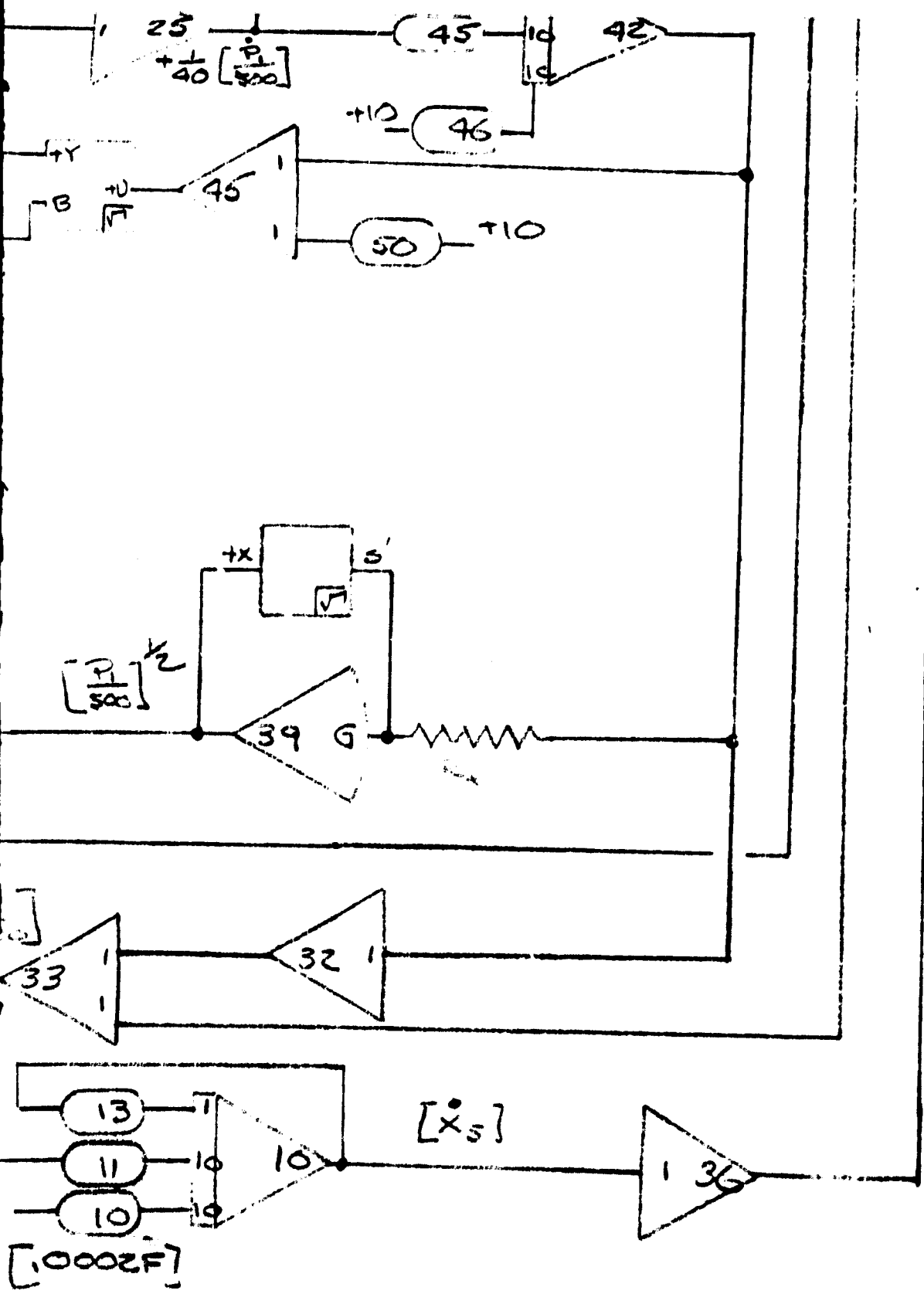
FOLDOUT FRAME 1




# RAULIC COMPUTER SCHEMATIC

HR 739000

FOLDOUT FRAME 2




R 73900000

w/o 54011
NAS8 20730
HYDRAULIC INTEGRATOR
SMG 4-20-67

FOLDOUT FRAME 3

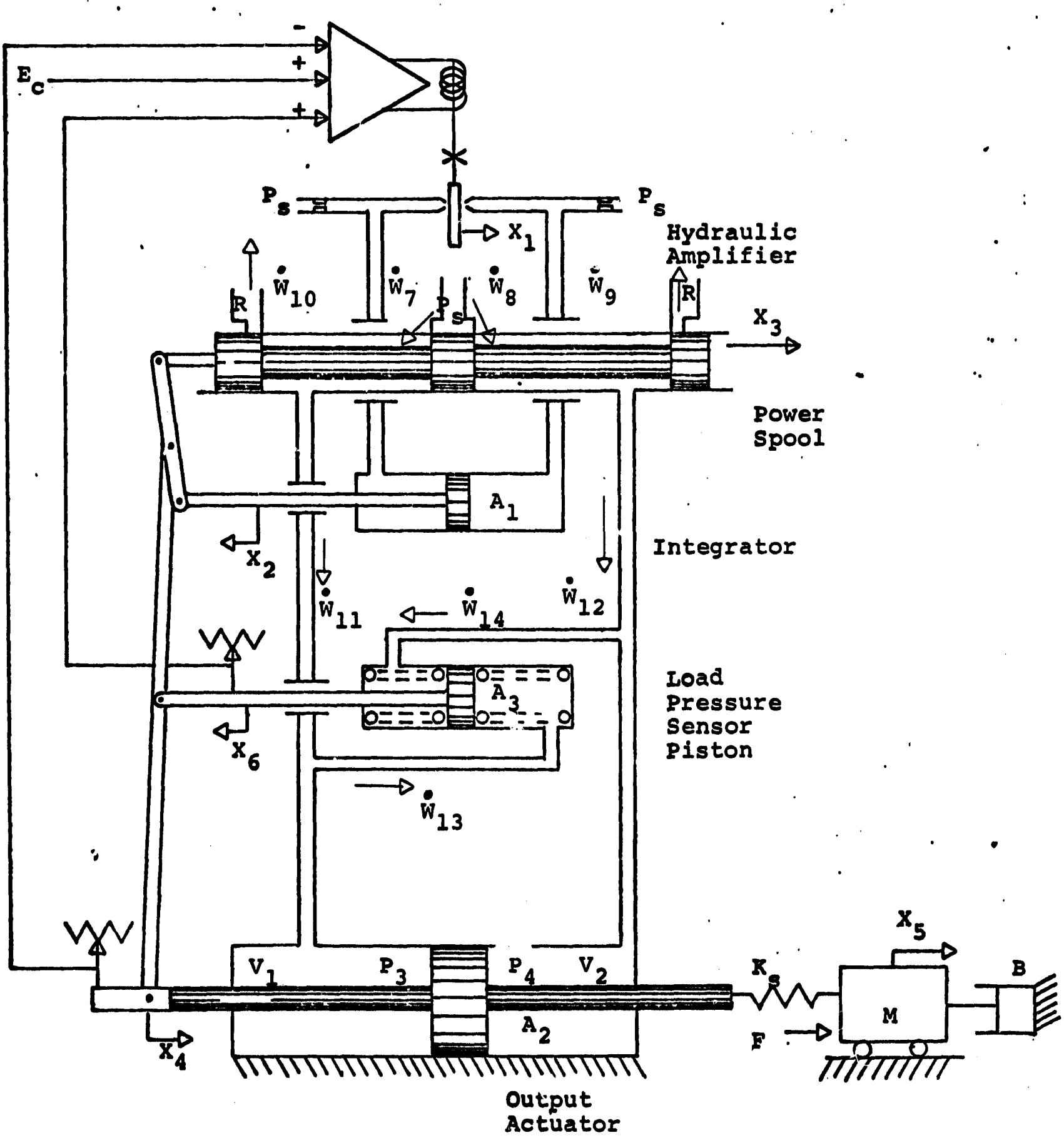



Figure 9. Pneumatic Inner Loop Integrator Schematic

$$\dot{W}_{11} - \dot{W}_{13} = \frac{d}{dt}(\rho\, v_1) = \rho \frac{dv_1}{dt} + v_1 \frac{d\rho}{dt}$$

where $v_1$ = control chamber volume
$\rho$ = density ...(2.3.1)

By assumption 2

$$\rho = \left(\frac{p}{c}\right)^{\frac{1}{k}},$$

where k = specific heat ratio,
c = a constant, ...(2.3.2)

log differentiating 2.3.2,

$$\frac{1}{\rho}\frac{d\rho}{dt} = \frac{1}{kp}\frac{dp}{dt}. \quad ...(2.3.3)$$

Substituting 2.3.3 into 2.3.1,

$$\dot{W}_{11} - \dot{W}_{13} = \rho \frac{dv_1}{dt} + \frac{\rho v_1}{kp}\frac{dp}{dt}, \quad ...(2.3.4)$$

$$\text{since } \frac{dv_1}{dt} = A_2\, \dot{x}_4 \quad ...(2.3.5)$$

$$\dot{W}_{11} - \dot{W}_{13} = \rho\, A_2\, \dot{x}_4 + \frac{\rho v_1}{kp_3}\dot{p}_3 \quad ...(2.3.6)$$

Rewriting (6),

$$\dot{p}_3 + \frac{kp_3}{v_1}\left(A_2\, \dot{x}_4 - \frac{\dot{W}_{11} - \dot{W}_{13}}{\rho}\right) = 0 \quad ...(2.3.7)$$

Since a positive flow to $v_1$ gives a negative flow from $v_2$, the equation for the other side of the piston can be written:

$$\dot{p}_4 + \frac{kp_4}{v_2} \left(- A_2 \dot{x}_4 - \frac{\dot{W}_{12} - \dot{W}_{14}}{\rho}\right) = 0 \qquad \ldots(2.3.8)$$

## ANALOG EQUATIONS - PNEUMATIC INTEGRATOR

Assume $\dot{W}_{HA} = i\ K_{sv}$

where $K_{sv}$ = #/sec/ma

$$\therefore\ \dot{X}_2 = \frac{1}{\rho A_1}\ K_{sv} i \qquad \ldots(2.3.9)$$

$$\dot{W}_7 = (Cbx_3 + A_{leak})\ \frac{P_s S}{RT} \qquad \begin{cases} C = 0 & X_3 \leq 0 \\ C = 0.63 & X_3 > 0 \\ S = f(P_3/P) \end{cases} \qquad \ldots(2.3.10)$$

$$\dot{W}_8 = (-Cbx_3 + A_{leak})\ \frac{P_s S}{RT} \qquad \begin{cases} C = 0 & X_3 \geq 0 \\ C = 0.63 & X_3 < 0 \\ S = f(P_4/P) \end{cases}$$

$$\dot{W}_9 = (Cbx_3 + A_{leak})\ \frac{P_4}{RT}\ S \qquad \begin{cases} C = 0 & X_3 \leq 0 \\ C = 0.63 & X_3 > 0 \\ \text{Sonic } S = f(k) \end{cases} \qquad \ldots(2.3.11)$$

$$\dot{W}_{10} = (-Cbx_3 + A_{leak})\ \frac{P_3 S}{RT} \qquad \begin{cases} C = 0 & X_3 \geq 0 \\ C = 0.63 & X_3 < 0 \\ \text{(Sonic) } S = f(k) \end{cases} \qquad \ldots(2.3.12)$$

$$\dot{W}_7 - \dot{W}_{10} = \dot{W}_{11} \qquad \ldots(2.3.13)$$

$$\dot{W}_8 - \dot{W}_9 = \dot{W}_{12} \qquad \ldots(2.3.14)$$

Load Pressure Sensor

$$A_3\ (P_3 - P_4) = K_p\ X_6 \qquad \ldots(2.3.15)$$

POWER ACTUATOR, NEGLECTING VOLUME OF LOAD PRESSURE SENSOR:

$$\dot{W}_{14} = \dot{W}_{13} = 0$$

$$\dot{P}_3 + k \frac{P_3}{V_1} \left\{ A_2 \dot{X}_4 - \frac{\dot{W}_{11}}{\rho} \right\} = 0 \qquad \ldots(2.3.16)$$

$$\dot{P}_4 + \frac{k P_4}{V_2} \left\{ - A_2 \dot{X}_4 - \frac{\dot{W}_{12}}{\rho} \right\} = 0 \qquad \ldots(2.3.17)$$

Actuation Equations

$$(P_3 - P_4) A_2 = k_s (X_4 - X_5) = (MS^2 + BS) X_5 - F \qquad \ldots(2.3.18)$$

Feedback Linkage

$$X_2 = K_1 X_2 - K_L X_6 - K_P X_4 \qquad \ldots(2.3.19)$$

$$i = K_{amp} (E_c + K_p X_6 - K_p X_4) \qquad \ldots(2.3.20)$$

From the Hydrogen Handbook, AFFTC 60-19, the following values for density of $GN_2$ apply at 540°R.

| P psia | 500 | 750 | 1000 | 1500 | 2000 |
|---|---|---|---|---|---|
| $\rho$ lb/ft$^3$ | 2.43 | 3.64 | 4.84 | 7.22 | 9.49 |

For the purposes of this study, the density, $\rho$, may be approximated by a straight line.

$$\rho = 4.84 \times 10^{-3} P \qquad \ldots(2.3.21)$$

## PNEUMATIC INTEGRATOR

$$\dot{X}_1 = \frac{1720\ K_{sv}}{A_1}\ i \qquad \text{Where } \rho = 2.43 \text{lb/ft}^3 \text{ @ 500 psi} \quad \text{3.64 @ 750 psi} \quad \text{4.84 @ 1000 psi} \qquad \ldots(2.3.22)$$

$$\dot{W}_7 = (0.63\ X_3 + A_{leak})\ \frac{P_s\ S}{23.2 \times 7.41} \qquad s = f\ (P_5/P) \ldots(2.3.23)$$

$$\dot{W}_8 = (-0.63\ X_3 + A_{leak})\ \frac{P_s\ S}{23.2 \times 7.41} \qquad s = f\ (P_3/P)$$

$$\dot{W}_9 = (0.63\ X_3 + A_{leak})\ \frac{3.88}{23.2 \times 7.41}\ P_4 \qquad \ldots(2.3.24)$$

$$\dot{W}_{10} = (-0.63\ X_3 + A_{leak})\ \frac{3.88}{23.2 \times 7.41}\ P_3 \qquad \ldots(2.3.25)$$

$$X_6 = \frac{A_3}{K_p}\ (P_3 - P_4) \qquad \ldots(2.3.26)$$

$$\dot{P}_3 + \frac{1.4}{14 \times 1.5 + 14\ X_4} \left\{ P_3\ 14\ \dot{X}_4 - \frac{\dot{W}_7 - \dot{W}_{10}}{4.84 \times 10_{-3}} \right\} = 0 \qquad \ldots(2.3.27)$$

$$\dot{P}_4 + \frac{1.4}{14 \times 1.5 - 14\ X_4} \left\{ -14 P_4\ \dot{X}_4 - \frac{(\dot{W}_8 - \dot{W}_9)}{4.84 \times 10_{-3}} \right\} = 0 \qquad \ldots(2.3.28)$$

$$(P_3 - P_4)\ 14 = 275 \times 10^3\ (X_4 - X_5) =$$

$$(110S^2 + 540S)\ X_5 - F \qquad \ldots(2.3.29)$$

$$X_3 = K_I\ X_2 - K_L\ X_6 - K_p\ X_4 \qquad \ldots(2.3.30)$$

$$i = K_{amp}\ (E_c + K_1\ X_6 - K_p\ X_4) \qquad \ldots(2.3.31)$$

## SCALED EQUATIONS

$$[10X_2] = \frac{1720\ K_{sv}}{S\rho A_I}\ 20\ [0.5\ i] \qquad \ldots(2.3.32)$$

$$[10\dot{W}_7] = \begin{cases} (0.63\ [100X_3] + 0.03)\ \frac{S}{10}\ 1.16\ [\frac{P}{200}] & X_3<0 \\ 0.03\ \frac{S}{10}\ 1.16\ [\frac{P}{200}] & X_3\geq 0 \end{cases}$$

$$S = f(P_s/P) \qquad \ldots(2.3.33)$$

$$[10\dot{W}_8] = \begin{cases} (-0.63\ [100X_3] + 0.03)\ \frac{S}{10}\ 1.16\ [\frac{P}{200}] & X_3>0 \\ 0.03\ \frac{S}{10}\ 1.16\ [\frac{P}{200}] & X_3\leq 0 \end{cases}$$

$$S = f(P_6/P) \qquad \ldots(2.3.34)$$

$$[10\dot{W}_9] = \begin{cases} (0.63\ [100X_3] + 0.03)\ \frac{1}{10}\ [\frac{P_6}{200}] & X_3<0 \\ 0.03 \times \frac{4.52}{10}\ [\frac{P_6}{200}] & X_3\geq 0 \end{cases} \qquad \ldots(2.3.35)$$

$$[10\dot{W}_{10}] = \begin{cases} (-0.63\ [100X_3] + 0.03)\ \frac{1}{10}\ [\frac{P_5}{200}] & X_3>0 \\ 0.03 \times \frac{4.52}{10}\ [\frac{P_6}{200}] & X_3\leq 0 \end{cases} \qquad \ldots(2.3.36)$$

$$[10X_6] = 0.3\ \left(\frac{[P_5]}{200} - \frac{[P_6]}{200}\right) \qquad \ldots(2.3.37)$$

$$\frac{[\dot{P}_3]}{200} = 70\ \frac{10}{7.5 + [5X_4]}\left(1.28[10\dot{W}_7] - 5.8\right.$$

$$\left.[10\dot{W}_{10}] - \frac{P_3}{200}\ \frac{[\dot{X}_4]}{10}\right) \qquad \ldots(2.3.38)$$

$$\frac{[\dot{P}_4]}{200} = 70\ \frac{10}{7.5 - [5X_4]}\left(1.28[10\dot{W}_8] - 5.8\right.$$

$$\left.[10\dot{W}_9] + \frac{[P_4]}{200}\ x\ \frac{[\dot{X}_4]}{10}\right) \qquad \ldots(2.3.39)$$

$$[\ddot{X}_5] = 25.2\ \left(\frac{[P_5]}{200} - \frac{[P_6]}{200}\right) + 9.1\ [0.001F] - 4.92[\dot{X}_5] \qquad \ldots(2.3.40)$$

$$[\dot{X}_4] = 0.71\ \frac{1}{7C}\left(\frac{[\dot{P}_5]}{200} - \frac{[\dot{P}_6]}{200}\right) + [\dot{X}_5] = [\dot{X}_4] \qquad \ldots(2.3.41)$$

$$[100X_3] = 10K_I[10X_2] - 10K_L[10X_6] - 100K_p[X_4] \qquad \ldots(2.3.42)$$

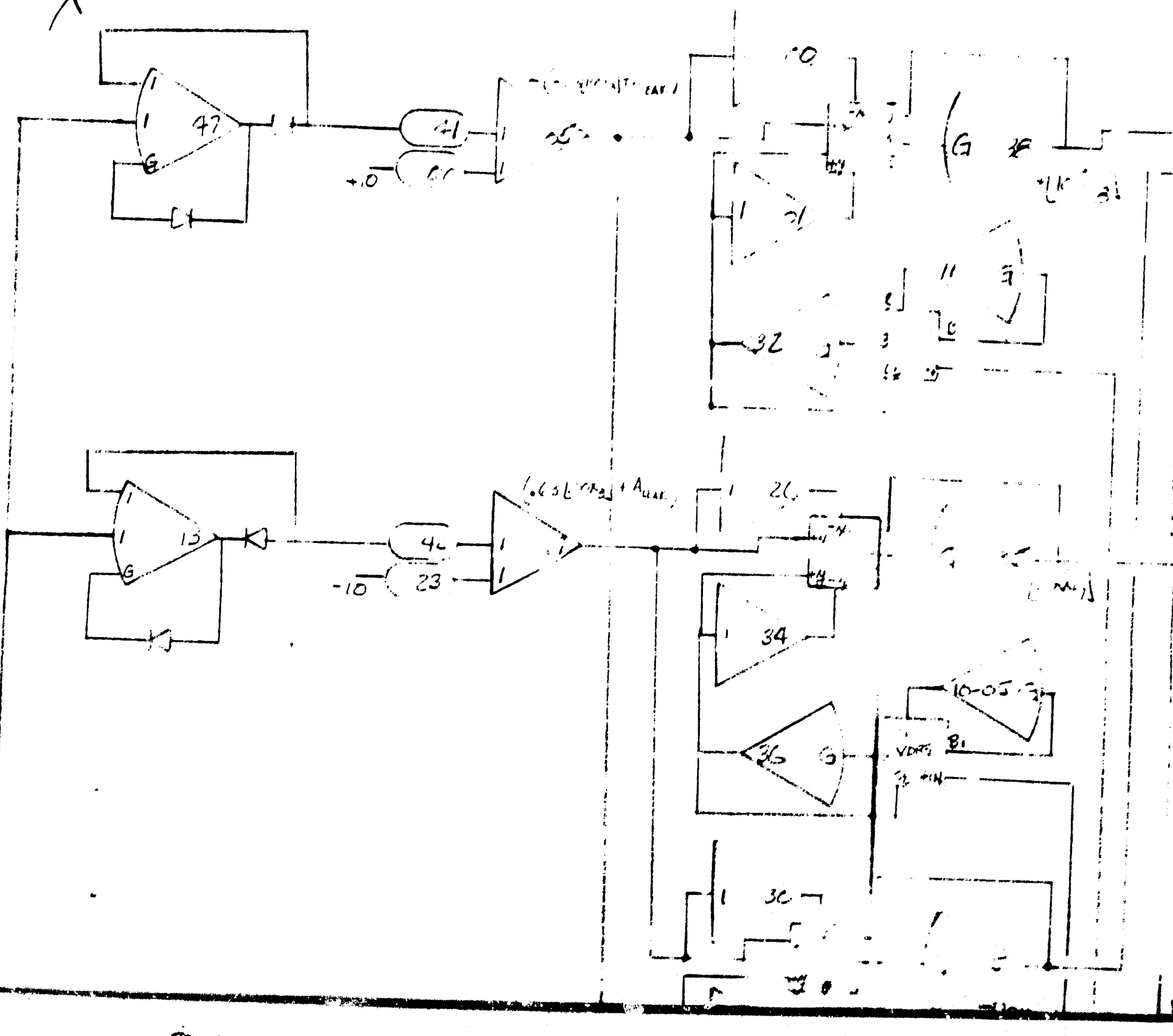
$$[0.5i] = .5\ K_{amp}\ (E_c + \frac{K_{Lp}}{10}\ [10X_6] - K_{PA}[X_4]) \qquad \ldots(2.3.43)$$

| $[10\ P_4/P]$ | S | $P_s$ | $[10\ P_4/P]$ |
|---|---|---|---|
| 1 | 3.88 | 2000 | $\frac{[P_4]}{200}$ |
| 2 | 3.88 | | |
| 3 | 3.88 | 1500 | $1.33\ \frac{[P_4]}{200}$ |
| 4 | 3.88 | | |
| 5 | 3.88 | 1000 | $2\ \frac{[P_4]}{200}$ |
| 6 | 3.84 | | |
| 7 | 3.62 | | |
| 8 | 3.18 | | |
| 9 | 2.40 | | |
| 10 | 0 | | |

The scaled equations of 2.3.32 through 2.3.43 permit development of the computer simulation of Fig. 10.

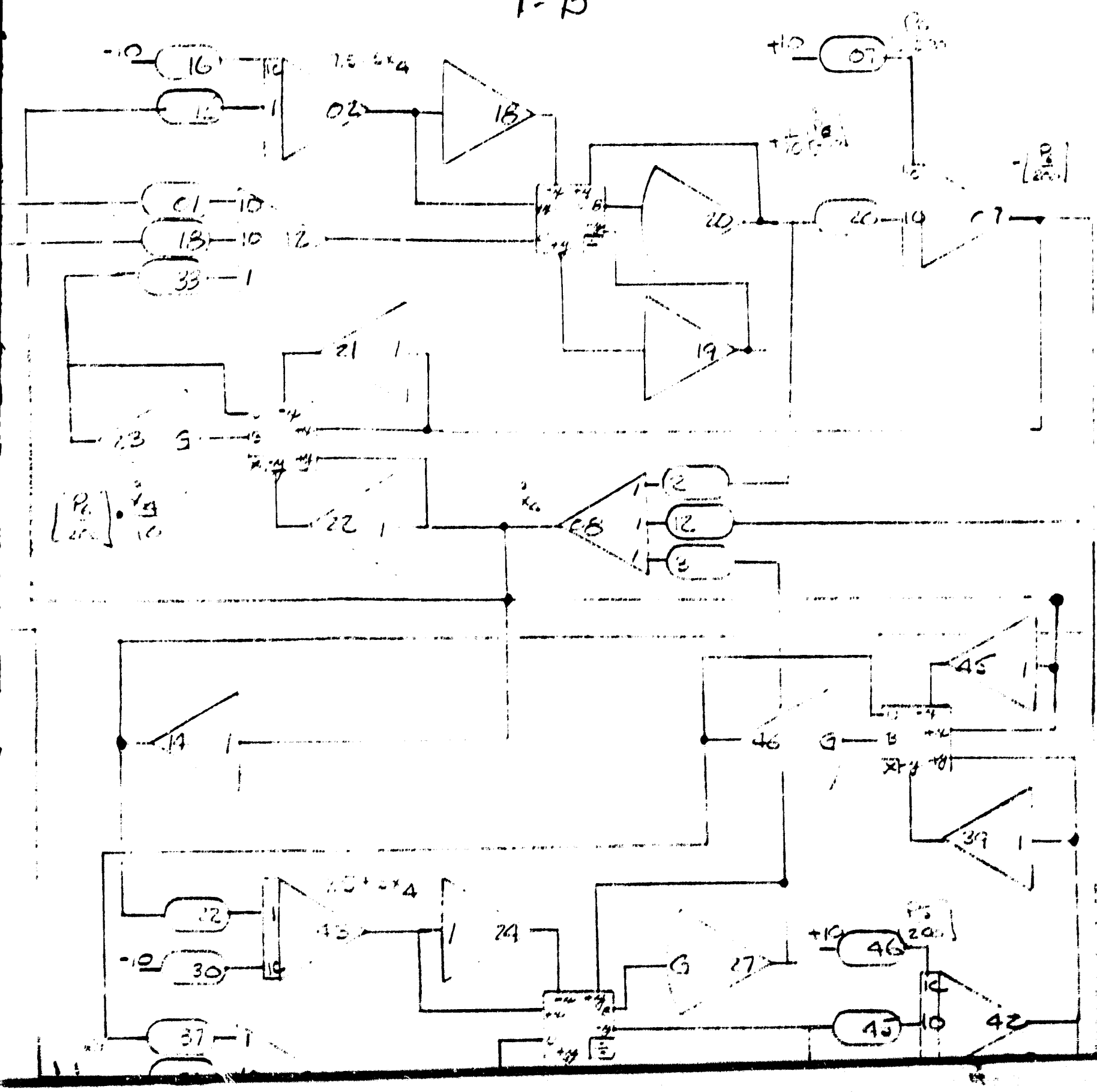
REPRODUCIBILITY OF THE ORIGINAL PAGE IS POOR.

Page 34
Fold out frame
1-A

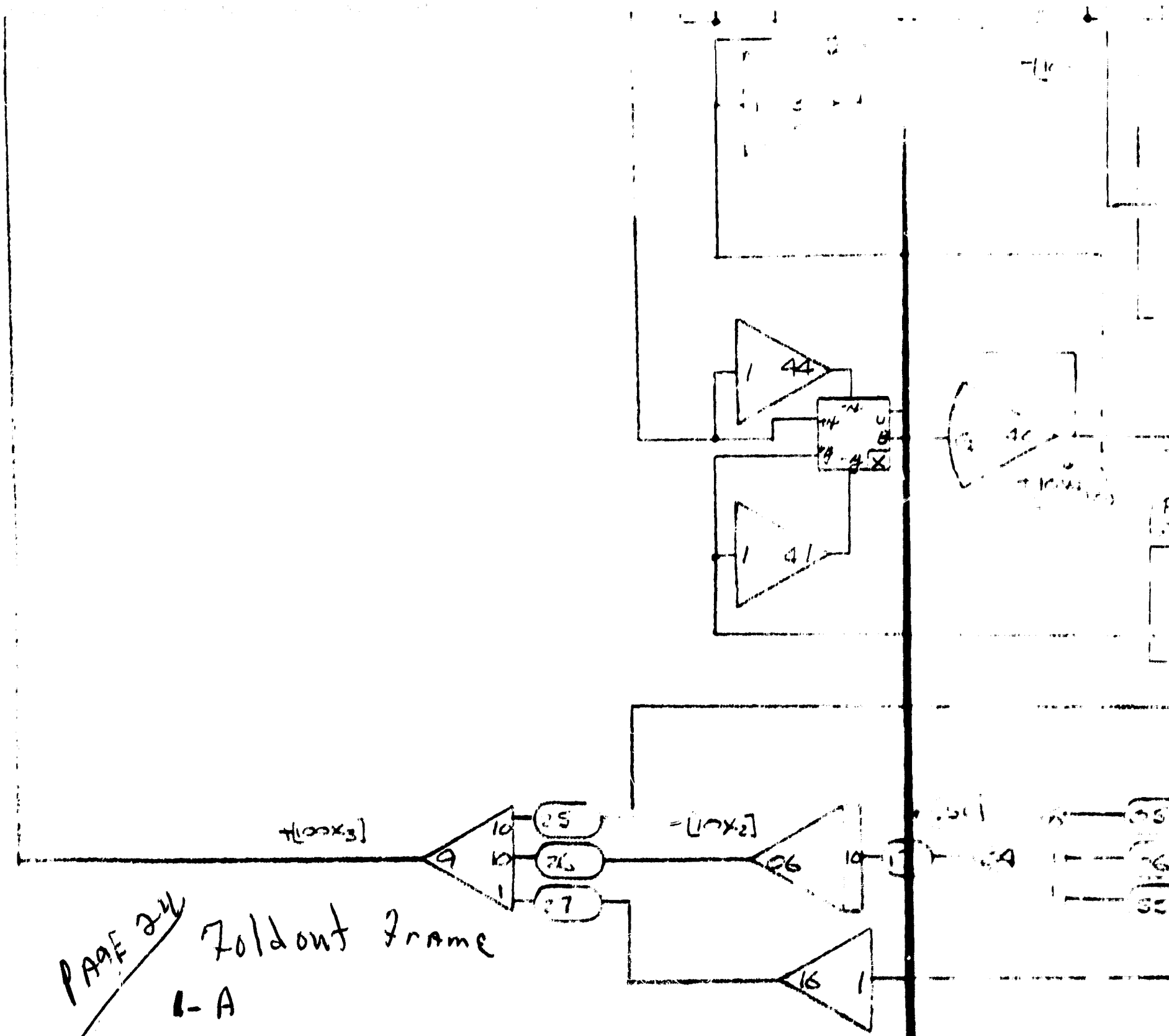


REPRODUCIBILITY OF THE ORIGINAL PAGE IS POOR.

Fold out Frame
1-B



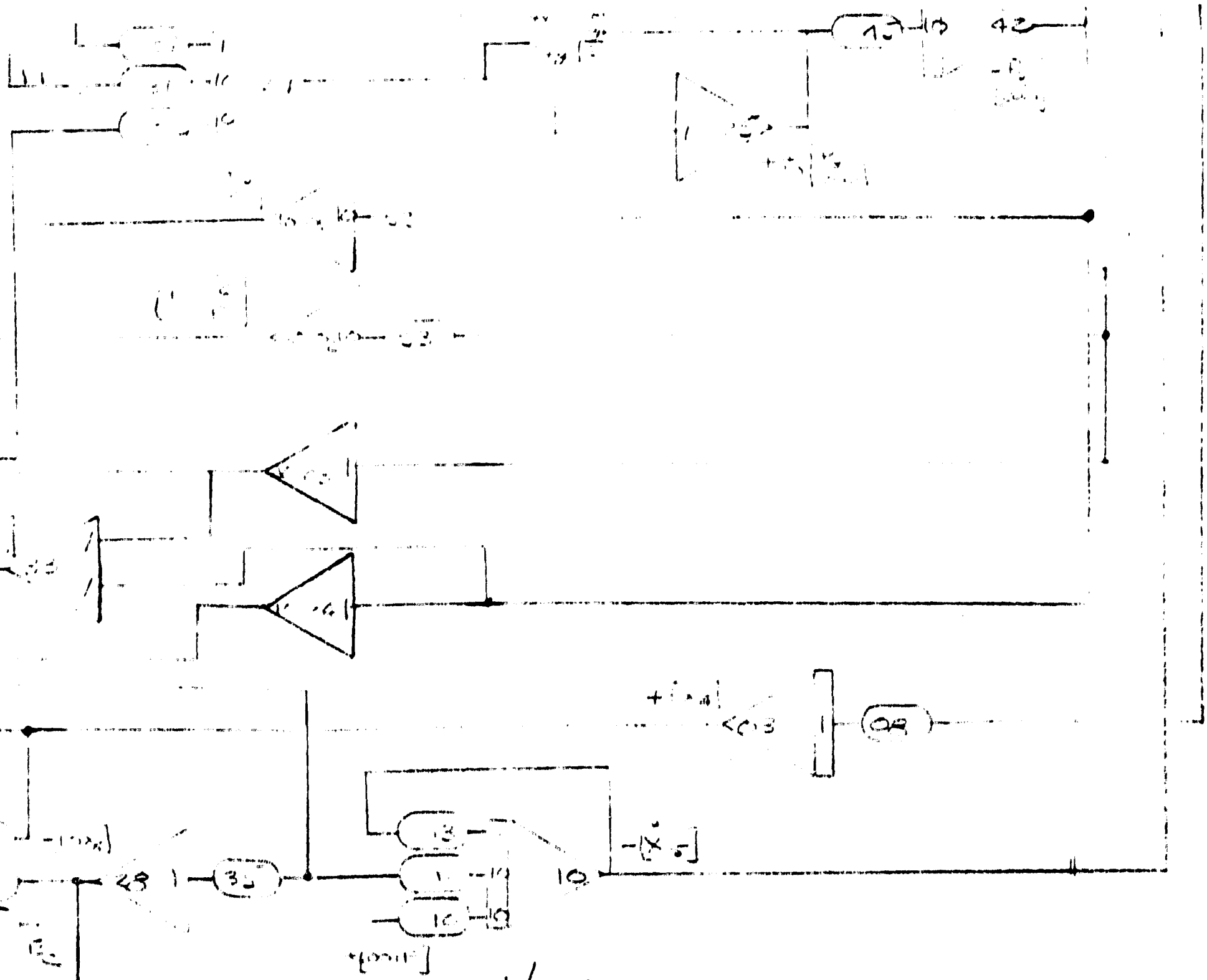
REPRODUCIBILITY OF THE ORIGINAL PAGE IS POOR.




PAGE 24 Foldout Frame 1-A

FIGURE 10. PNEUMATIC CO[illegible] E [illegible]

REPRODUCIBILITY OF THE ORIGINAL PAGE IS POOR.



Foldout Frame
1-B

CONTRACT NAS8-20730
V1.0 84011
PNEUMATIC INTEGRATOR
5-8-67 SMG

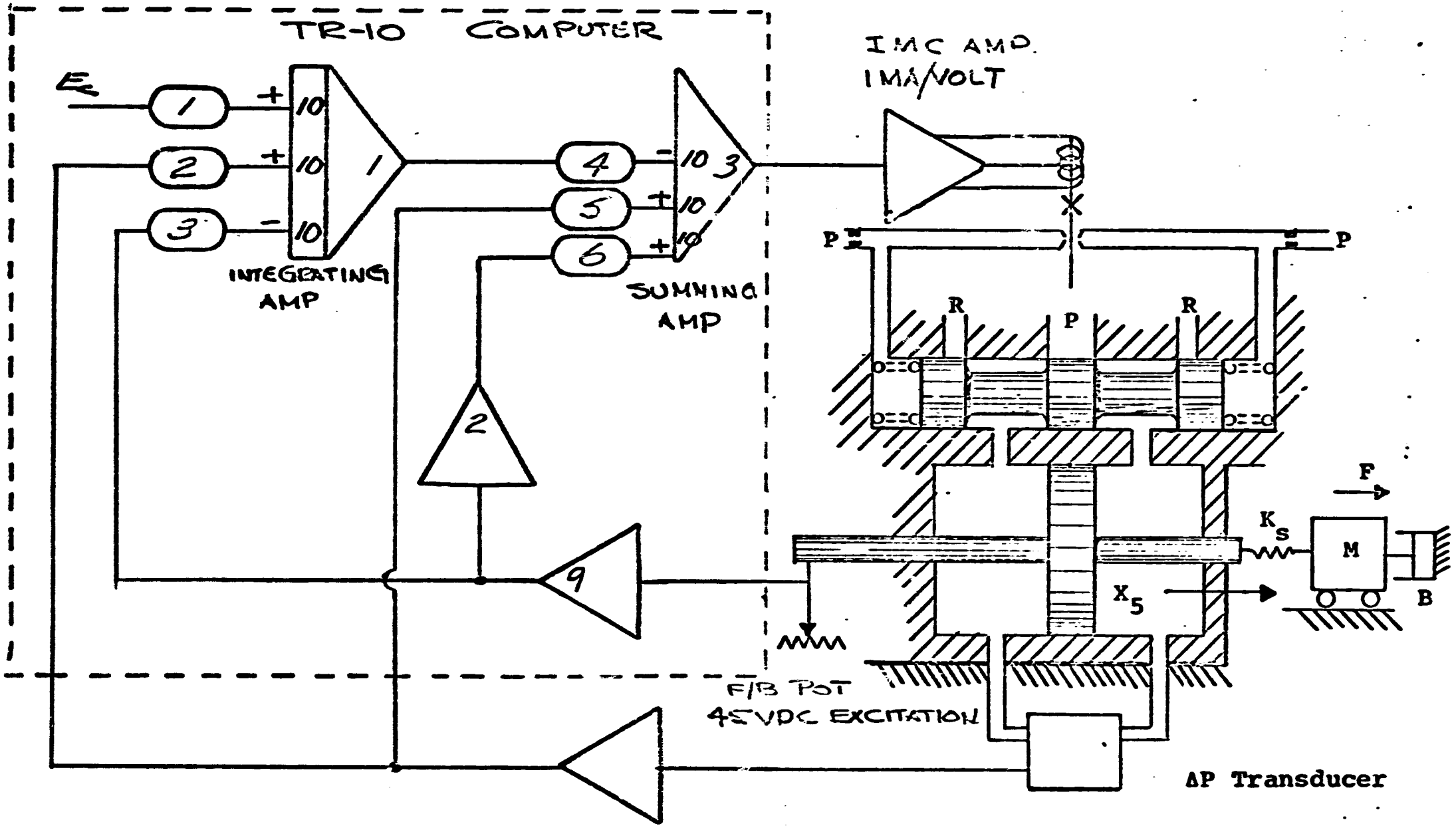
HP 7390000

## 2.4 Electrical Implementation Tests

A hybrid test series was undertaken in order to demonstrate the validity of the analytical models of sections 2.1, 2.2, and 2.3. A G.F.E. servo actuator HR&M P/N 1052350 was functionally modified by removing the dynamic load damping (DLD) package. As shown in Fig. 11, a TR-10 analog computer was connected to the actuator, and used to simulate the contemplated modifications.

A ΔP transducer was connected across the cylinder ports to provide load damping by means of negative feedback to the summing amplifier, and load spring rate compensation by positive feedback to the integrating amplifier. Negative electrical position feedback was provided to both the inner loop (summing amplifier) and outer loop (integrating amplifier). This actuator was installed in the HR&M load simulator. The loop gains were adjusted by iteration until the system step and frequency response characteristics most closely satisfied the desired envelopes. Gain values determined from this hybrid testing were then compared with those found from the previous analytical studies.

FIGURE 11
HYBRID-FREE INTEGRATOR
FEASIBILITY STUDY.




NOTE:

1. CONNECT XDUCER SUCH THAT A + SIGNAL TO SERVO VALVE YIELDS A + SIGNAL FROM XDUCER
2. CONNECT F/B POT SUCH THAT IN EXTEND DIRECTION OUTPUT OF POT IS POSITIVE.

HR 73900000

## 2.5 Feasibility Study Results

The inner loop integrator, as proposed in HR&M report 73400170, can provide a significant improvement in static sensitivity when implemented on an S-II servoactuator HR&M P/N 1052350. However, this is accomplished with an increase in low frequency phase shift as manifest by delayed time response to a position step command. The simulation study indicated this delay could be substantially reduced by the addition of lead compensation.

Correlation between linear analysis, analog simulation, and hybrid electrical testing provided confidence in the gains selected for detail designs in phase II. The power spool position equations allows the following comparison of component gains, as determined by analysis and test.

1) Linear Analysis:

$$X_{3P} = 0.77 \times 10^{-5} P_L - 0.081 X_4 + \frac{1}{S} (KE_c - 1.25 X_4 + 0.645 \times 10^{-4} P_L)$$

2) Analog Simulation:

$$X_{3P} = 0.4 \times 10^{-5} P_L - 0.1 X_4 + \frac{1}{S} (KE_c - 1.34 X_4 + 0.69 \times 10^{-4} P_L)$$

3) Hybrid Testing:

$$X_{SP} = 3 \left[0.415 \times 10^{-5} P_L - 0.98 X_4 + \frac{1}{S} (KE_c - 1.38 X_4 + 0.5 \times 10^{-4} P_L)\right]$$

It can be seen from the above equations that except for a factor of 3, close correlation exists in the results of the simulation and hybrid test series. The specific cause of this observed discrepancy has not been determined, although a variation between the first-stage servovalve gain and the value used in the simulation study may be significant. The deviation is not considered serious, since the servo amplifier gain may be adjusted and nominal gains of the mechanical loop components have been established with high confidence.

During static sensitivity tests on both the analog simulation and load simulator, it was observed that stability margin decreased as static load force increased.

This was most significant on load simulator tests with the appearance of a limit cycle approaching 0.5% of full stroke travel at 80% of maximum load force. Causes of and correction for this characteristic have not been determined. However, it can be seen from the load simulator static sensitivity curve of Fig. 37 that both hysteresis and dead band exist in the test setup. Excess play in the actuator rod end bearings and load simulator linkages is a major contributor to this condition. It would be desirable to investigate the problem and some additional system configurations such as derivative load pressure feedback, power spool lapping conditions,

and lead compensation. Further studies along these lines would permit the design of a more optimum modification to P/N 1052350. Results of the analog simulation study employing 2000 psi ambient temperature nitrogen gas indicate that a flight type actuator can be designed that is insensitive to static load forces.

A unit of this type operating on pneumatic media would be limited in response characteristics, and would be more susceptible to dynamic load force disturbance inputs such as those arising from engine vibrations and vehicle bending modes. However, the amount of performance degradation does not appear excessive, as indicated by a comparison of the enclosed hydraulic and pneumatic command and load force response plots.

A series of 54 runs was made on the analog computer in which both the hydraulic and pneumatic integrator systems were investigated. The configuration proposed in HR&M report 73400170 exhibits low frequency phase shift and step response delay as shown in Fig. 14 and at the bottom plot of Fig. 12. The load force characteristics are shown in Figs. 15, 16, and 17. The +6 db/octave low frequency slope of Fig. 17 demonstrates the inherent ability of this system to compensate for static load force.

Lead compensation can be added to the actuator by summing a piston whose position is proportional to first-stage flow with the integrator piston displacement. This type of compensation was

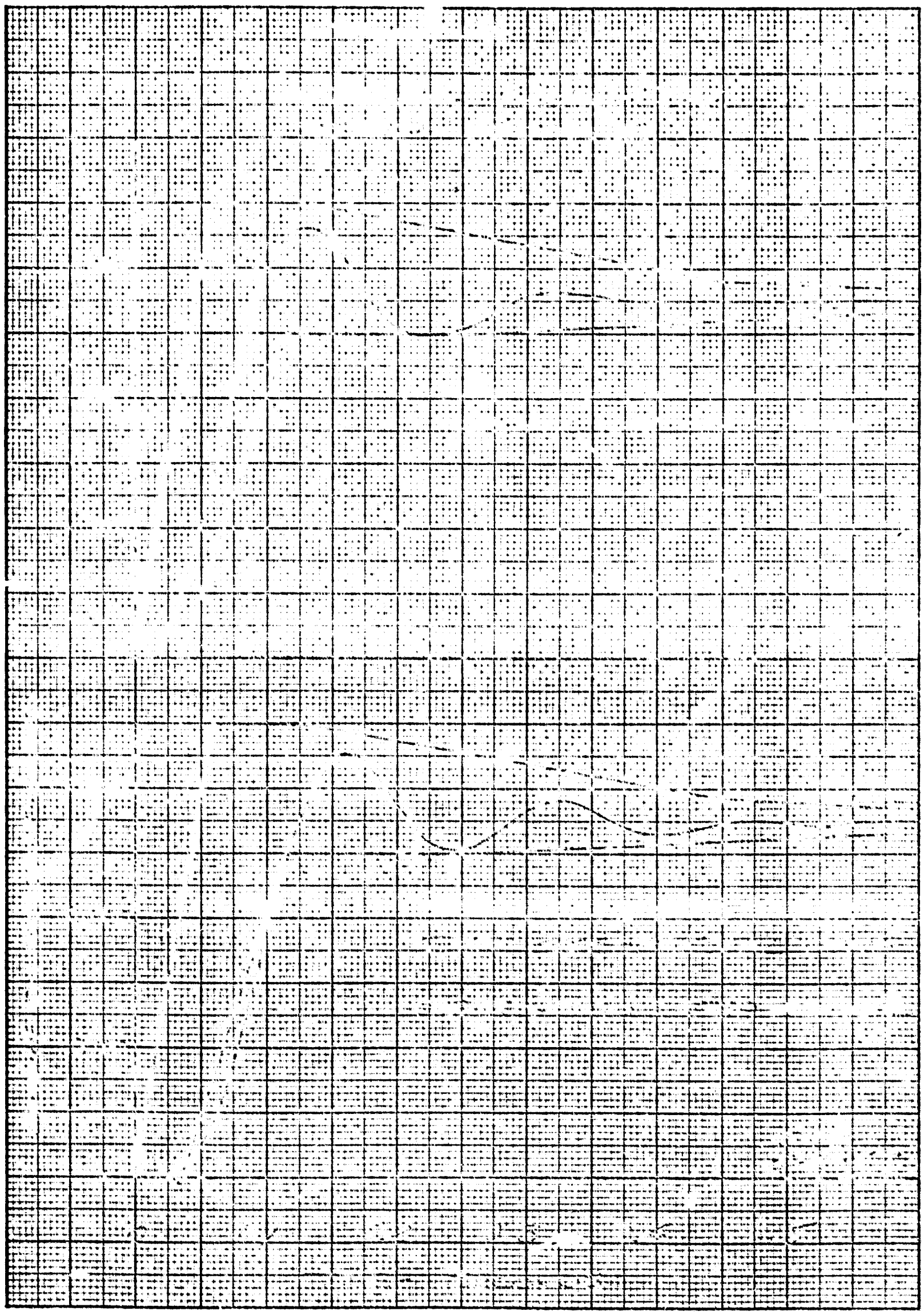
investigated on the computer as one method of correcting for excessive low-frequency phase shift. This modification allowed the step and frequency response envelopes to be satisfied, as shown at the top of Fig. 2 and Figs. 18 and 19. Comparison of Figs. 20, 21 and 22 with 17, 18 and 19 respectively indicates that the load force response characteristics are satisfactory.

Figures 23 through 33 define performance of the pneumatic inner loop integrator system. Again the actuator was studied with and without lead compensation. Although, as shown in Fig. 23, some improvement in low frequency phase shift is noticeable, the increase in mechanical complexity does not seem justified. The characteristic of zero static load force position error is indicated by the +6 db/octave low frequency slope in Figs. 28 and 33. Decreased dynamic stiffness (as compared with that of the hydraulic system) is seen in the load force step response plots of Figs. 26 and 31. With the actuator at null, an applied load force step of 20,000 lb causes the actuator to deflect as much as 0.300 in., 20 percent of rated stroke, before returning to null.

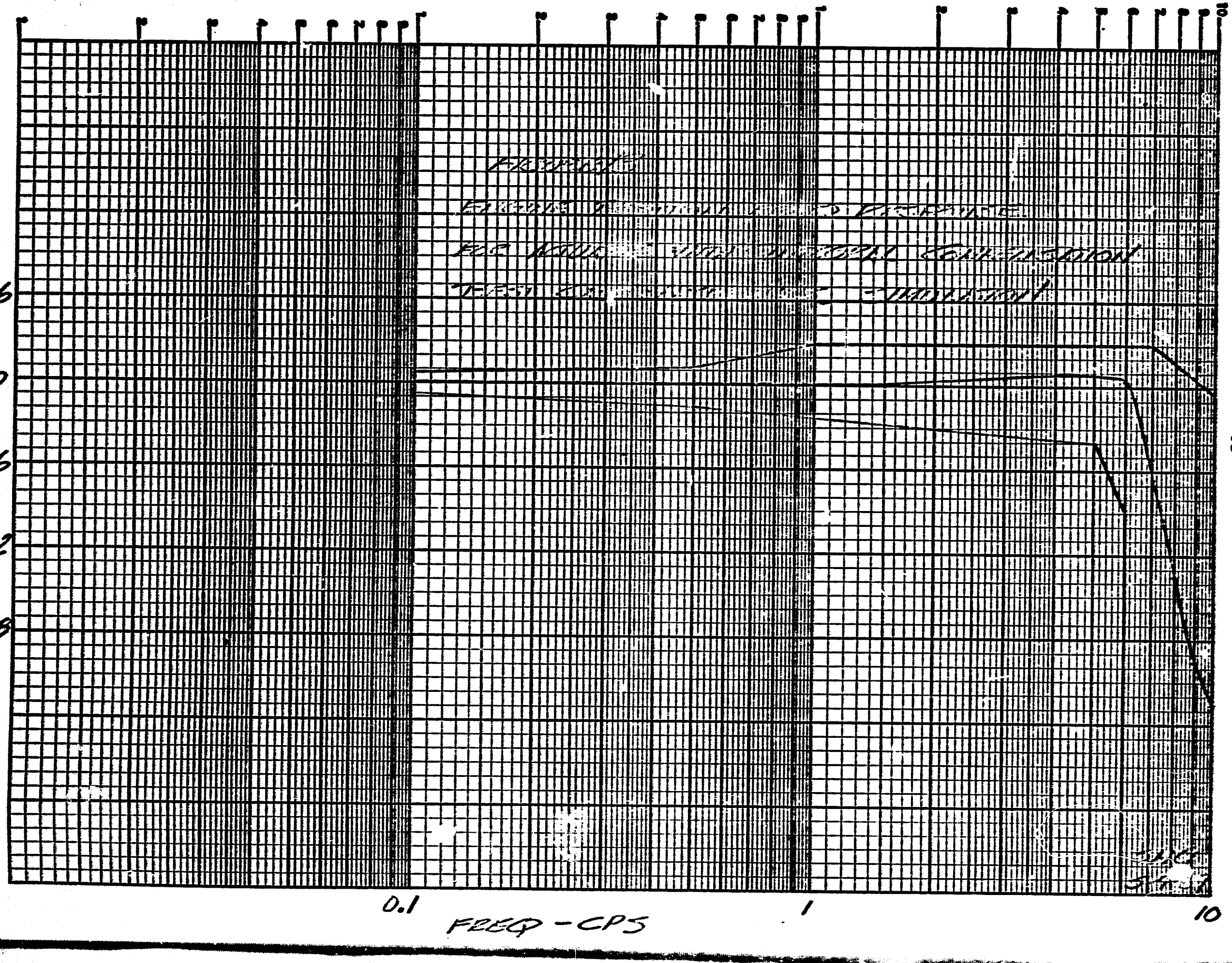
Static load sensitivity plots for the simulated actuator have not been shown. Data were taken, and in all cases an infinite static stiffness curve was exhibited by plotting engine position against load force.

Electrical implementation testing was accomplished on the HR&M load simulator. Engine position step response is shown in figure 34. This correlates well with the analog computer results shown at the bottom of figure 12. Simulator tests seem to exhibit a somewhat lower natural frequency. This may be attributed to variations in the load simulator or different moments of inertia and spring rates from those calculated and assumed for the analog study.

Frequency response is shown in figures 35 and 36. The static sensitivity characteristic of Figure 37 shows a negative slope. This is attributed to excessive gain in the positive pressure feedback loop. It is interesting to note that the engine position can be made to grow against a load force. Hysteresis in Figure 37 appears to be characteristic of the HR&M SI-C load simulator, and has been observed in previous tests. Apparent deadband is attributed to play in the actuator and simulator attach point bearings and bushings.



KEUFFEL & ESSER CO. 7 X 10 IN. • ALBANENE • TO V. .327

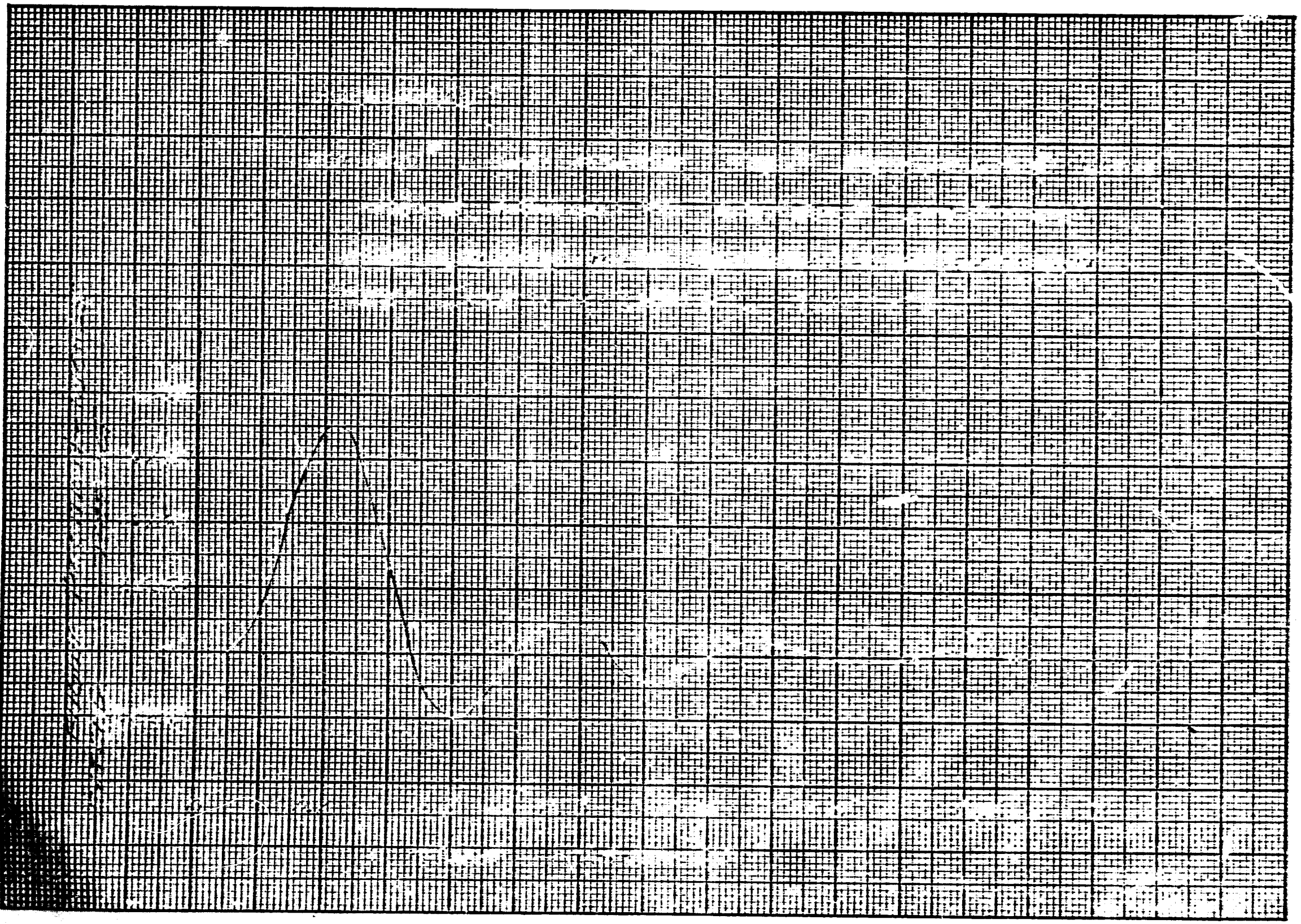

6
0
-6
-12
-18
GAIN - DB
0.1
1
10
FREQ - CPS

KEUFFEL & ESSER CO.

0
30
60
90
120
150
180
210
240
270

0.1 FREQ-CPS 1 10

K&E 10 X 10 TO ½ INCH 46 1327
7 X 10 IN. • ALBANENE MADE IN U.S.A.
KEUFFEL & ESSER CO.



REPRODUCIBILITY OF THE ORIGINAL PAGE IS POOR

HR 73900000

K&E SEMI-LOGARITHMIC 3 CYCLES X 80 DIVISIONS KEUFFEL & ESSER CO. MADE IN U.S.A. 537

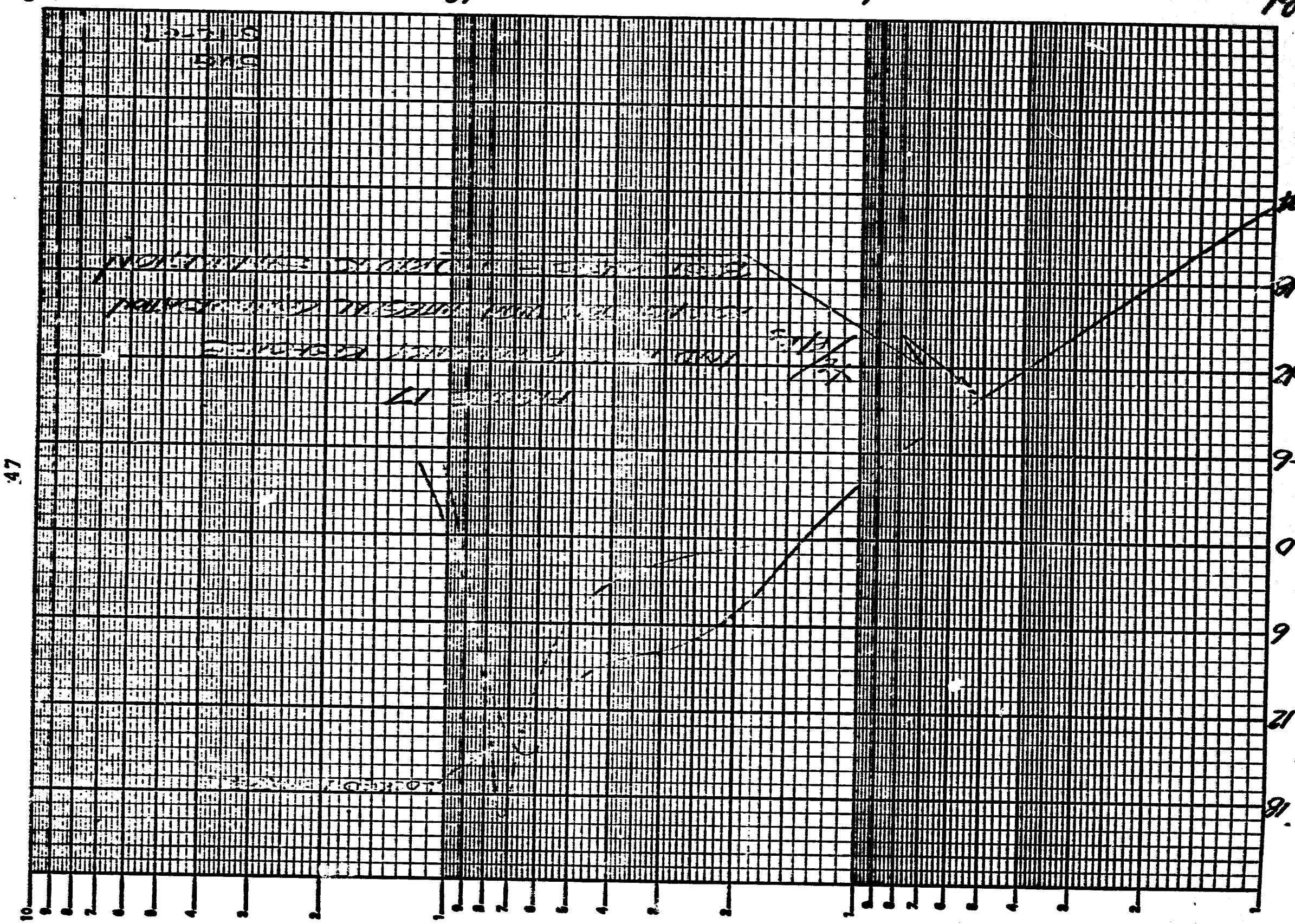
12
6
0
-6
-12
-18

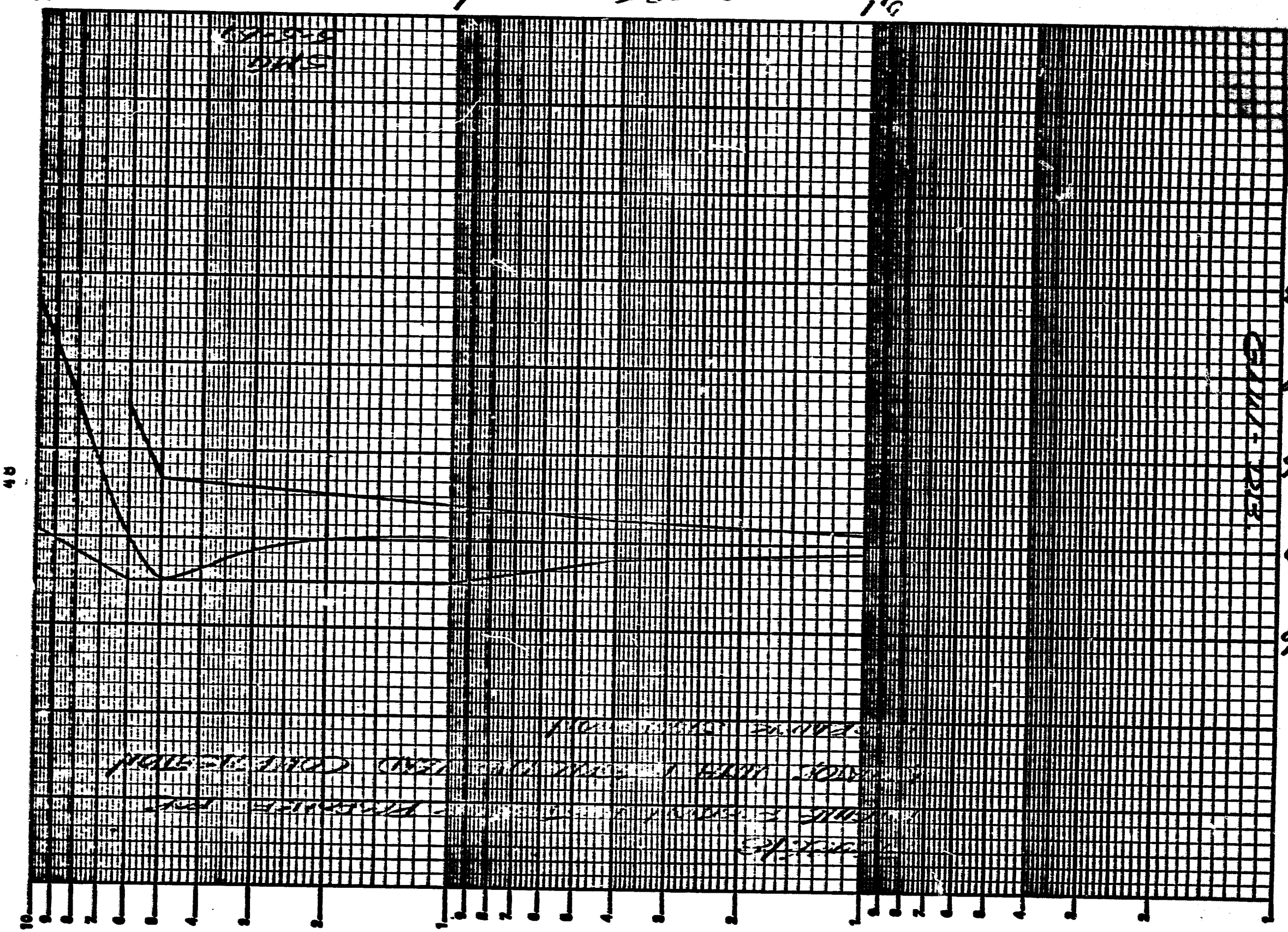
PHASE LAG - DEGREES

90
120
150
180

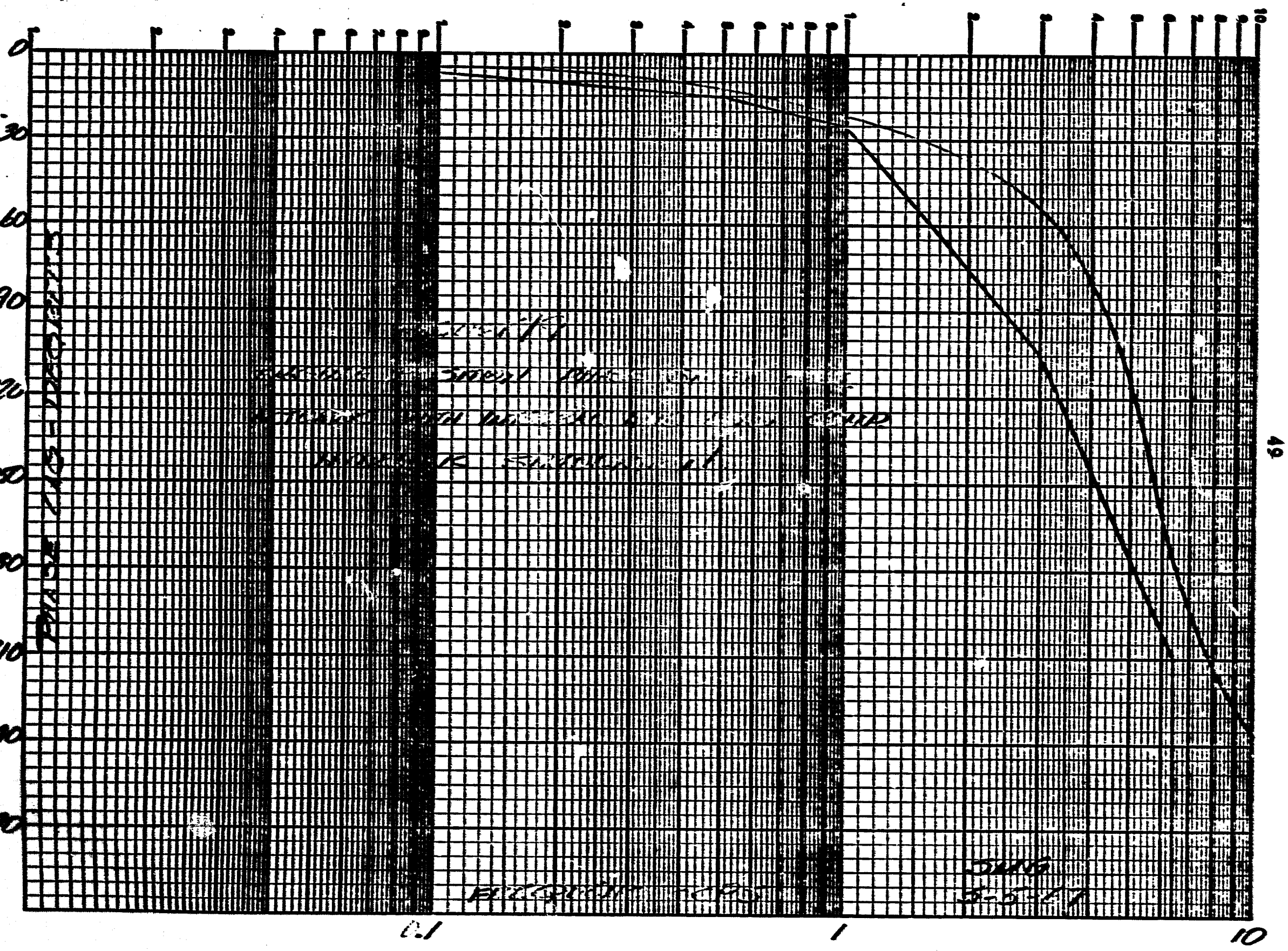
0.1
1
10

FREQUENCY - CPS



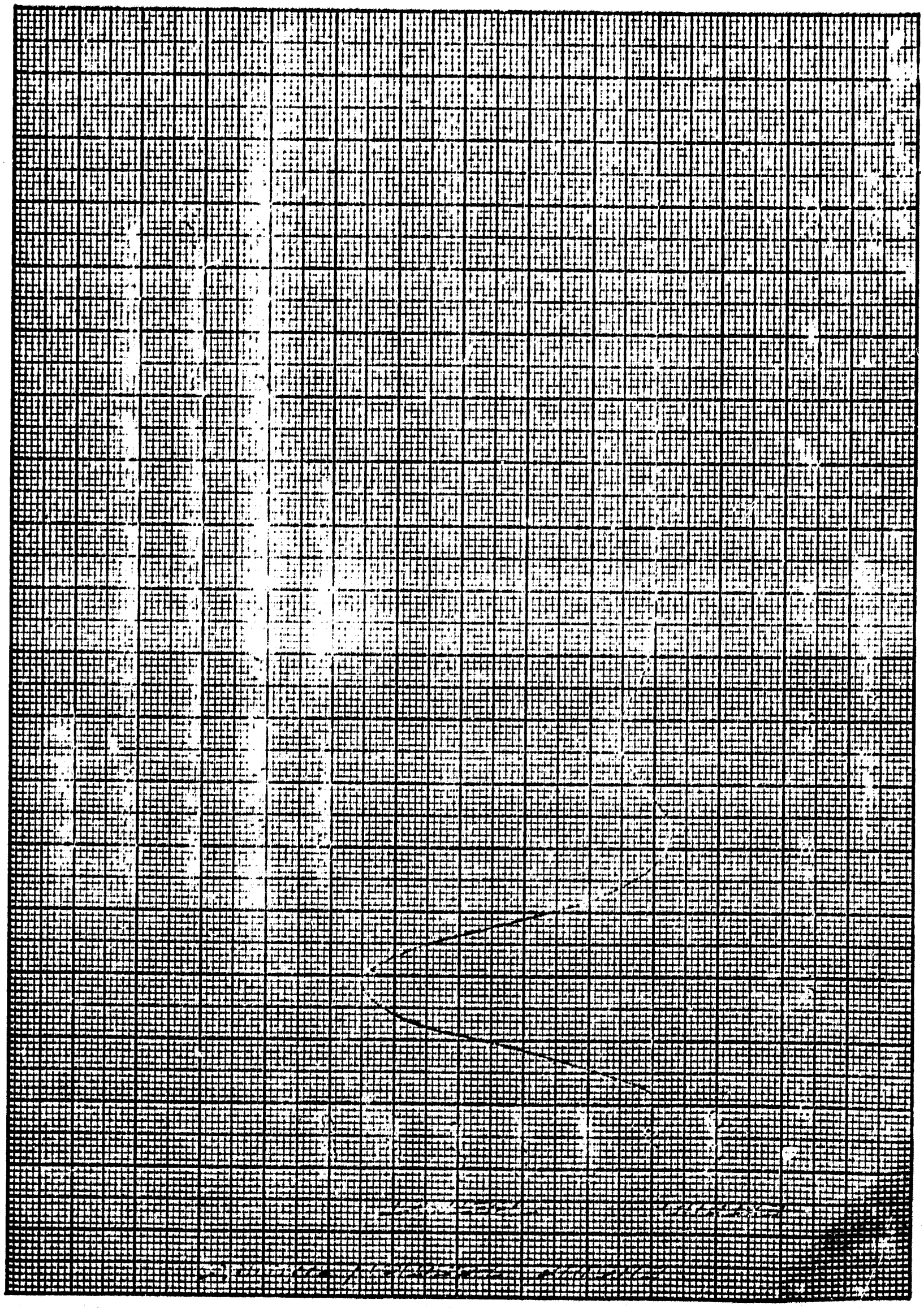


HR 73900000

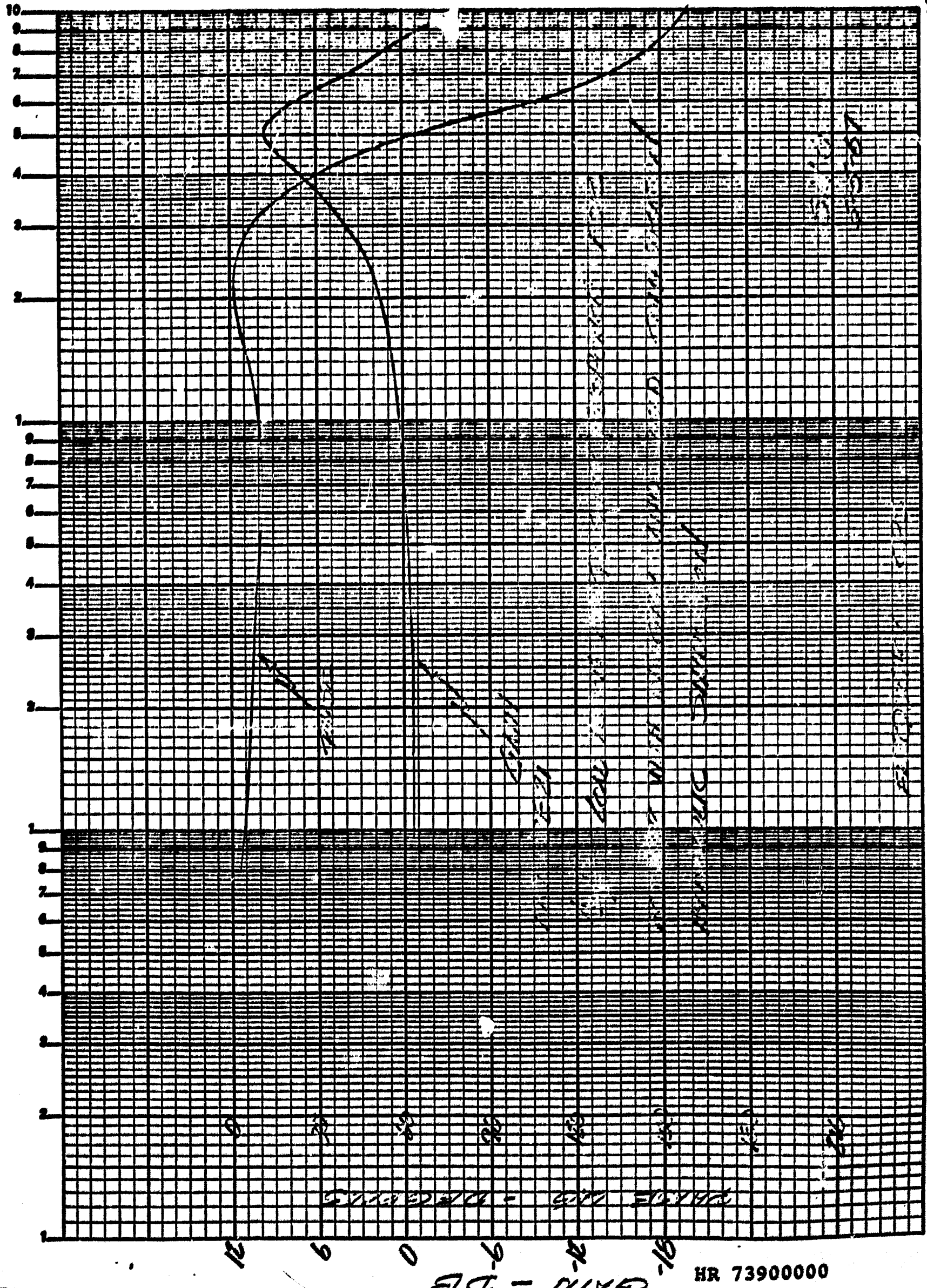

0
30
60
90
120
150
180
210
240
270
0.1
1
10

REPRODUCIBILITY OF THE ORIGINAL PAGE IS POOR

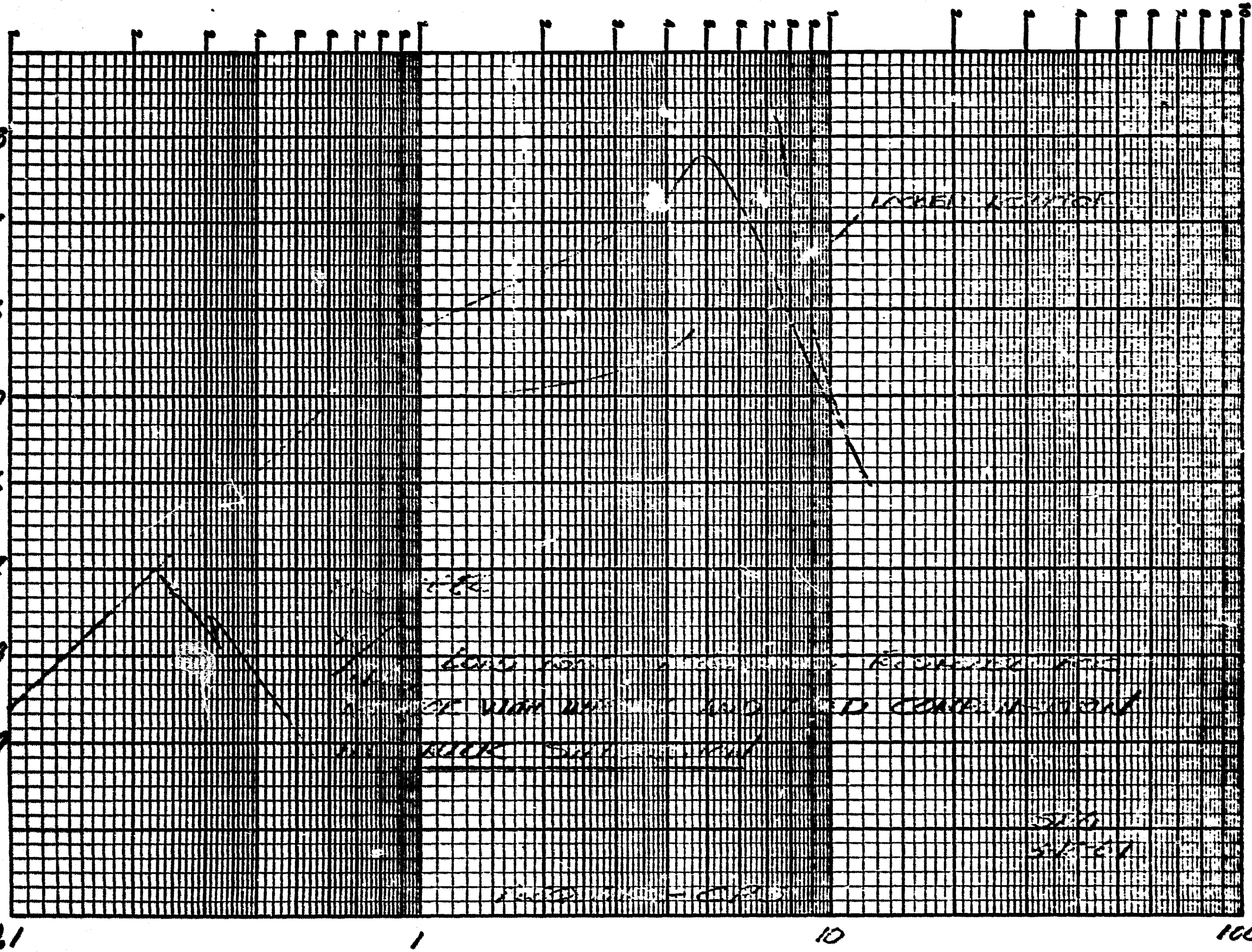




HR 73900000


GAIN - DB
HR 73900000

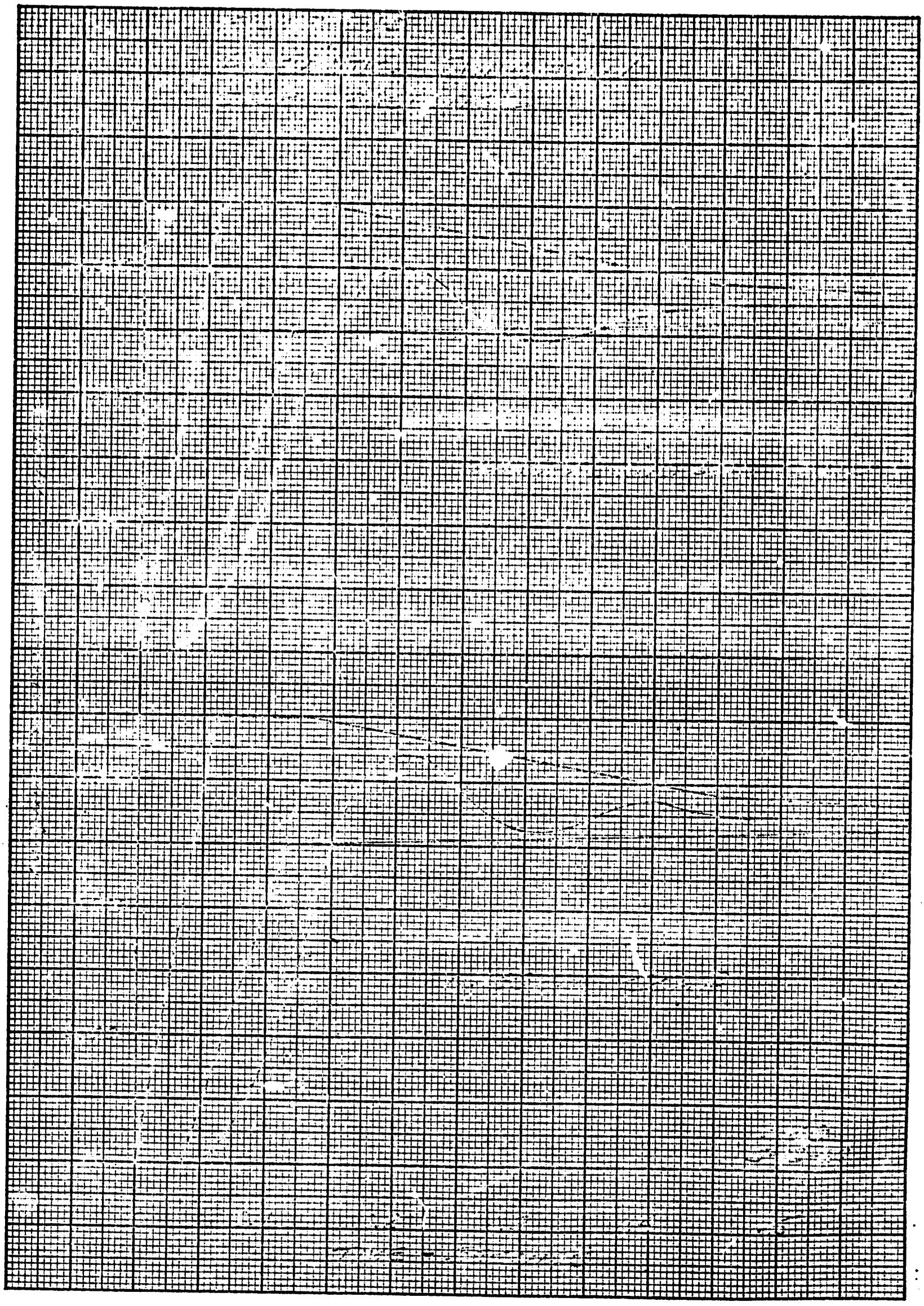
K&E SEMI-LOGARITHMIC 46 5...
3 CYCLES X 90 DIVISIONS MADE IN U.S.A.
KEUFFEL & ESSER CO.




HR 73900000

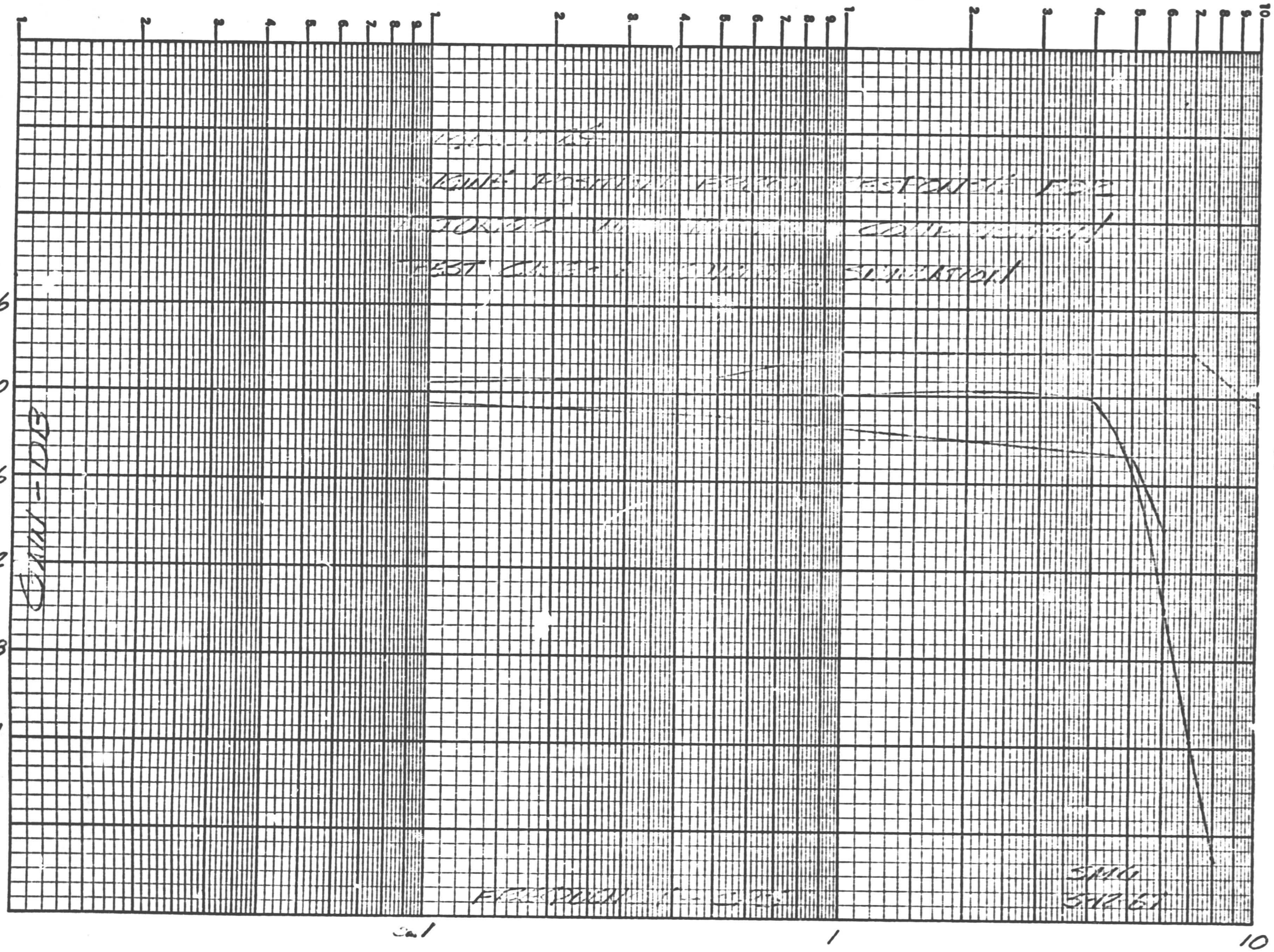
REPRODUCIBILITY OF THE ORIGINAL PAGE IS POOR.





KEUFFEL & ESSER CO. MADE IN U.S.A. 7 X 10 IN. • ALBANENE®

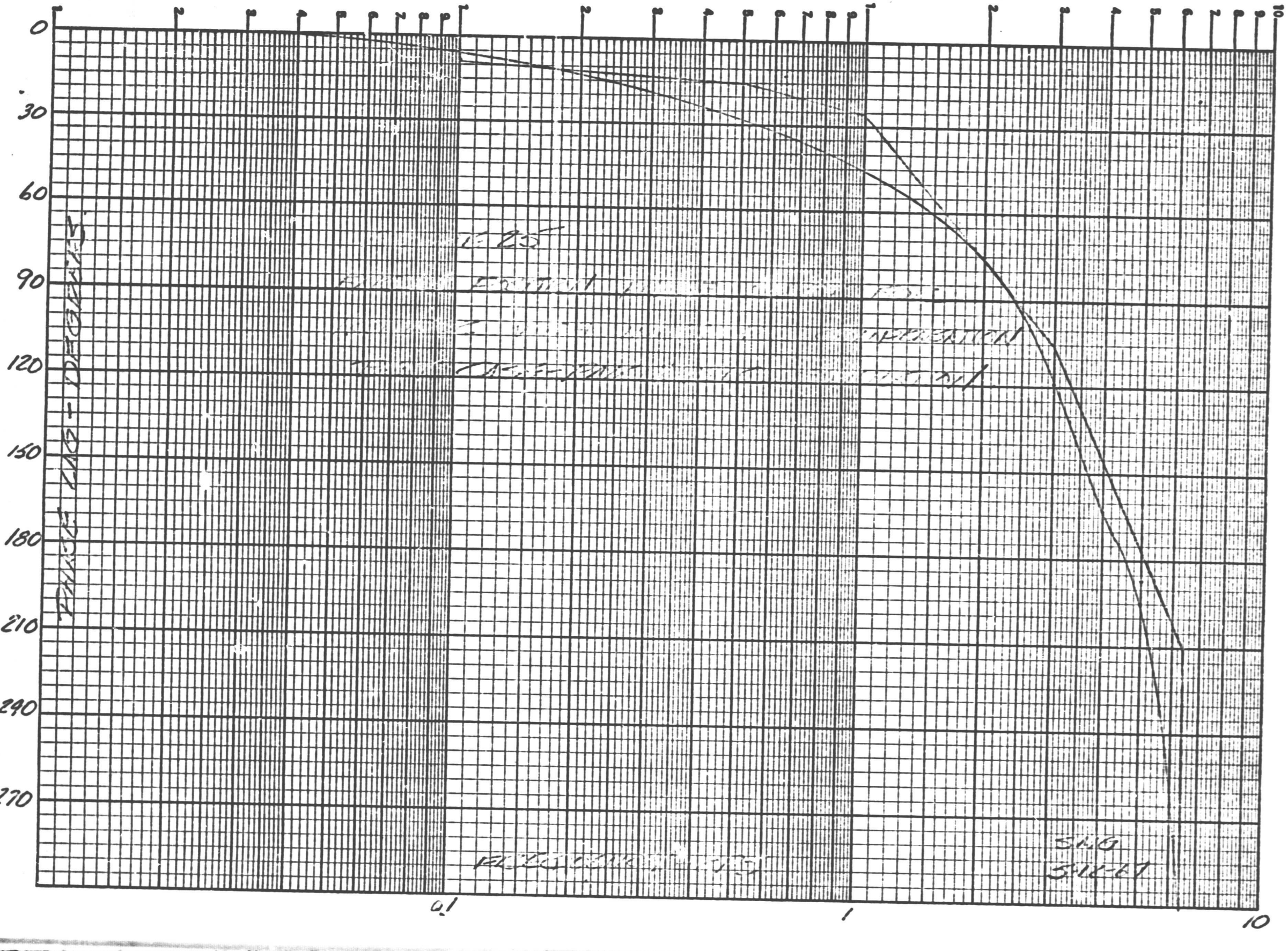
K&E LOGARITHMIC 5 53
3 CYCLES X 60 DIVISIONS MADE IN U.S.A.
KEUFFEL & ESSER CO.




HR 73900000

54

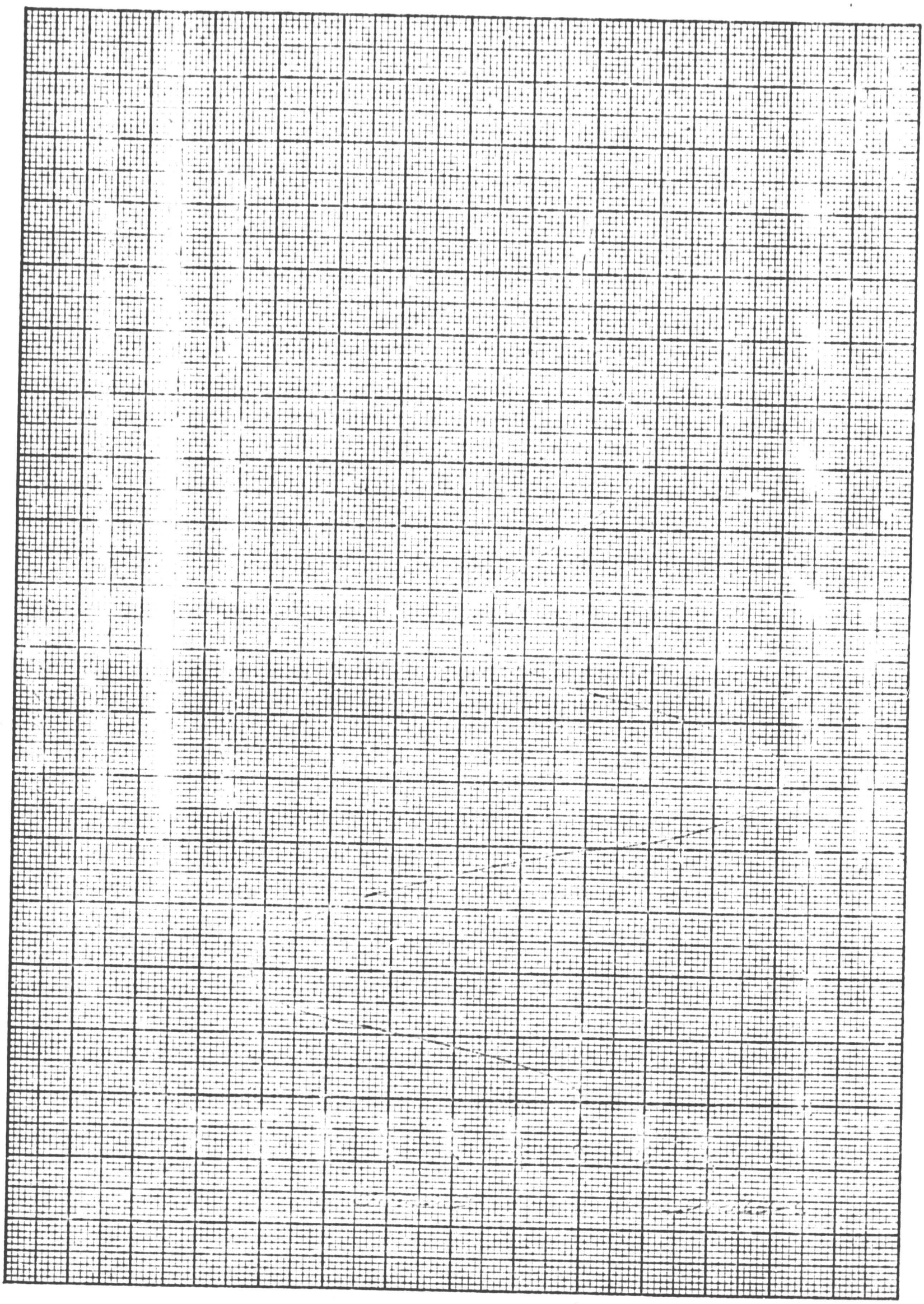
K&E SEMI-LOGARITHMIC 3 CYCLES X 60 DIVISIONS KEUFFEL & ESSER CO. MADE IN U.S.A.




HR 7390000

55

REPRODUCIBILITY OF THE ORIGINAL PAGE IS POOR.



K+E 7 X 10 IN. • ALBANENE® KEUFFEL & ESSER CO.

K&E LOGARITHMIC 3 CYCLES X 60 DIVISIONS MADE IN U.S.A.
KEUFFEL & ESSER CO.

GAIN - DB

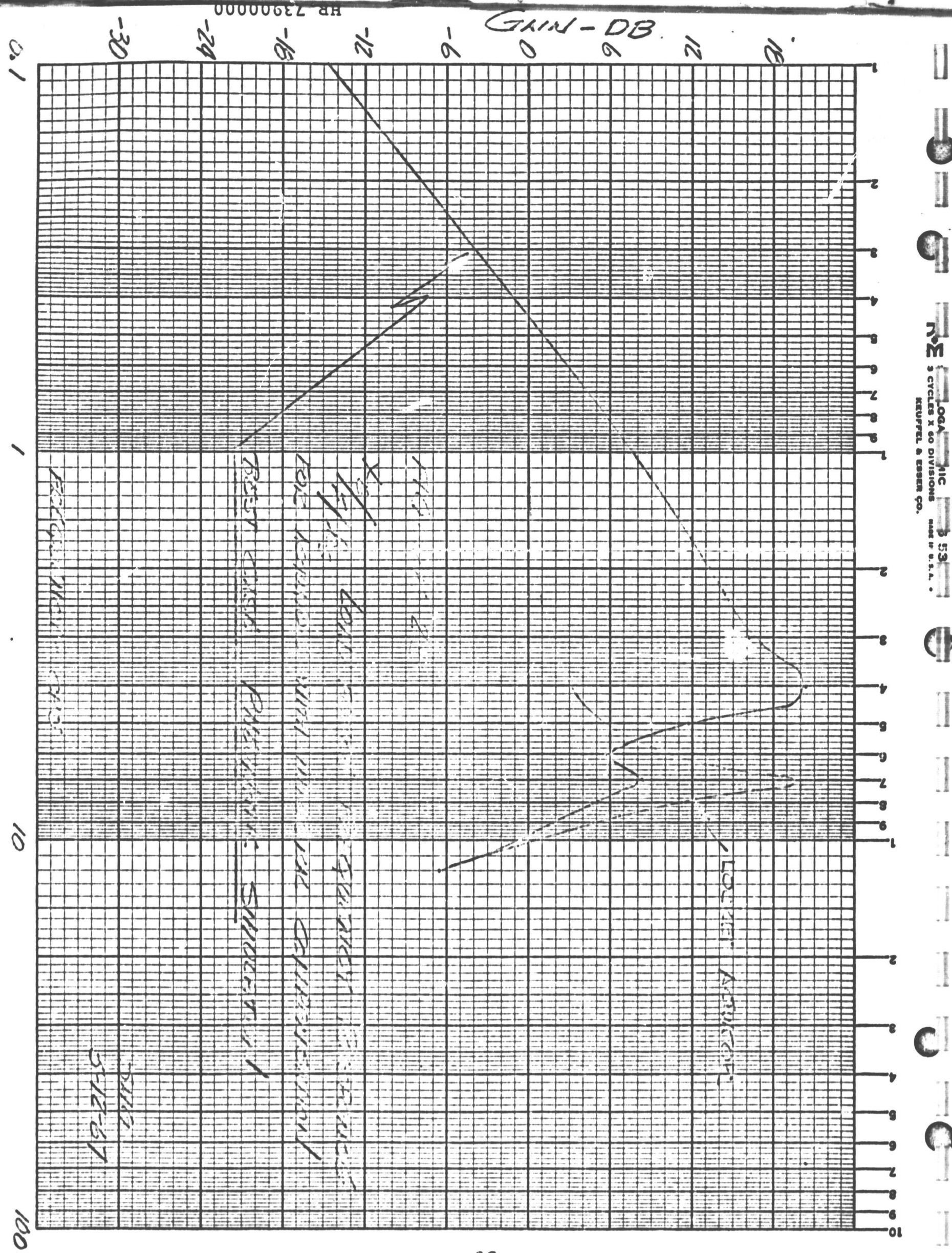
18
12
6
0
-6
-12
-18

0
30
60
90
120
150
180

1
.1
10

57

HR 73900000


GAIN-DB
-30
-24
-18
-12
-6
0
6
12
18
0.1
1
10
100
HR 7390000
KEUFFEL & ESSER CO.
58

KEUFFEL & ESSER CO.

6

0

-6

-12

-18

-24

0.1

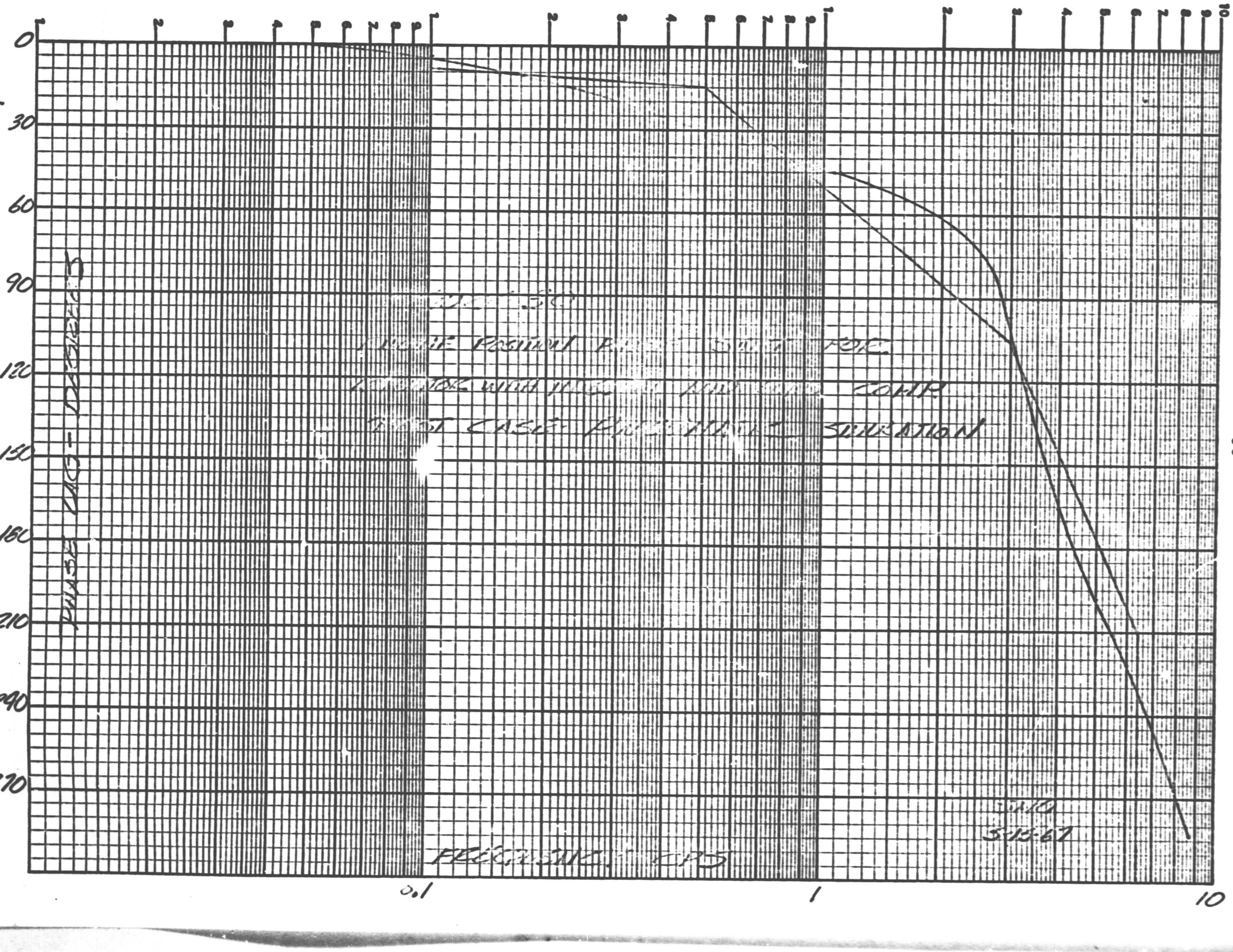
1

10

59

HR 73900000

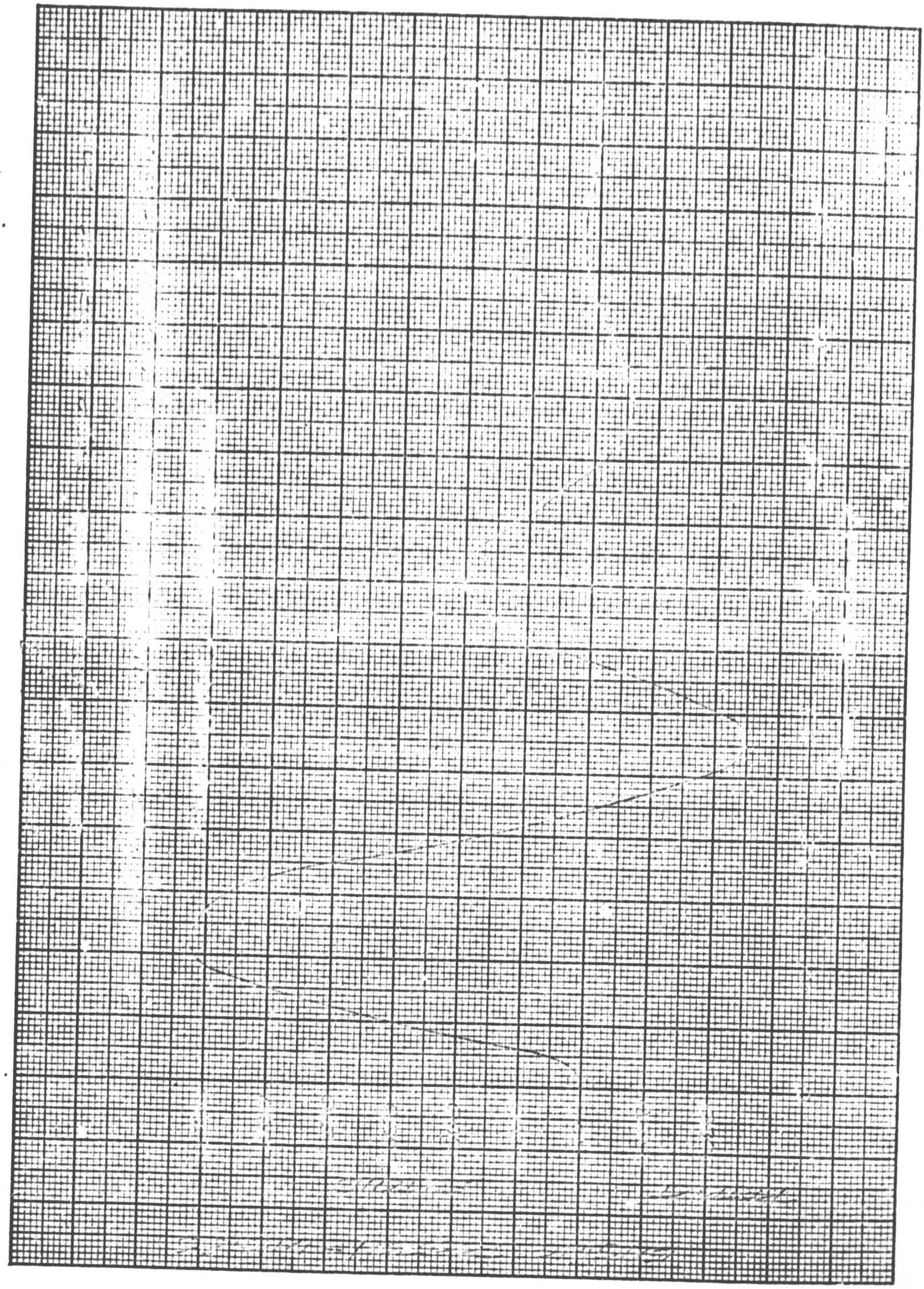
K&E LOG MIC 6 5:
3 CYCLES X 60 DIVISIONS MADE IN U.S.A.
KEUFFEL & ESSER CO.




HR 73900000

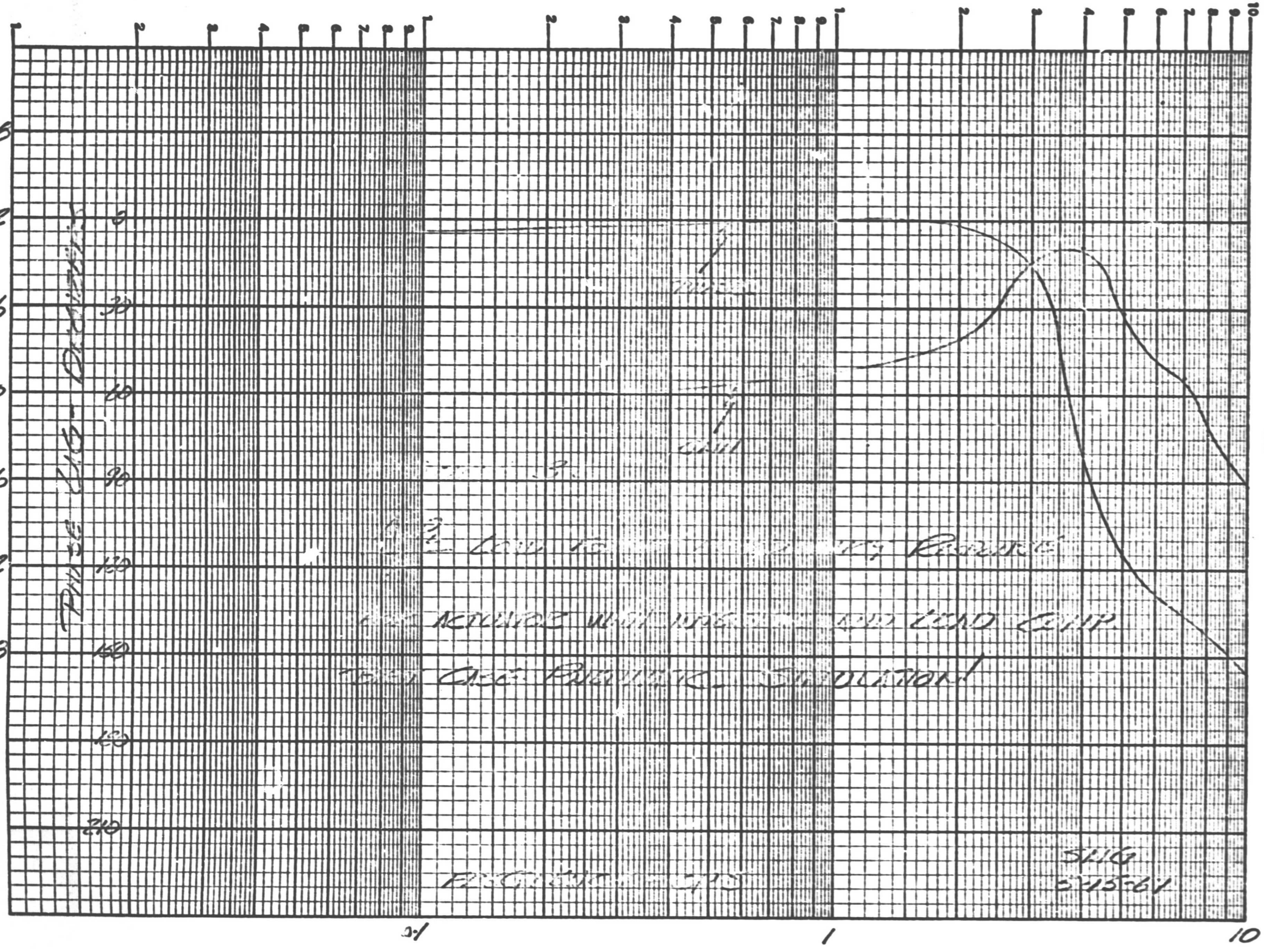
REPRODUCIBILITY OF THE ORIGINAL PAGE IS POOR.



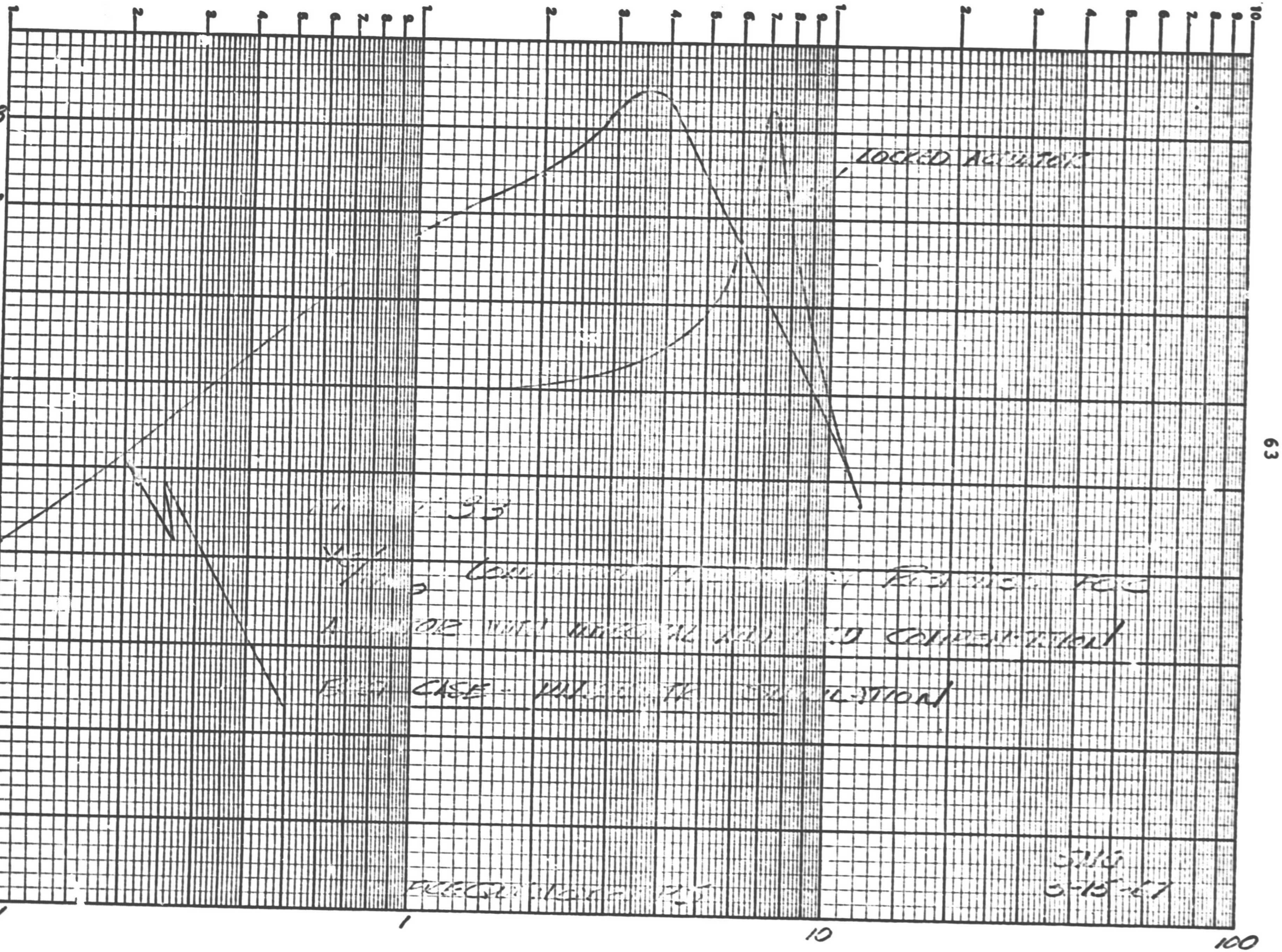


KEUFFEL & ESSER CO. MADE IN U.S.A.

K&E ...I-LO ...HMIC ...46 ...
... CYCLES X 60 DIVISIONS MADE IN U.S.A.
KEUFFEL & ESSER CO.

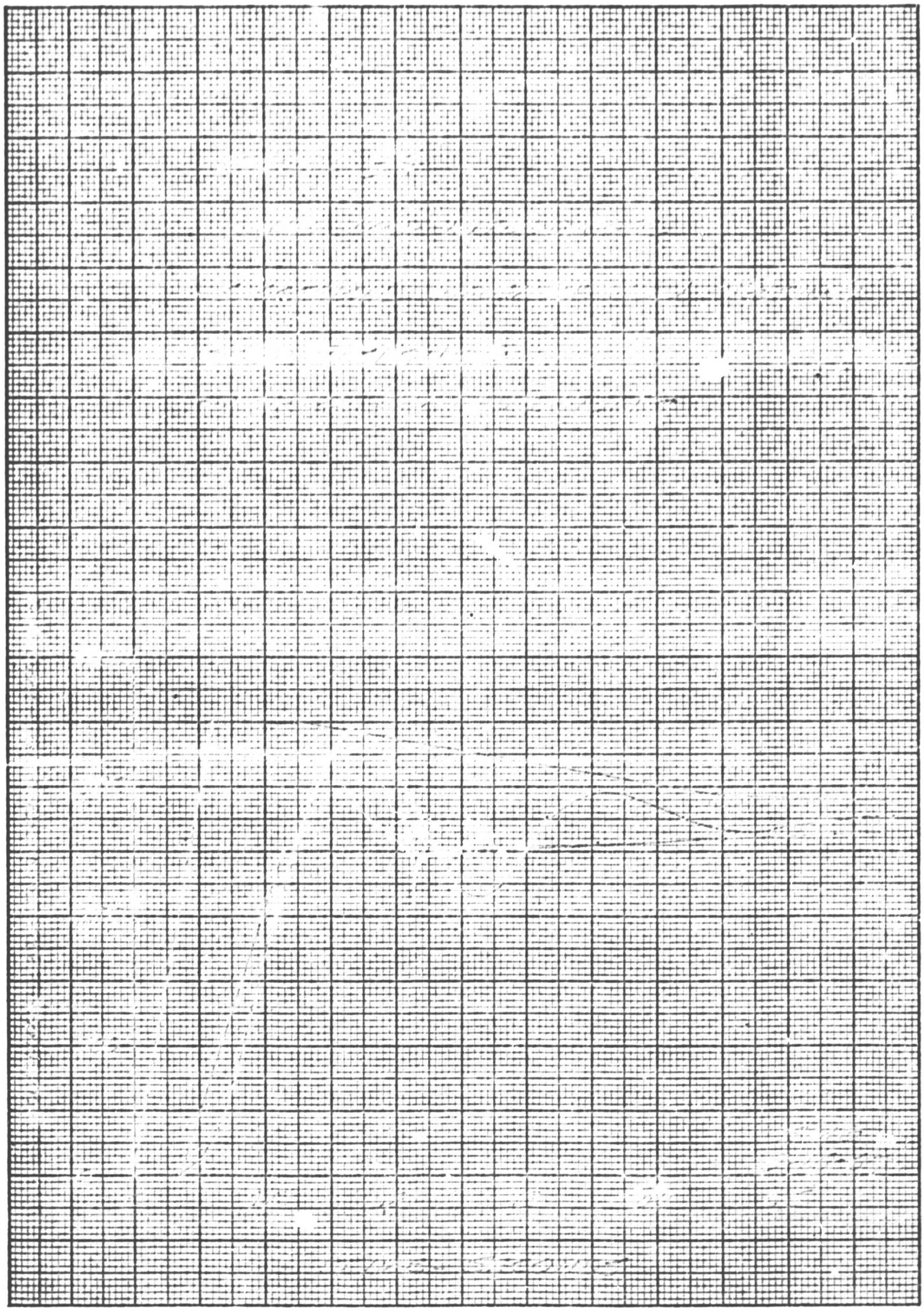


SEMI-LOG 373
3 CYCLES X 60 DIVISIONS MADE IN U.S.A.
KEUFFEL & ESSER CO.



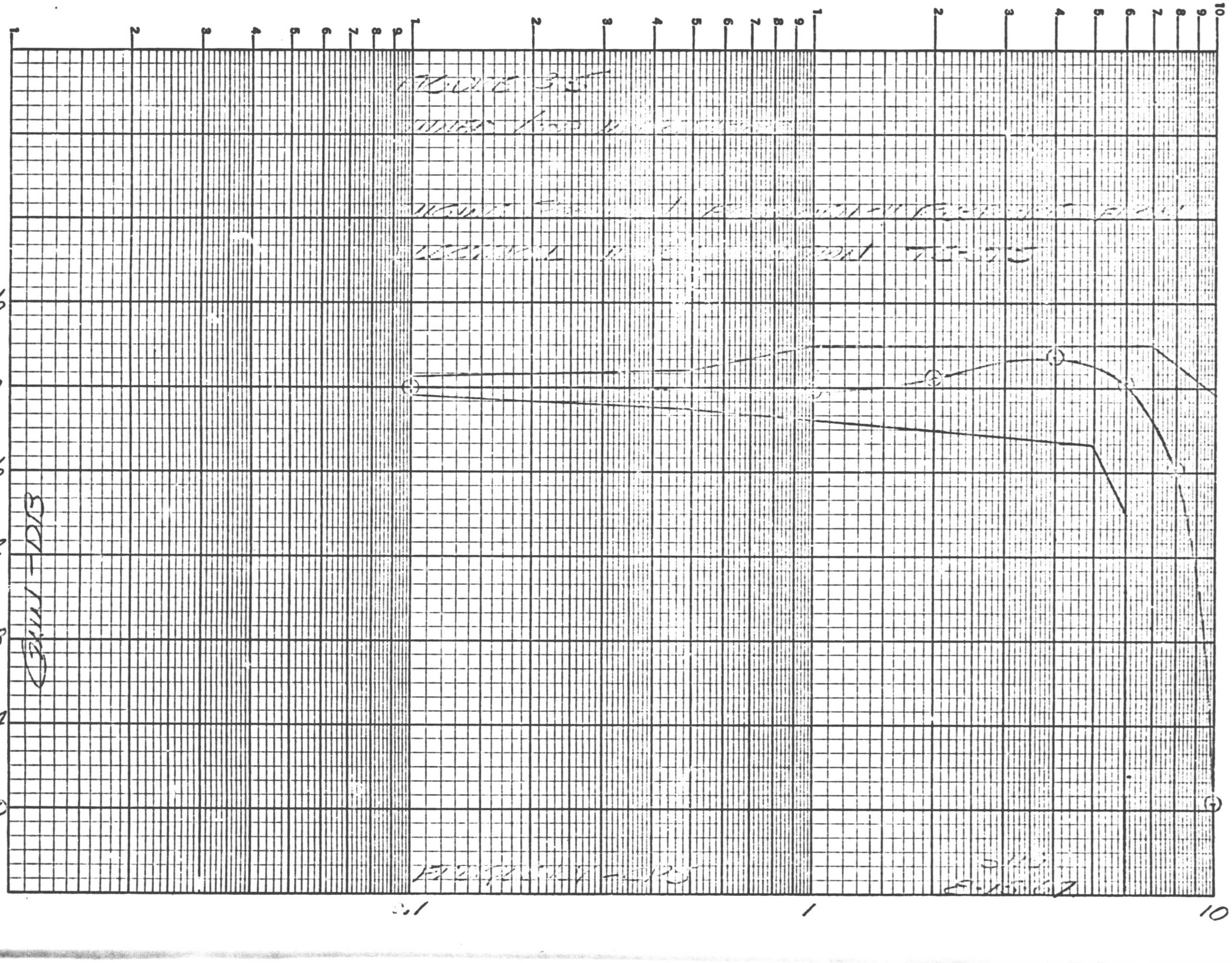
REPRODUCIBILITY OF THE ORIGINAL PAGE IS POOR.



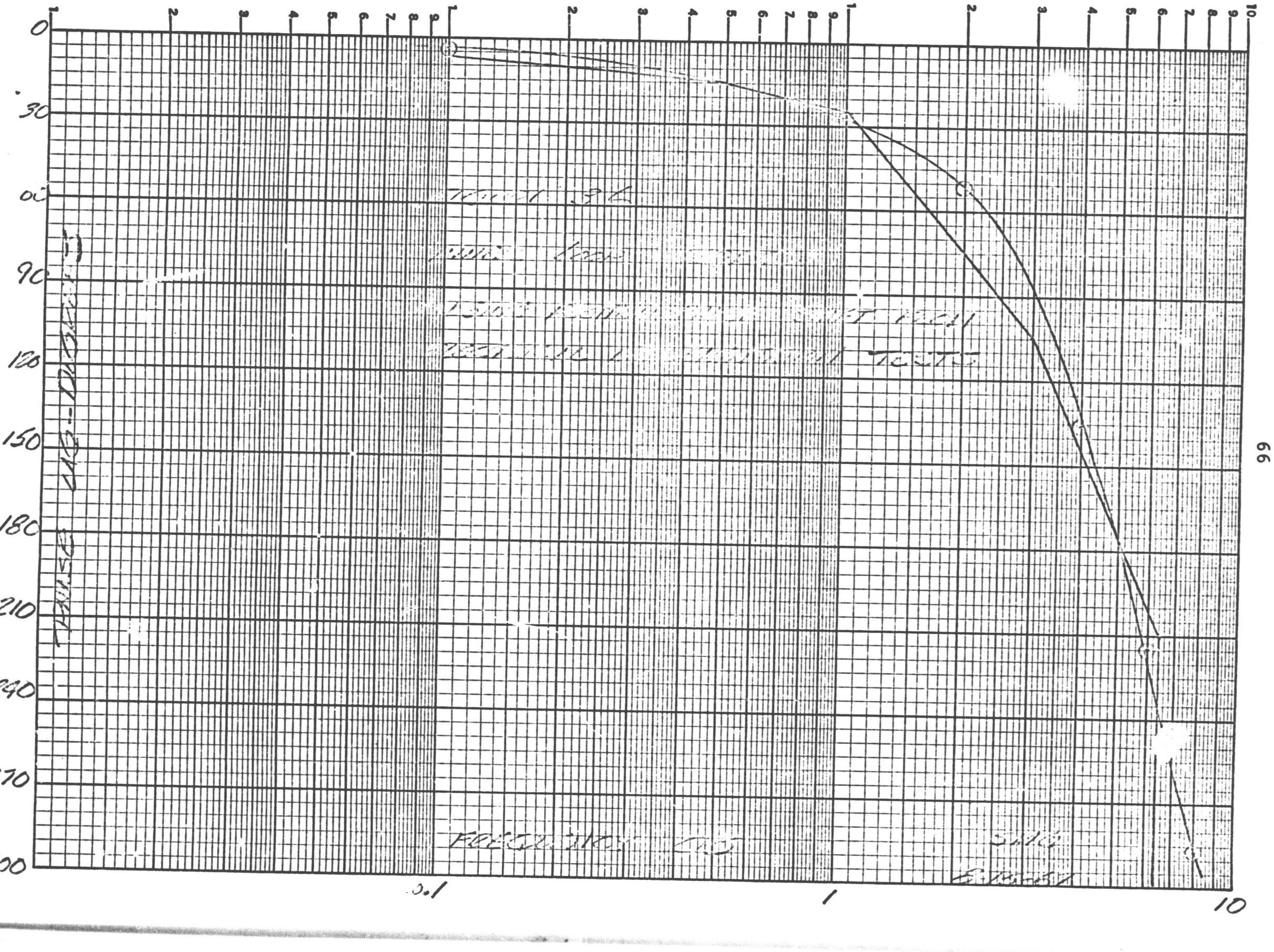


KEUFFEL & ESSER CO.

KEUFFEL & ESSER CO. 537 3 CYCLES X 60 DIVISIONS MADE IN U.S.A.



K+E LOGARITHMIC 6 53
3 CYCLES X 60 DIVISIONS MADE IN U.S.A.
KEUFFEL & ESSER CO.

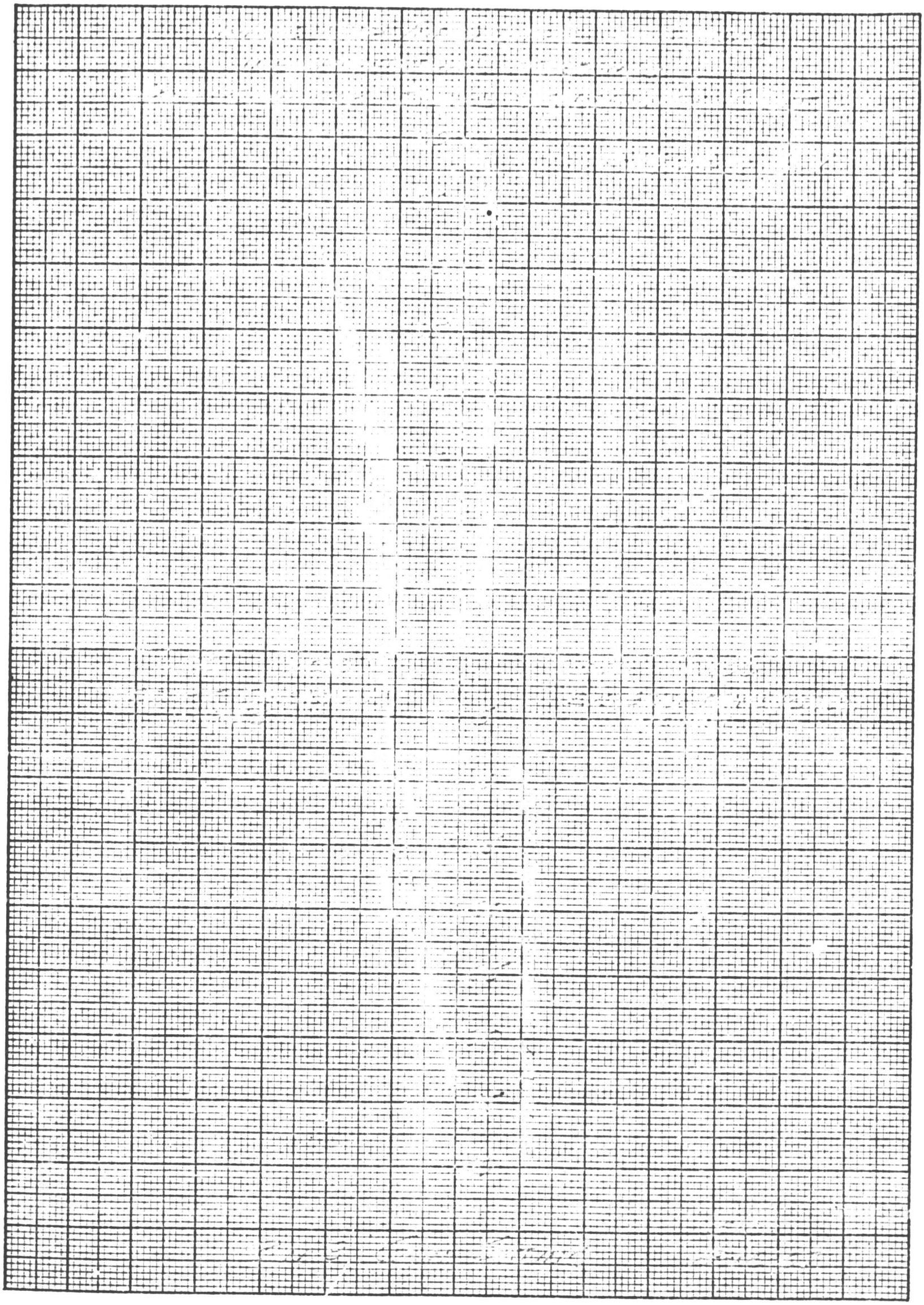



99

HR 73900000

REPRODUCIBILITY OF THE ORIGINAL PAGE IS POOR.





10 X 10 TO 1/2 INCH
7 X 10 IN. • ALBANENE
KEUFFEL & ESSER CO.

# 3.0 DESIGN AND FABRICATION

## 3.1 Initial Design Concepts

This discussion refers to the initial mechanization design concepts illustrated in Figure 9 of HR&M Proposal 73400170. When these preliminary sketches were executed, design concepts were still in the general case and not applicable to a specific actuator. Consequently, assumptions were made that the maximum travel of each input would be short relative to the wobble-plate length and the three legs of the wobble-plate would be of equal or near-equal length. The resulting mechanization concepts shown do, in fact, illustrate the wobble-plate legs of equal length. Suspension is achieved by S-shaped leaf springs. Angular motion between the wobble-plate and the power spool axis is accomplished by flexure of a wire drive system. Coupling between the input pistons of the wobble-plate is achieved by a cone and pin arrangement. This configuration is simple to manufacture, exhibits low friction characteristics, and compensates for misalignment and changes in lever arm length. Assembly and installation are also relatively simple. The combination of wobble-plate suspension and S-shaped springs provides insensitivity to shock and vibration.

## 3.2 Implementation

For purposes of this study program, HR&M hydraulic servo actuator, Part No. 1052350, was selected as the vehicle to demonstrate the innerloop integrator

concept. Mechanization of this concept on the subject actuator is illustrated in HR&M Drawing No. 31000020, No change and A change. The following basic design constraints were imposed.

1. The modified unit must fit test fixtures designed for the original actuator.

2. Maximum utilization with minimum modification of existing parts would be observed.

Initial design premises were that the innerloop integrator would be a self-contained unit mounted to the actuator by the four bolts which originally retained the servovalve. Feed-back was to be accomplished by means of a conic cam mounted directly on the actuator output shaft. The original servovalve first-stage assembly and second-stage sleeve were to be used. As a result of sizing studies undertaken as shown in Section 2.0, it was determined that the wobble-plate legs would necessarily be of different lengths. Preliminary design sketches and analysis were coordinated to arrive at the final wobble-plate configuration, which generates gain ratios of 1 to 1.5 for the feed-back cam, 1 to 3.4 for the integrator piston travel, and 1 to 10 for the load pressure sensor piston motion. The stroke requirements of the integrator piston and the feedback input to the wobble-plate resulted in angular rotation of the wobble-plate about its output axis of such a magnitude that the leaf-type support springs and the wire drive concept were no longer applicable. Consequently, these were replaced with a ball joint at the wobble-plate drive rod junction and a relatively rigid drive rod coupling the ball joint to the power spool. In order to retain the cone pin drives of the inputs in

proper alignment with the wobble plate, the leaf type support springs provide an antirotation constraint. Removal of these springs required that a guide pin be added through the wobble-plate and retained in the housing. This design approach requires that the power spool serve as the primary wobble-plate support. In order to minimize bearing load between the spool and sleeve contact surface, the spool lands were made longer than normal practice. Since the power spool is controlled only by the drive rod attached to the wobble-plate and has no integral stops, the added length lands are needed as a safety factor. With lands of conventional length during abnormal transient conditions, it might be possible to open a pressure port to the return cavity of the wobble-plate, thereby overpressurizing and damaging the unit. Long lands preclude this condition.

Actuator differential pressure piston and cylinder assemblies and the integrator piston assemblies were designed as cartridge units for convenience of manufacture and ease of replacement during development test. The cartridge construction also permits minor changes in the wobble-plate leg ratios for the actuator differential pressure and integrator inputs. This would be achieved by making the cylinder axis eccentric to the outside cartridge diameter.

A separate base plate for the servovalve first stage was designed. This houses the first stage filters and orifices and permits a complete subassembly to be adjusted, tested, and installed. The power stage body and wobble-plate housings were designed as

separate components to simplify machining and facilitate assembly. Mechanical clearance requirements dictated the necessity of removing the sample valve components from the filter. The port in the filter body was shortened and modified to an AND 10050 type. The sample valve was replaced by an AN 814 plug. The piston rod was shortened approximately 3/8 in., and new wrenching flats were machined. This permitted mounting of the cone type feedback cam without increasing mounting dimensions of the actuator.

## 3.3 Assembly and Subsequent Modification

Initial assembly indicated that the wobble-plate antirotation pin was not performing its function. A force-centered cone and pin drive such as is used here is essentially a toggle-action mechanism inherently unstable in the center position. As spring preload on the actuator differential pressure pistons was increased, the antirotation pin deflected, allowing the wobble-plate to rotate or toggle so that the cone drive pins exceeded their seating angle and snapped out of their seats. A first modification was undertaken by adding a second antirotation pin and changing to a higher strength material on both pins. This permitted initial pressurization of the unit; however, it was found that addition of pressure forces to the spring preload again allowed sufficient deflection to toggle the cone drive pins out of their seats. In addition, high frictional forces between the plate and pin impeded wobble-plate travel.

A universal joint with a single pin between the pistons was installed on the actuator differential pressure input to the wobble-plate. This universal joint allows rotation in two planes and compensates for changes in lever arm length. After assembly of the unit with this modification, no further tendency to unseat cone and pin was observed.

Direction reversals of the actuator showed improper follow-up, and dead-band effects. It was found that the follow-up problem was created by deflection of the power spool drive rod sufficient to cause the ball joint outer spring seat to rub against the housing bore. As the integrator piston reversed direction, the power spool drive rod deflected from one side of the housing bore to the other. The basic cause of this action was toggling of the integrator cone drive pins under hydraulic pressure force. The dead band effects were in the position feedback linkage. This was designed as an opposing spring mechanism which allowed a 2 to 1 stroke reduction of the feedback ratio at the wobble-plate. This approach was taken in order to use a high cam angle. Unfortunately, this mechanism inherently has a low force output at small displacements of the wobble-plate relative to the feedback arm. Since frictional and flow force on the wobble-plate joints and power spool was high, large relative displacements between the feedback arm and wobble-plate were required. This had the effect of creating a dead-band between the feedback arm lever and the power spool motion. A second universal joint was installed at the integrator piston input to rectify the follow-up problem. Dead-band effects were minimized by installation of a spacer in the spring guide and removal of

one spring on the feedback input linkage. This allowed a direct connection to be made between the feedback cam and the wobble-plate through the feedback arm, and changed the function of the remaining spring to that of a load spring. This spring now serves the function of removing slack from the feedback linkage. A new cone cam was fabricated for installation on the piston rod, with a cam angle one-half that of the original. This was required in order to preserve integrity of the feedback gain selected for the first design.

## 3.4 Mechanization, Comments and Recommendations

The innerloop integrator would normally be part of the original design of a production actuator package requiring high static stiffness. The feedback mechanism would be internally housed, and the design should be a type where piston rod motion due to radial bearing clearance is not transmitted through to the wobble-plate. Wobble-plate ball joint should be as close as practical to the end of the spool, with the drive rod of a large diameter in order to increase rigidity and provide wobble-plate support. Depending on the particular unit design parameters, it might be advisable to add a third universal joint to the wobble-plate at the feedback input. By means of integral design, the wobble-plate configuration could be improved in order to optimize package envelope. This would also achieve a significant weight reduction. On a production unit, it would also be desirable to redesign the piston cartridges to reduce size of the hardened steel sleeve

and retain it with an aluminum cap. This again would provide a noticeable weight reduction. The cylinder differential pressure load spring adjustment and feedback spring adjustment could be eliminated. Initial adjustments of the unit would then consist of the following.

1. First stage servo calibration as a subassembly,

2. Centering of the feedback cam relative to actuator output rod stroke, and,

3. Null adjustments of the power spool relative to the wobble-plate, with the actuator rod centered and servo inputs at center.

Again, trade-off studies may be undertaken in order to reduce complexity and weight. For instance, Items 2 and 3 might be combined in a single adjustment.

# 4.0 ASSEMBLY AND TEST PROCEDURES

## 4.1 Assembly and No-Load Test Procedures

The first stage servovalve was removed from the 2-stage servovalve, HR&M P/N 241000, received with servo-actuator, HR&M P/N 1052350 SN 018. This was assembled to a base plate P/N 3100008 containing the 1st-stage filters and orifices to form the servovalve sub-assembly P/N 31000029. Flow and pressure gain tests were performed and 1st-stage flow gain was calibrated.

The power spool was flow-ground to establish a line-to-line lapping condition between the spool and sleeve assembly (P/N 31000055).

The modified piston (P/N 31000062) was installed in the actuator body. Potentiometer null was aligned with the mechanical null of the actuator by measuring the total piston stroke between snubber contact and then setting the minimum value of wiper to center tap resistance at the midpoint of this dimension. This null adjustment could be in error by a distance equal to one-half the difference between each snubber's travel. Since this error would have no effect on performance, it was not considered critical.

Assembly of the inner loop integrator feedback and power spool package subassembly, P/N 31000021, was accomplished by reference to assembly dwg 31000020, Rev B and PL 31000020, Rev B. This was then bolted

The outer electrical position loop was closed using an Industrial Measurements Corp. servo amplifier, model 914 A as shown in Fig. 38. A H.P. Model 202 A function generator was used to supply input command. External positive load pressure feedback was not connected since these tests were accomplished without an inertia load with which to develop significant load pressure. Command and position voltage were plotted against each other on an X-Y recorder. The function generator was set to produce a triangular wave of 0.01 cps with an amplitude adequate to yield 90 percent of full-stroke actuator travel. Linearity and hysteresis plots were made with supply pressure as a parameter. The actuator was positioned at the extreme ends of its stroke to observe its operation in the snubber regions.

## 4.2 Tests with Inertia Loads

The HR&M load simulator was set to provide an inertia of 0.291 slug $ft^2$ (107.5 lb $\frac{sec^2}{in.}$) and a structural spring of 275,000 lb/in. The inner loop integrator actuator was then mounted on the simulator. The load differential pressure transducer and d-c amplifier were calibrated to give 5 vdc output with supply pressure at 3000 psig and the actuator bottomed at either end. Position and load pressure feedback loops were closed as shown in the test schematic, Fig. 38. Data traces were taken of function generator output, servo current, load pressure, supply pressure, actuator position, and engine position. Position traces were calibrated by reference to a dial indicator placed between the

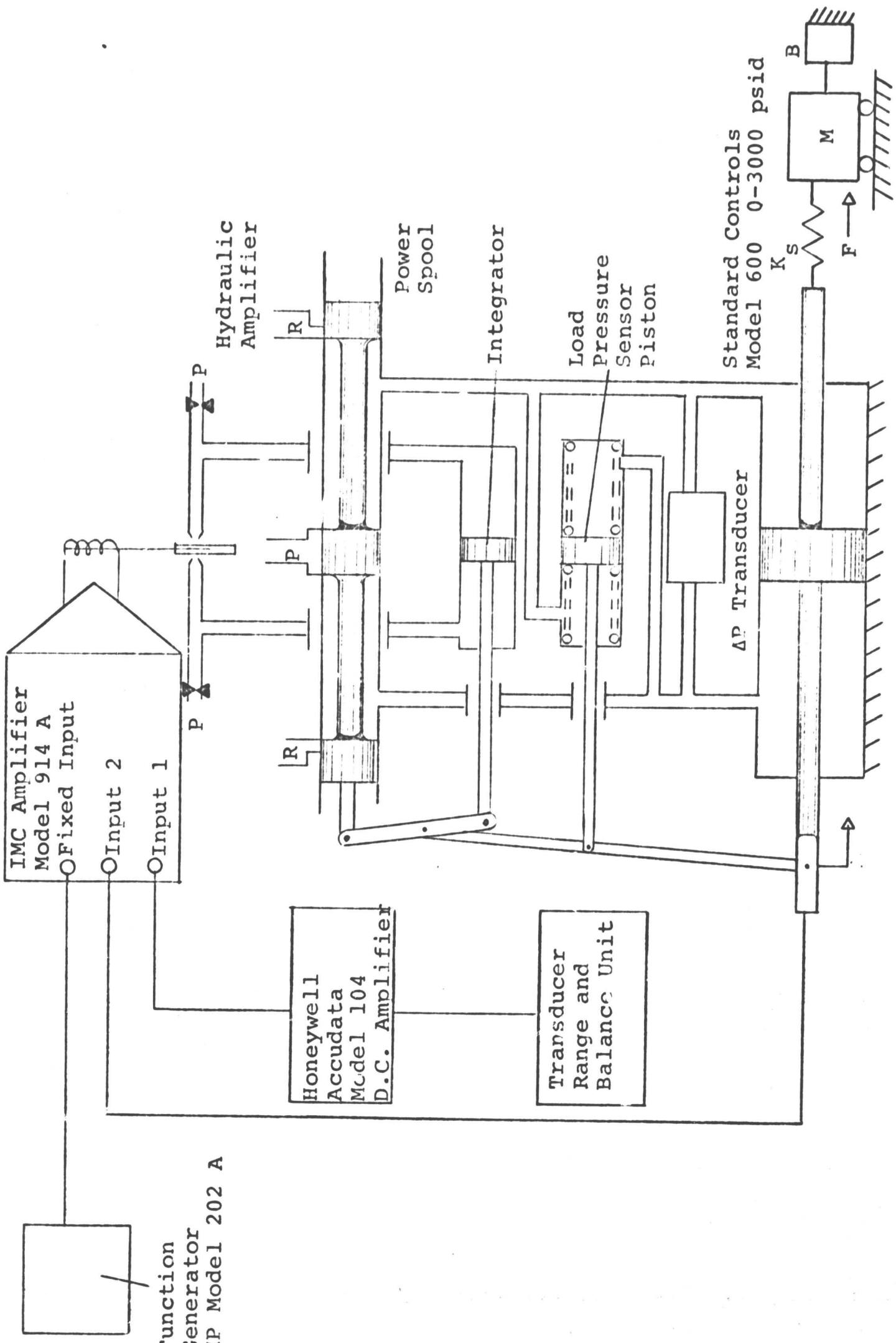



Figure 38. Inner Loop Integrator Test Schematic

to a mating test block. It was then installed on a flow bench capable of supplying 3000 psi oil, MIL-H-5606, to permit adjustment of the power spool null.

The integrator piston sleeve, P/N 31000028, and end caps, P/N 31000027 were removed. The integrator centering springs, P/N 31000026, were replaced with solid rods in order to lock the integrator piston, P/N 31000025, in its approximate center position. The end caps were reinstalled. The power spool rod access cap, P/N 31000032, and bottom cover plate, P/N 31000022, were removed. Supply pressure was adjusted to 500 psig. The two AN340C2 (2-56 UNC) nuts were adjusted on the power spool valve rod, P/N 31000058, until a no-flow condition existed and the springs, P/N 31000039, compressed the ball, P/N 31000036, and seat, P/N 31000037, without binding. The bottom cover plate was reinstalled and this subassembly was bolted to the actuator subassembly, P/N 1052352 and PL 1052350. The assembled inner loop integrator servoactuator was connected to a MIL-H-5606 oil supply variable from 0 to 3000 psig. A voltage $\pm$ 22 1/2 vdc was connected across Element 2 of the feedback potentiometer. Pressure was set at 500 psig and the AN3CH3A machine-bolt was adjusted on the feedback spring compressor until the wiper to center-tap voltage was minimum. The power spool rod access cap was replaced and the null adjustment was verified at 3000 psig. Integrator piston centering rods were removed and the centering springs reinstalled.

actuator body and the simulator "T" bar inertia beam at the actuator attach point.

Supply pressure was adjusted to 3000 psig and function generator output was set for a triangular wave of 0.01 cps, with an amplitude sufficient to create actuator travel of 0.250 in. peak-to-peak. Amplifier "input 2" gain was adjusted by iteration to provide satisfactory response to a step input. A static force of approximately 15,000 pounds was applied to the load. The "input 1" gain was adjusted until engine position deflection created by this force was negated. Frequency and step response data were taken both with and without this load pressure feedback compensation. Amplifier gain levels were recorded.

## 4.3 Load Force Tests

The actuator was installed on the HR&M load simulator as in Section 4.2. The function generator was disconnected so as to maintain position at null. Positive load pressure feedback at "input 1" of the I.M.C. servo amplifier was disconnected. With supply pressure at 3000 psig, extend static load force was incrementally increased to approximately 75 percent of maximum value. Actuator and engine position deflection was recorded. This load force was gradually decreased and then reapplied in the retract direction in order to define any mechanical hysteresis. This procedure was repeated with the load pressure feedback signal connected to "input 1" of the servo amplifier. For each case, plots were made of applied load force versus engine and actuator deflection.

With the inner loop integrator actuator still in the load simulator, an S1-C actuator HR&M P/N 301100 S/N 057 was installed, as shown in Fig. 39. Fig. 40 shows the two actuators at their attach points in relation to the inertial beam support bearing. Fig. 41 illustrates the integrator actuator with the S1-C actuator in the background. A load pressure ΔP transducer was connected across the cylinder ports of the S1-C actuator. Supply pressure was set at 2500 psig due to design limits of P/N 301100. Commanded position of the integrator actuator was adjusted until negligible load pressure was observed on either actuator. A sinusoidal load force of approximately 10,000 pounds peak-to-peak was applied to the P/N 31000020 actuator by commanding position of the S1-C actuator and monitoring its load pressure. Data were taken to determine load force frequency response of the inner loop integrator actuator, with and without positive load pressure feedback.

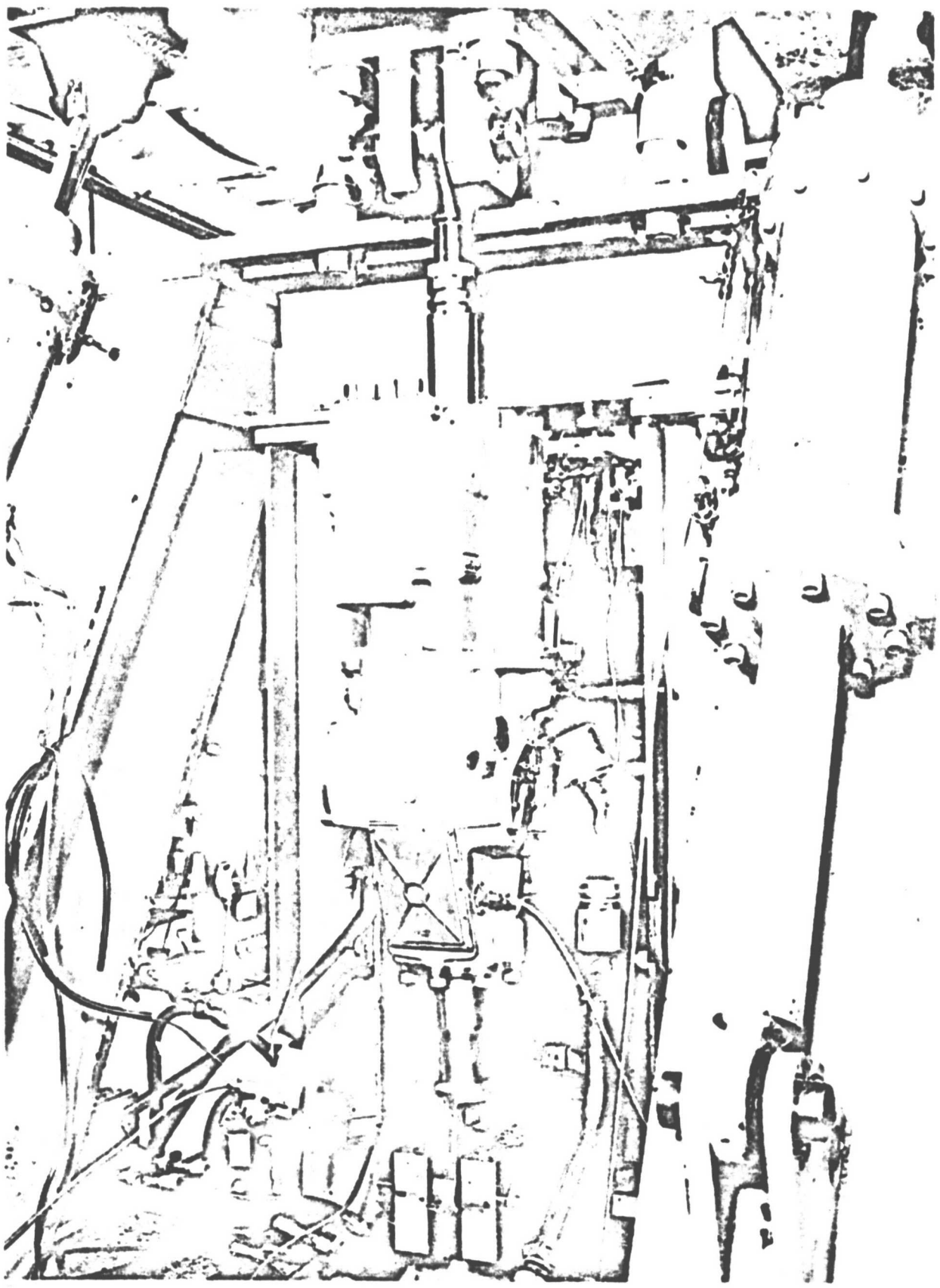
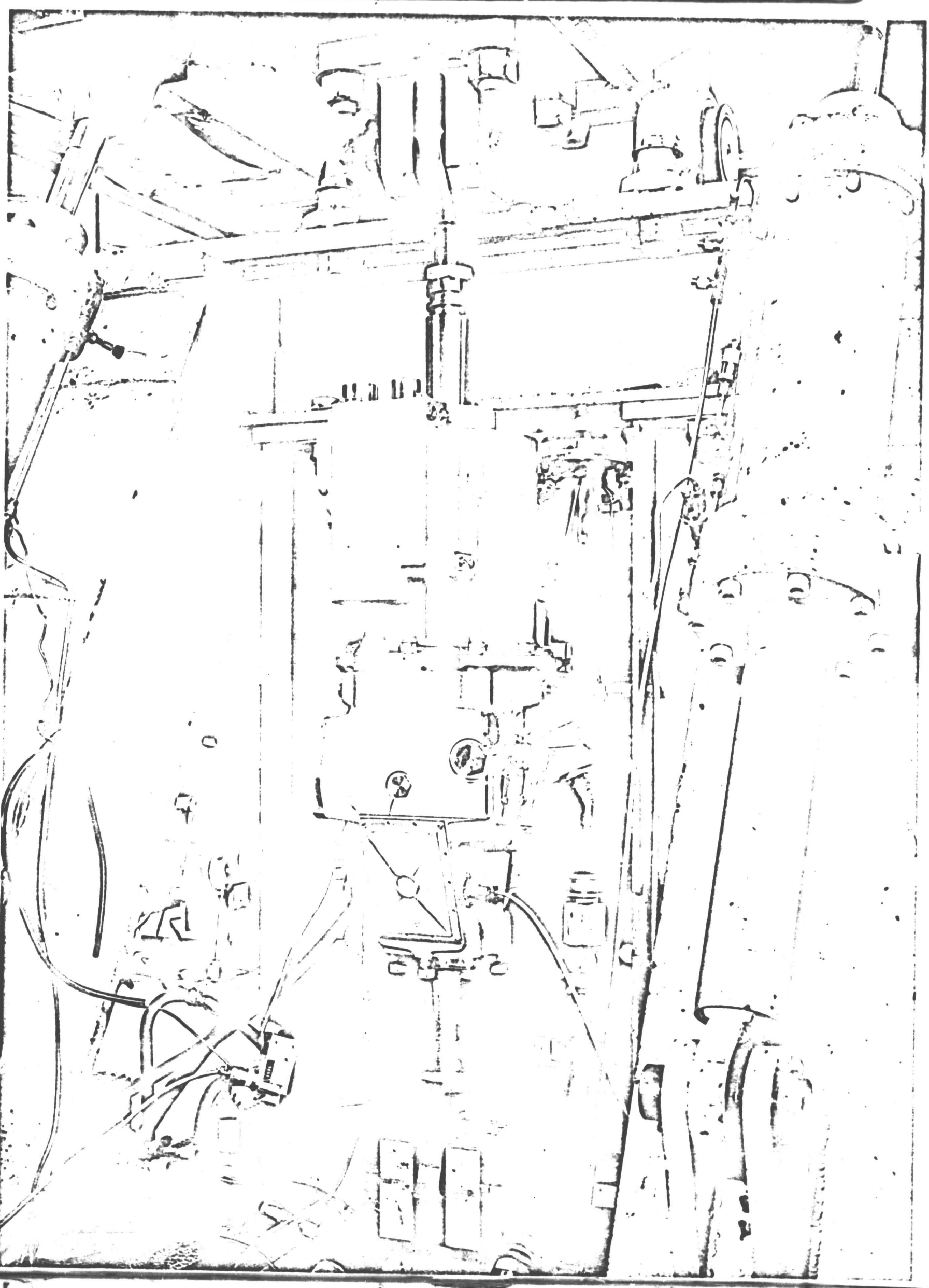
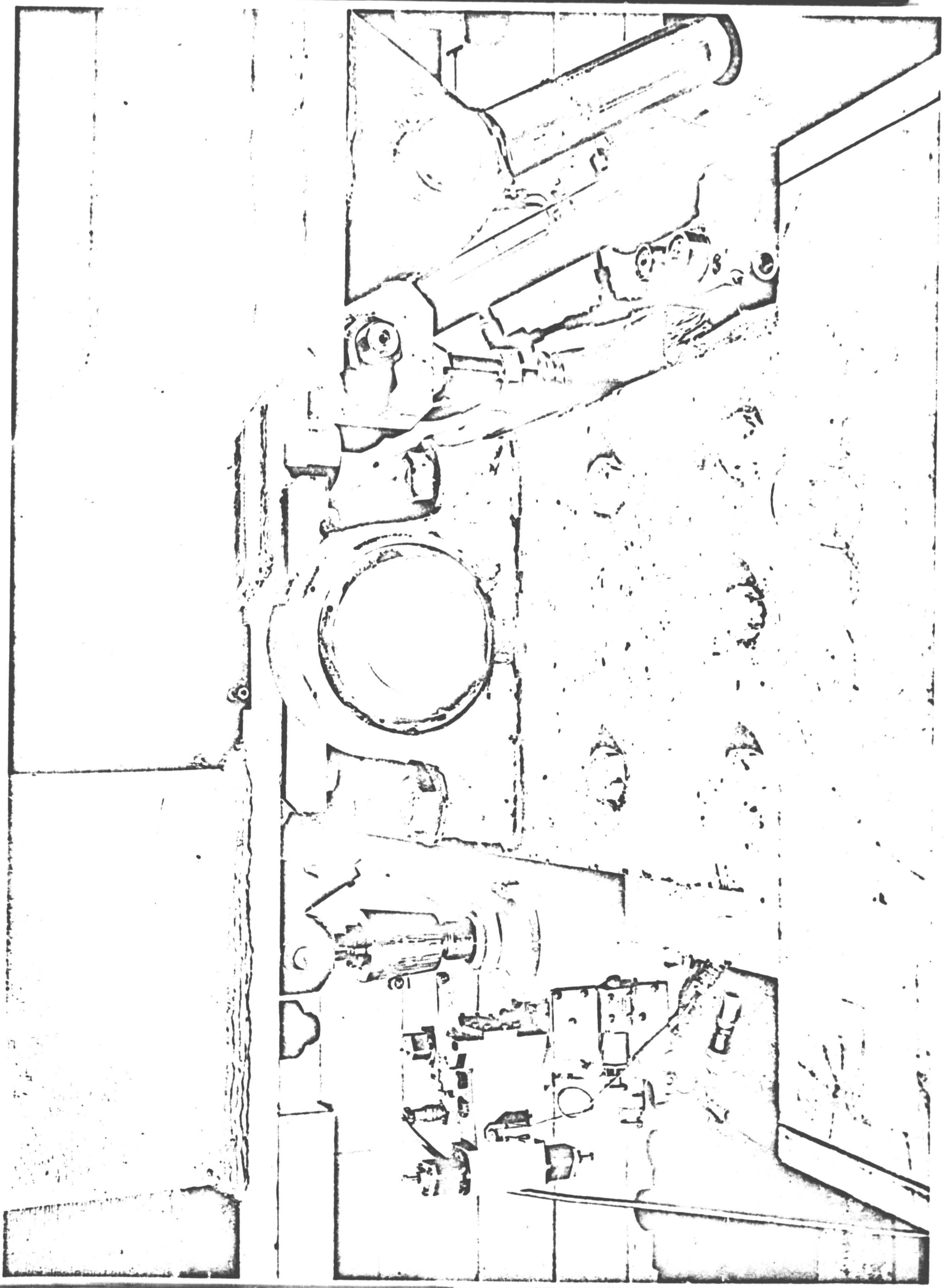


Figure 39. S1-C Actuator P/N 30110
S/N 057 On Load Simulator

REPRODUCIBILITY OF THE ORIGINAL PAGE IS POOR.



REPRODUCIBILITY OF THE ORIGINAL PAGE IS POOR.



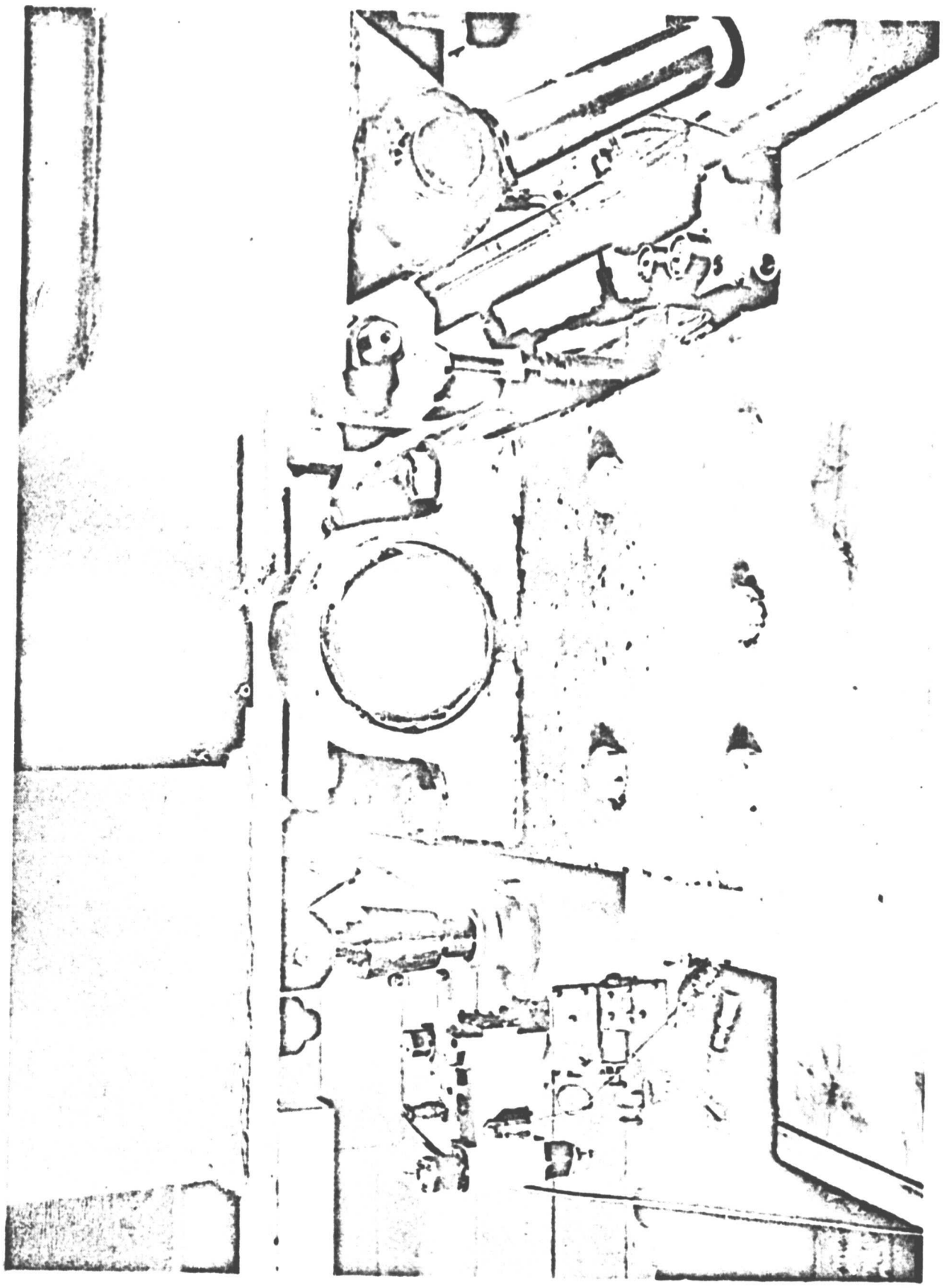
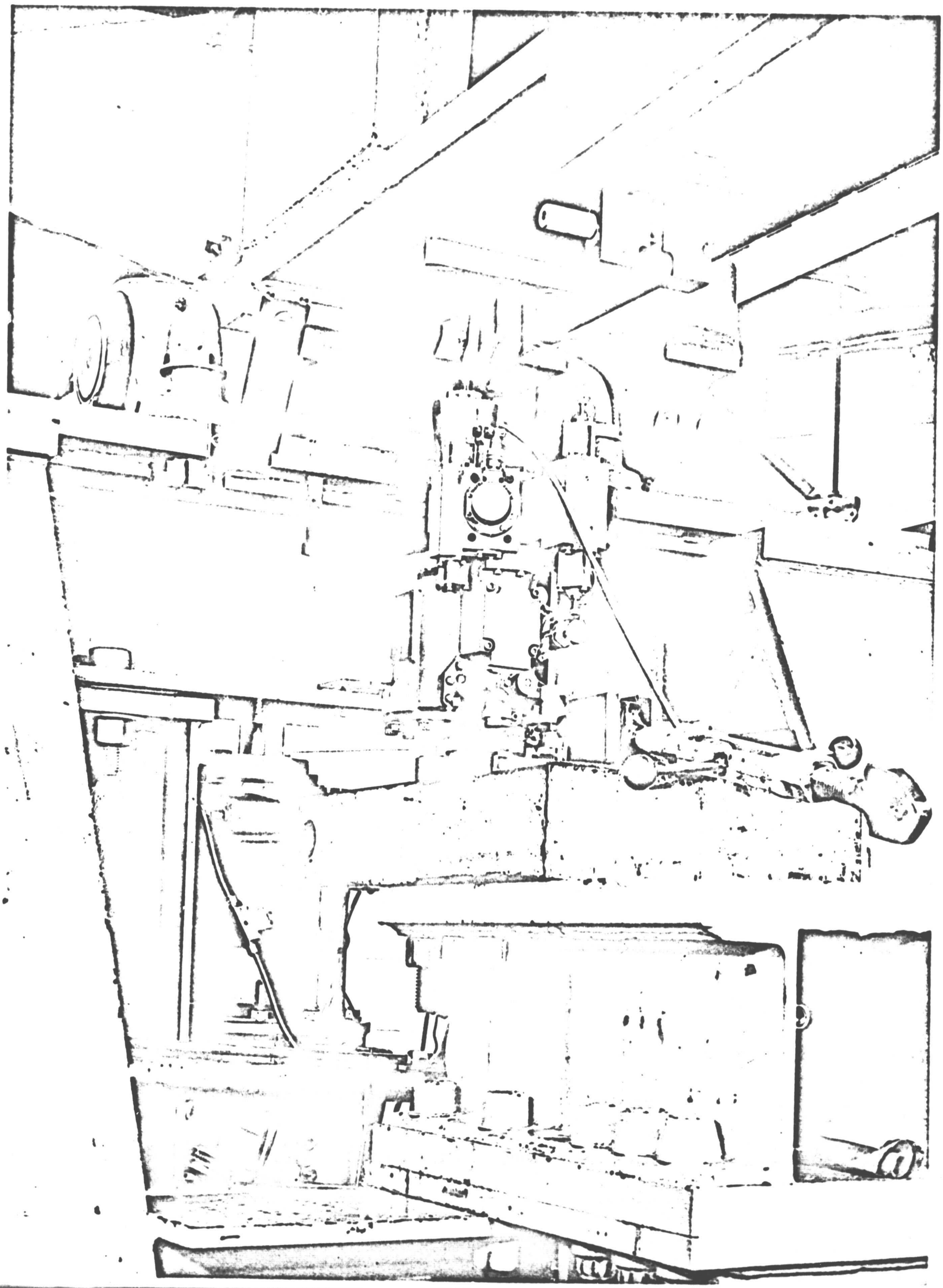


Figure 40. Inner Loop Integrator and Sl-C Actuators in Relation to Simulator Inertia Beam Bearing



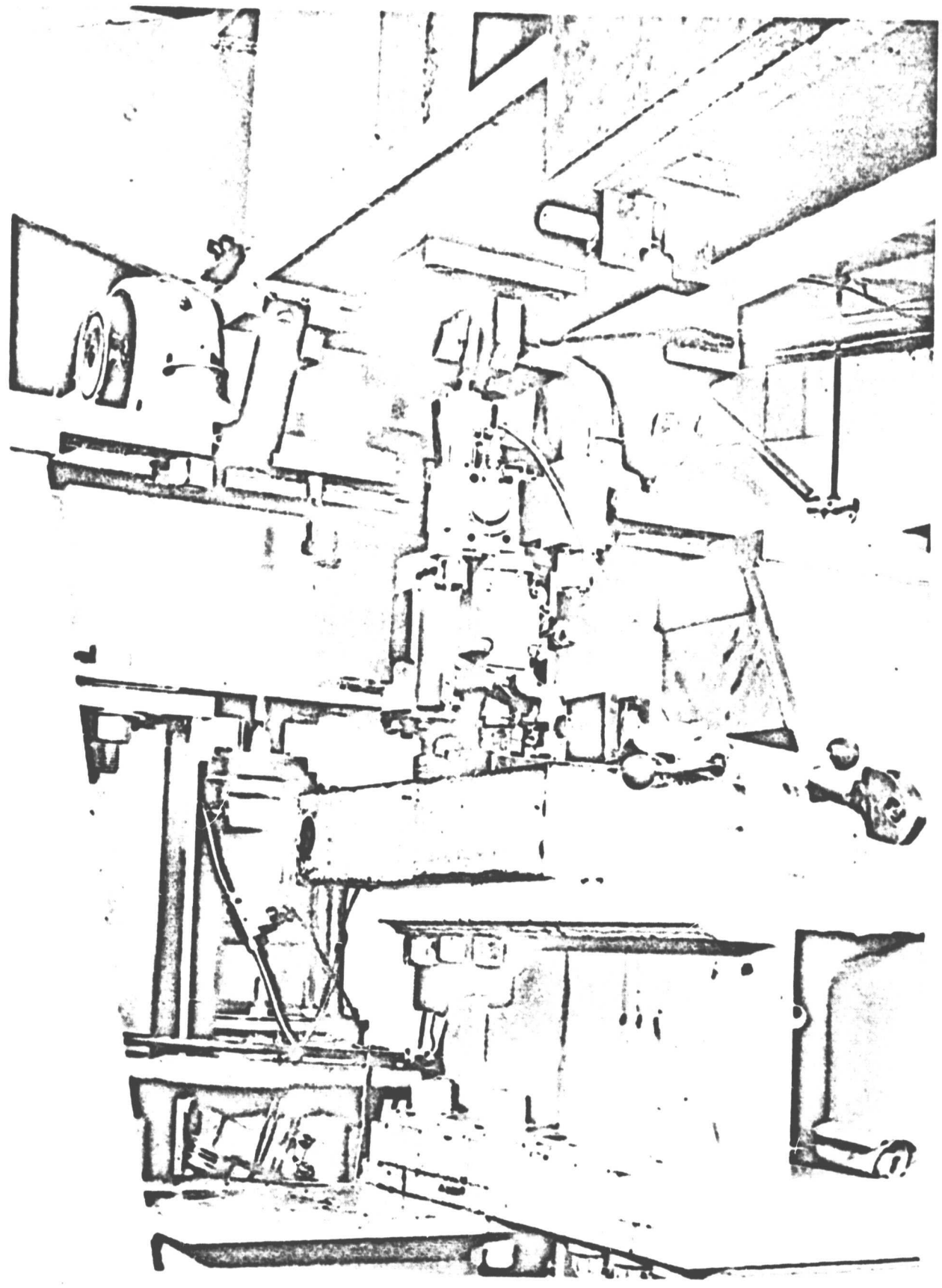


Figure 41. Inner Loop Integrator Actuator on Load Simulator

# 5.0 DISCUSSION OF RESULTS

## 5.1 Subassembly and No-Load Tests

Calibration and adjustment of the first-stage servo-valve assembly, P/N 31000029, indicated that serious limitations existed in its linear operating range. Fig. 42 shows the occurrence of a factor0of-11 change in flow gain at approximately 3 ma, with complete saturation apparent by 10 ma. The blocked port pressure gain shown in Fig. 43 is linear over the entire 24-ma current rating. Attempts to adjust flow gain for a linear characteristic over the desired 24-ma current range were not successful, due to basic sizing design limitations of this valve. Spring rates, nozzles, and orifices were originally chosen to yield a linear pressure gain that would permit positioning of a 2nd-stage spool. In the present application, negligible load pressure is required to move the integrator piston of P/N 31000020, but its rate of travel is proportional to flow. Consequently it would be desirable to redesign the first stage to obtain flow linearity.

It was anticipated the 1st-stage problem could be reflected in the actuator dynamic performance, and not in the static-stiffness characteristics. Due to program limitation and the ease with which the valve may be replaced, it was decided to proceed without redesign.

Fig. 44 shows the no-load linearity and hysteresis plots for supply pressures between 500 and 2500 psig

REPRODUCIBILITY OF THE ORIGINAL PAGE IS POOR.



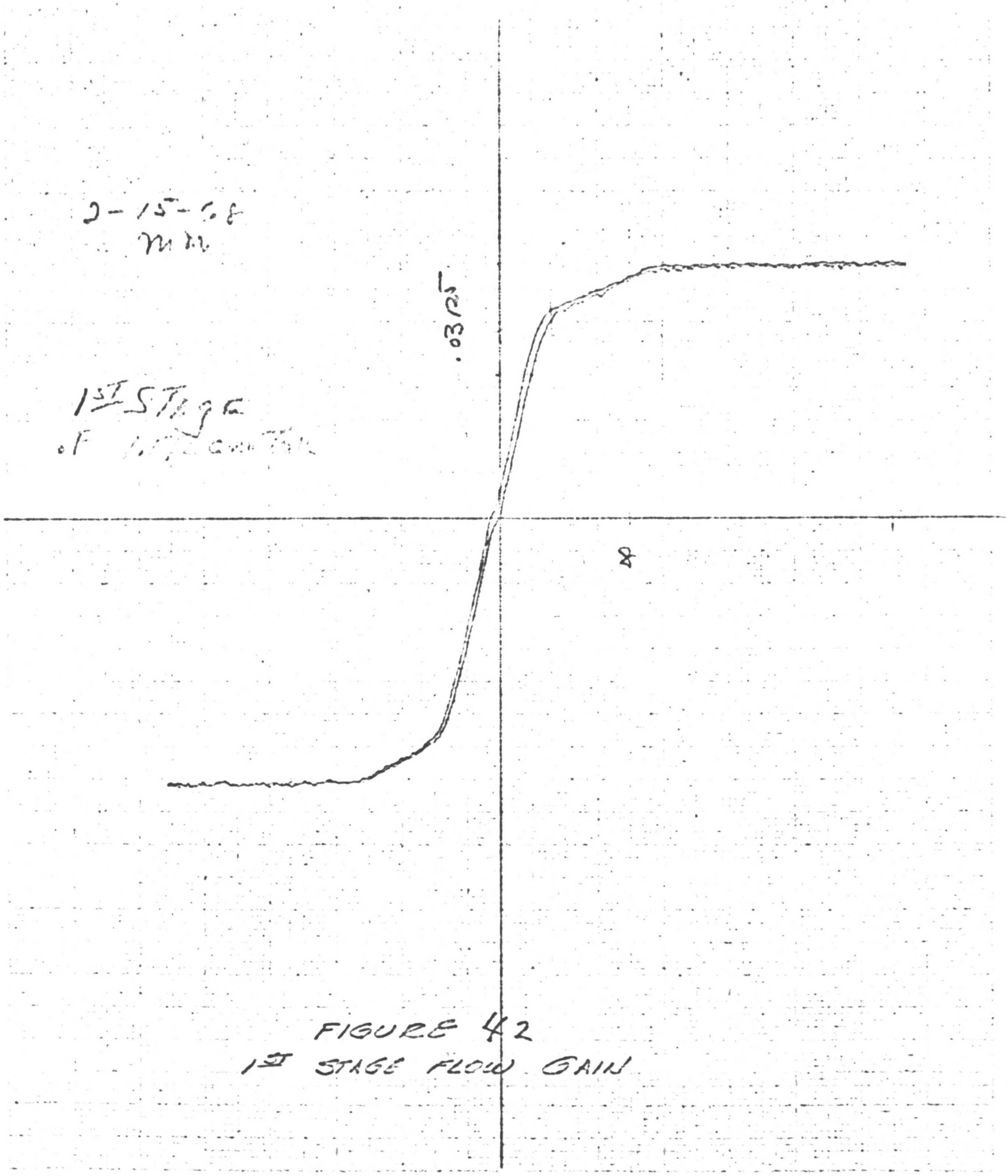



FIGURE 42
1ST STAGE FLOW GAIN

24/1000

3000

1-25-GF
Mil

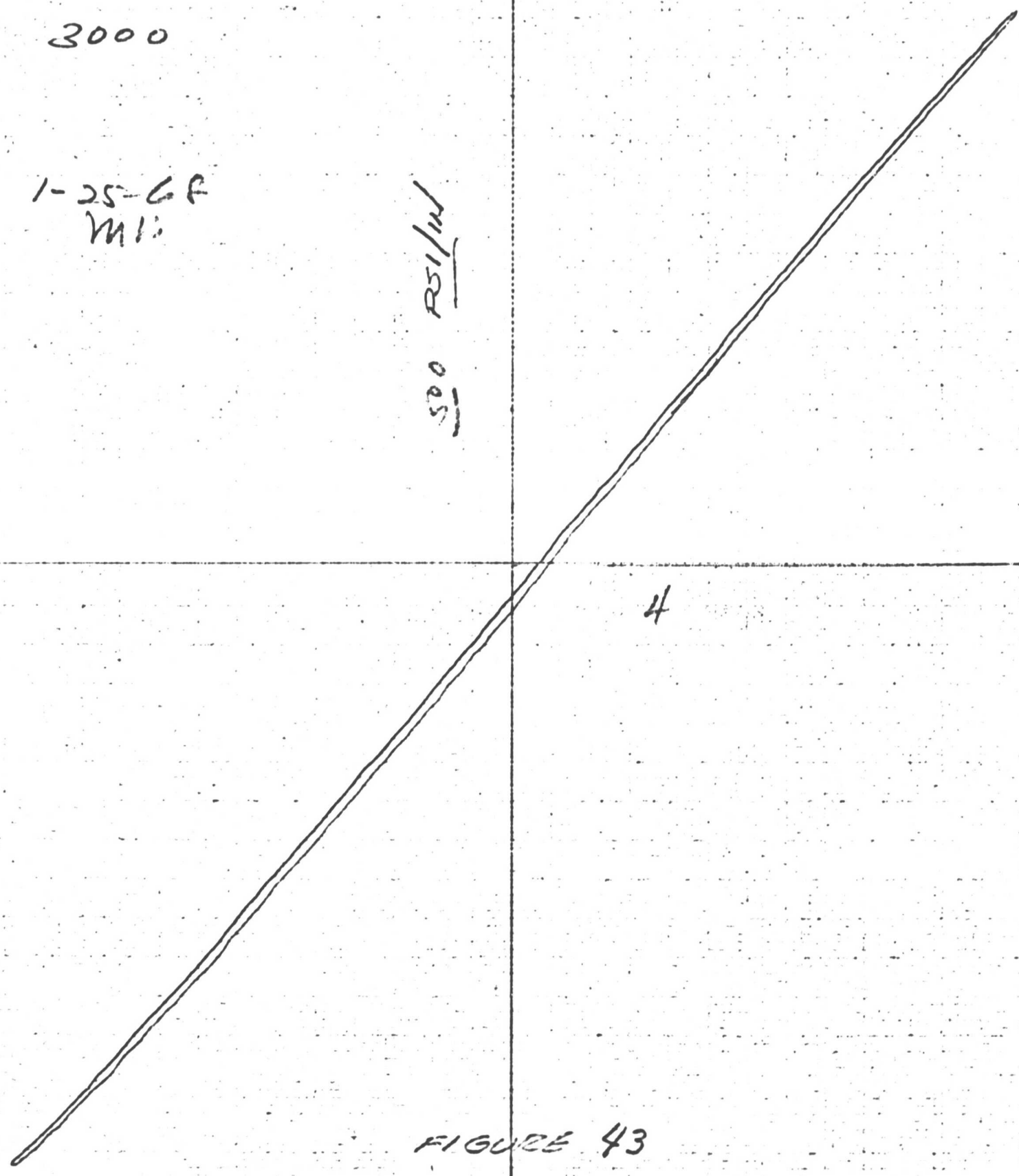


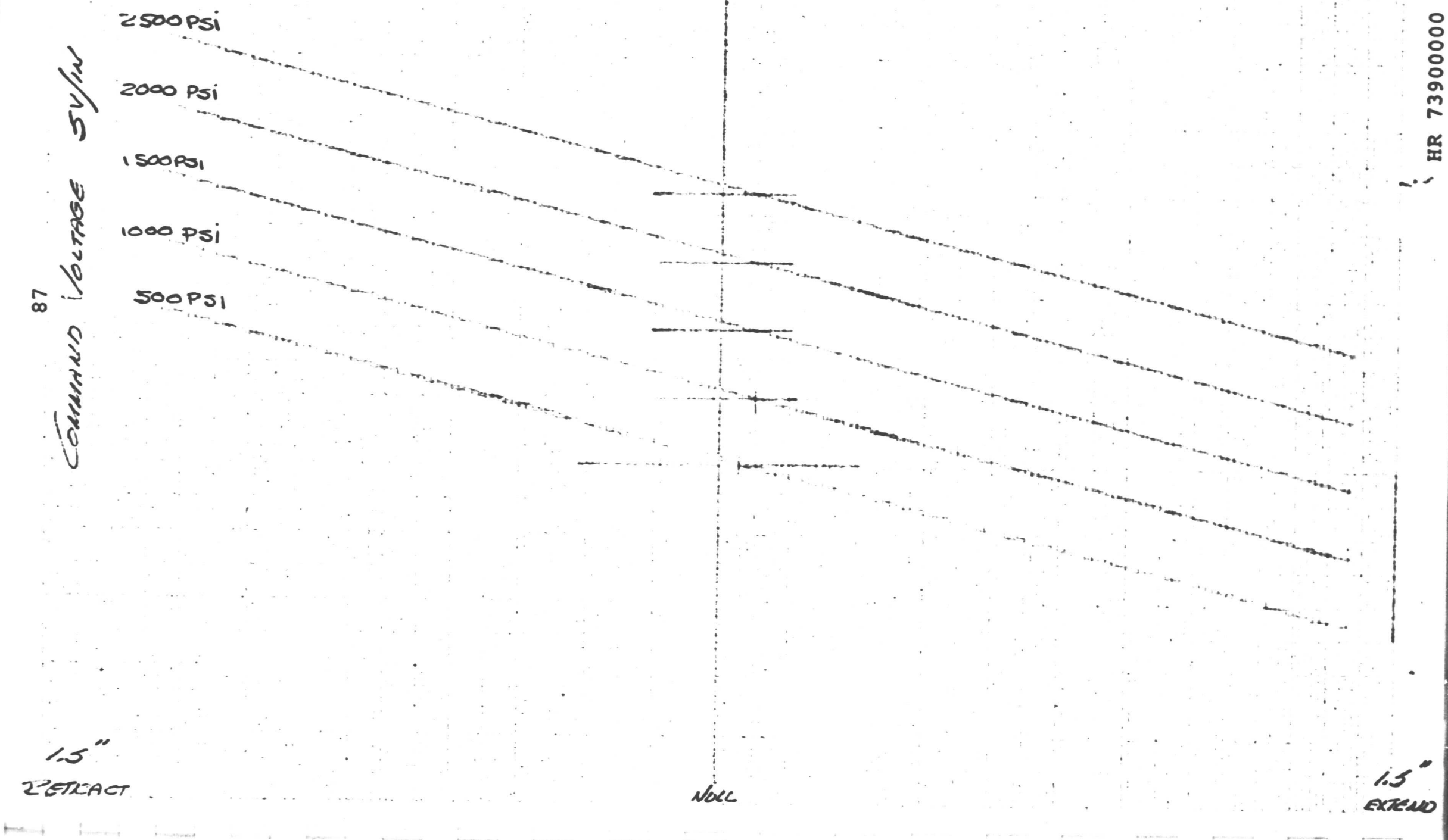

FIGURE 43

1ST STAGE BUCKED PORT
PRESSURE GUN

REPRODUCIBILITY OF THE ORIGINAL PAGE IS POOR.

INNER LOOP INTEGRATOR - P/N 31000020
NO LOAD HYSTERESIS 2-23-68

FIGURE 4.4



in 500-psi increments. A 3 percent null shift is apparent between the 500-psi plot and subsequent pressures. Above 500 psi, hysteresis is obscured by the width of the recorder pen. The plots were taken by commanding position of the actuator with a triangular input. It can be observed that disturbances from the peak of the wave cause lightly damped ringing. This was also observed during initial tests on the load simulator. It was found that increasing the preload on the springs at the "Y"-bar ball joint decreased damping. There apparently was a relative motion between the power spool and "Y"-bar linkage under dynamic conditions. This was caused by a restriction in the flow of oil from the cavity on the pin end of the power spool rod. A groove had been provided in the valve rod, P/N 31000058; however, it appeared inadequate. An "A" change on the rod provided flats to increase flow area and eliminate the problem. A 10-lb spring preload is recommended in order to negate flow forces on the power spool.

## 5.2 Simulated Load Tests

Simulated load tests were conducted on the HR&M load simulator as described in Section 4.3. Positive pressure feedback can be employed to compensate for structural deflection. This in essence has the effect of causing the inner loop integrator to "grow" in length against a static load. Tests were conducted both with and without this feedback. The reduced data shown in Fig. 47 through 54 show that almost no change was observed in dynamic characteristics. However, the raw data with positive pressure feedback exhibited a limit cycle approaching 0.030 in., peak-to-peak. This is due to mechanical hysteresis of

approximately 0.010 in., combined with bearing and rod-end play approaching 0.025 in., as seen in the static sensitivity plot of Fig. 45.

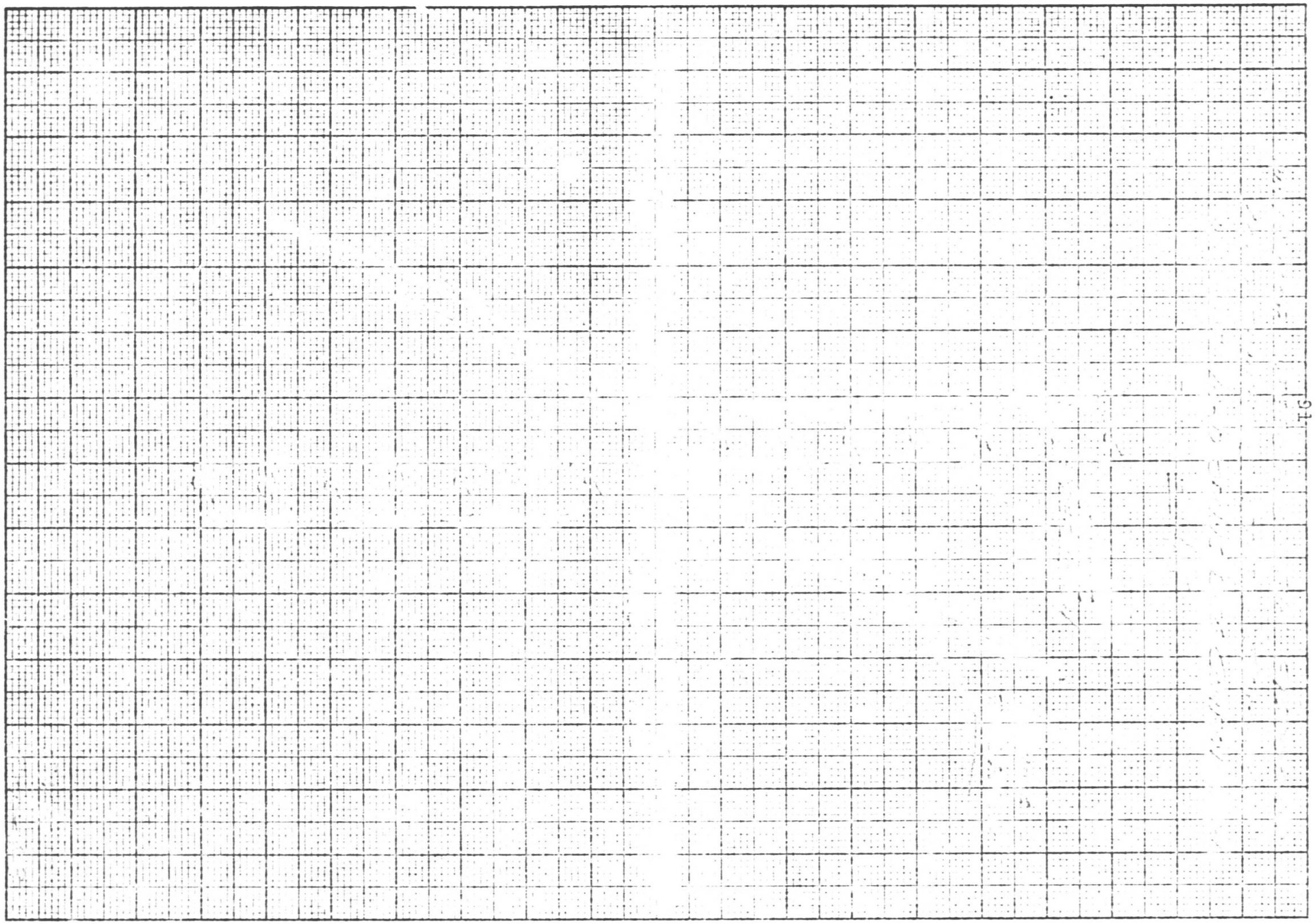
Figs. 45 and 46 show the static sensitivity of the inner loop integrator actuator without and with positive load pressure feedback respectively. In Fig. 45 it can be seen that, within instrumentation accuracy, there is virtually no actuator deflection with static loads to 75 percent of rated capacity. The static sensitivity of the inner loop integrator with load spring compensation, shown in Fig. 46, indicates that with static load forces up to 75 percent of rated capacity, the engine deflection is of the same order of magnitude as the mechanical hysteresis of the load simulator. The null shift of approximately 0.020 in. is the result of d-c bias in the pressure feedback amplifier, and can be minimized.

Amplitude response curves of Figs. 47 and 49 show little comparative change resulting from positive pressure feedback. In both cases, the actuator appears underdamped with approximately 5 db peaking at 2 cps. A secondary peak occurs at the load resonance of 7 cps. The corresponding phase shift curves of Figs. 48 and 50 indicate that phase lag is marginally within the desired performance band up to about 3 cps. The step response of Fig. 51 shows excessive delay from the instant of commanded motion to the commencement of (simulated) engine motion, along with overshoot approaching 63 percent. Damping is low, and the second overshoot is also out of bounds. This is in agreement with the amplitude response discussed previously. The

load force frequency response curves, $\frac{AP_L}{F}$, of Figs. 53 and 54 exhibit approximately 18 db peaking at the 7 cps load resonance. This is approximately 6 db higher than anticipated from the simulation and may be attributed to first-stage gain saturation. The position, $\frac{X_5}{F/k_5}$, amplitude response of Fig. 54 shows a +6 db slope in the low frequency region, which is characteristic of infinite load static stiffness. Peaking at the load resonance is 9 db above the anticipated level.

The amplitude response derived from P/N 31000020 actuator test data is compared with that resulting from hybrid simulation tests and response predicted from linear analysis in Fig. 55. The actuator data exhibit a double peaking characteristic similar to that from linear analysis, with a greater spread between the frequencies at which peaking occurs. Attempts to correlate this in terms of loop gains were not informative. Fig. 56 compares the step response from actuator tests with the results of hybrid simulation tests. The delays of response and rise times are similar and expected, as discussed in Section 2.5.

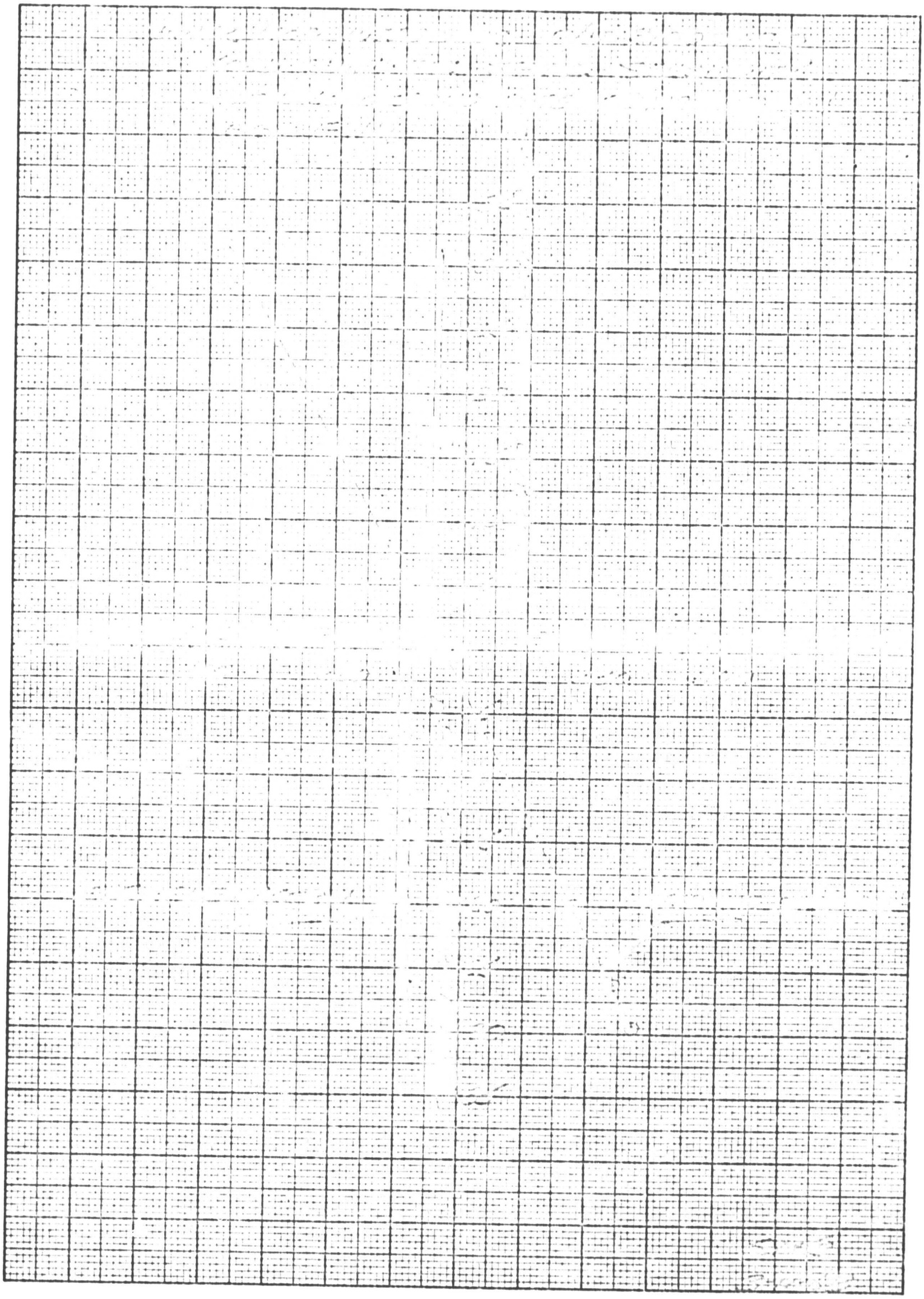
K+E 10 T[illegible]INCH 46 1[illegible]
7½ X 10 IN. • ALBANENE® MADE IN U.S.A.
KEUFFEL & ESSER CO.



HR 73900000

REPRODUCIBILITY OF THE ORIGINAL PAGE IS POOR.





KEUFFEL & ESSER CO.
7½ x 10 IN. • ALBANENE® MADE IN U.S.A.
HR 73900000

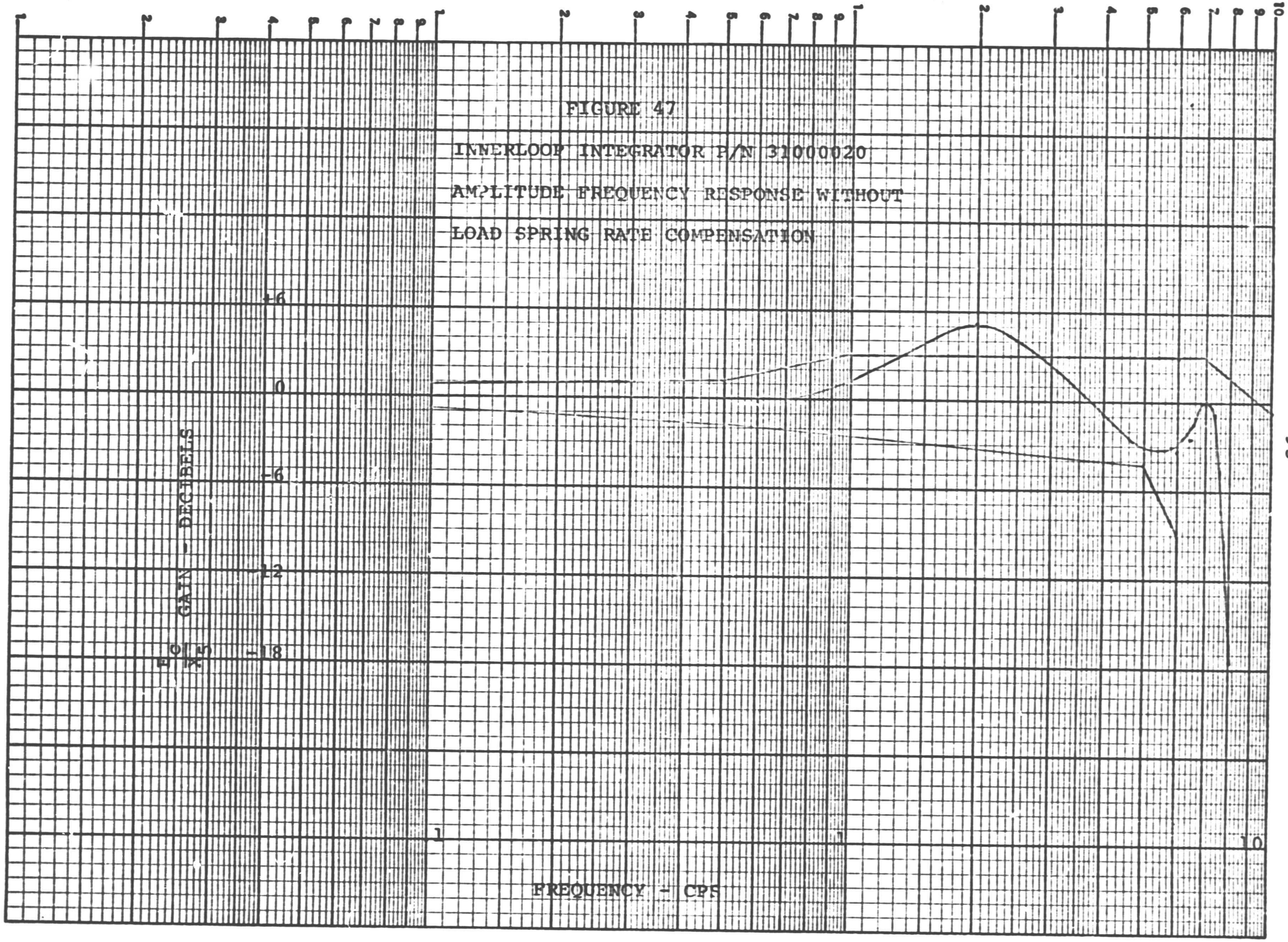
K•E 1-LOC HMIC 46 5
3 CYCLES X 60 DIVISIONS MADE IN U.S.A.
KEUFFEL & ESSER CO.

FIGURE 47

INNERLOOP INTEGRATOR P/N 31000020

AMPLITUDE FREQUENCY RESPONSE WITHOUT

LOAD SPRING RATE COMPENSATION



K&E 1-LOC ...AMIC 46 5...
3 CYCLES X 60 DIVISIONS MADE IN U.S.A.
KEUFFEL & ESSER CO.

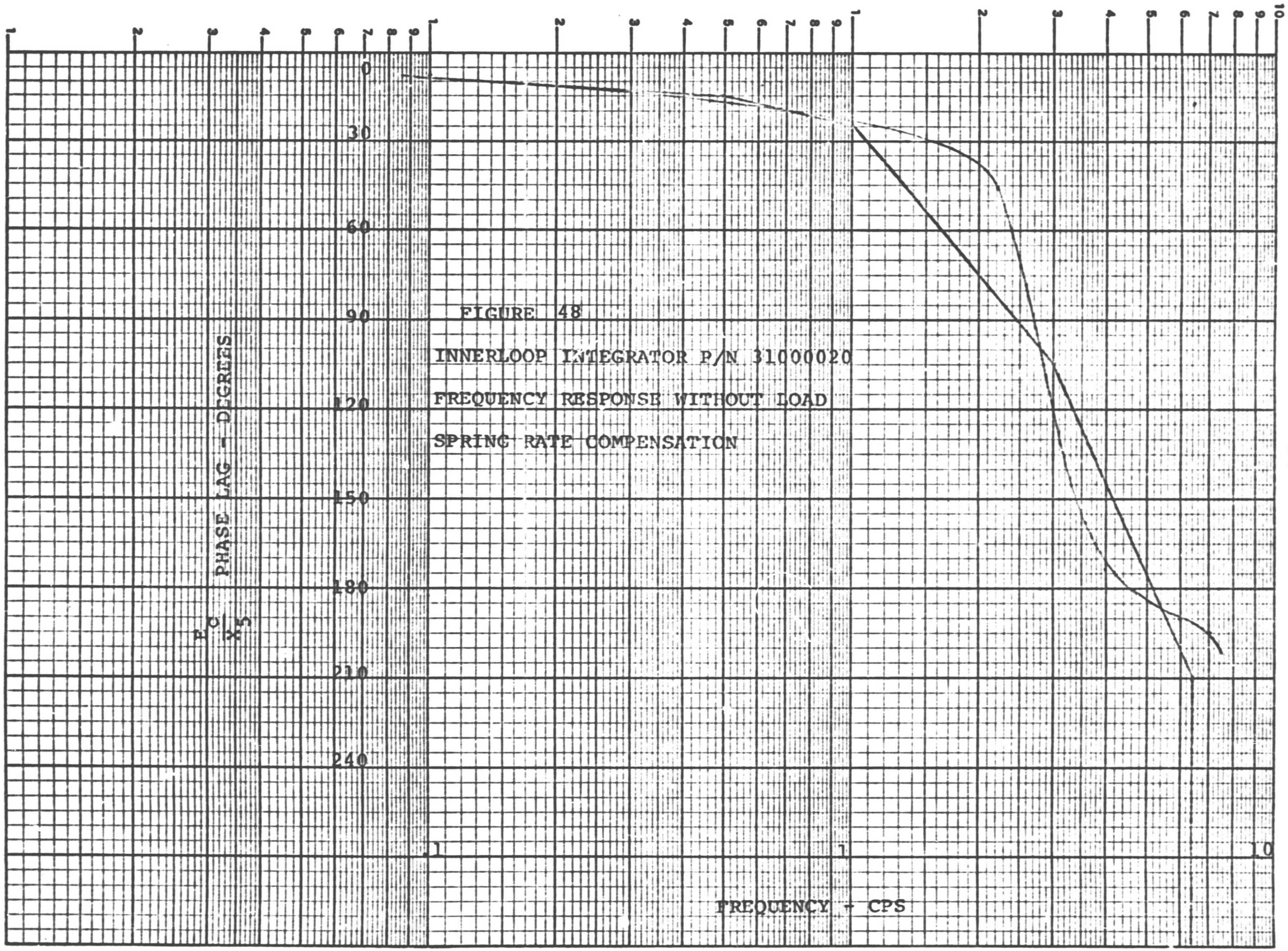



FIGURE 48

INNERLOOP INTEGRATOR P/N 31000020

FREQUENCY RESPONSE WITHOUT LOAD

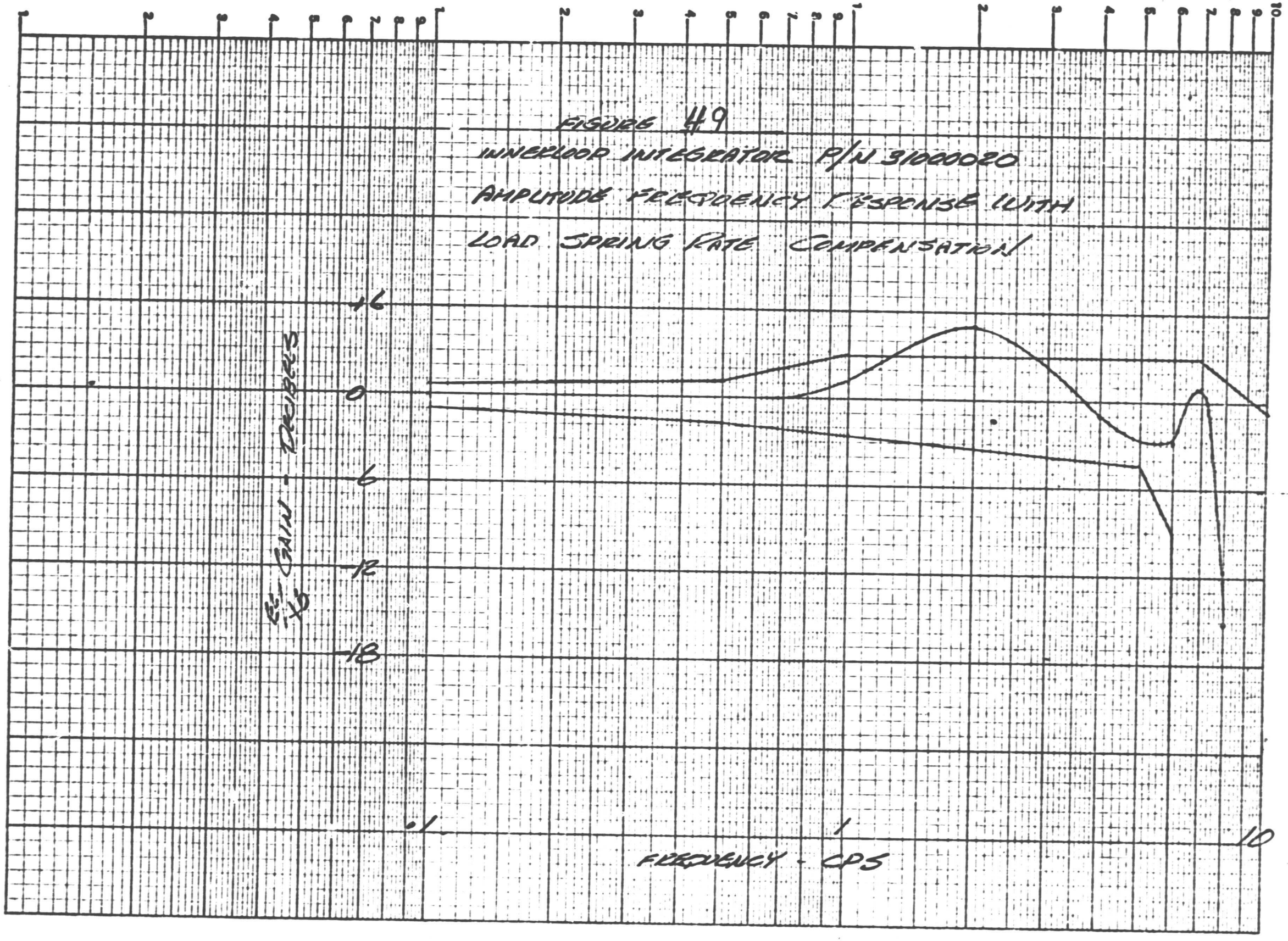
SPRING RATE COMPENSATION



HR 73900000

K&E -LOG IMIC 36 5
3 CYCLES X 60 DIVISIONS MADE IN U.S.A.
KEUFFEL & ESSER CO.

FIGURE 49
INNERLOOP INTEGRATOR P/N 31000020
AMPLITUDE FREQUENCY RESPONSE WITH
LOAD SPRING RATE COMPENSATION




HR 73900000

KEUFFEL & ESSER CO. MADE IN U.S.A. 3 CYCLES X 60 DIVISIONS

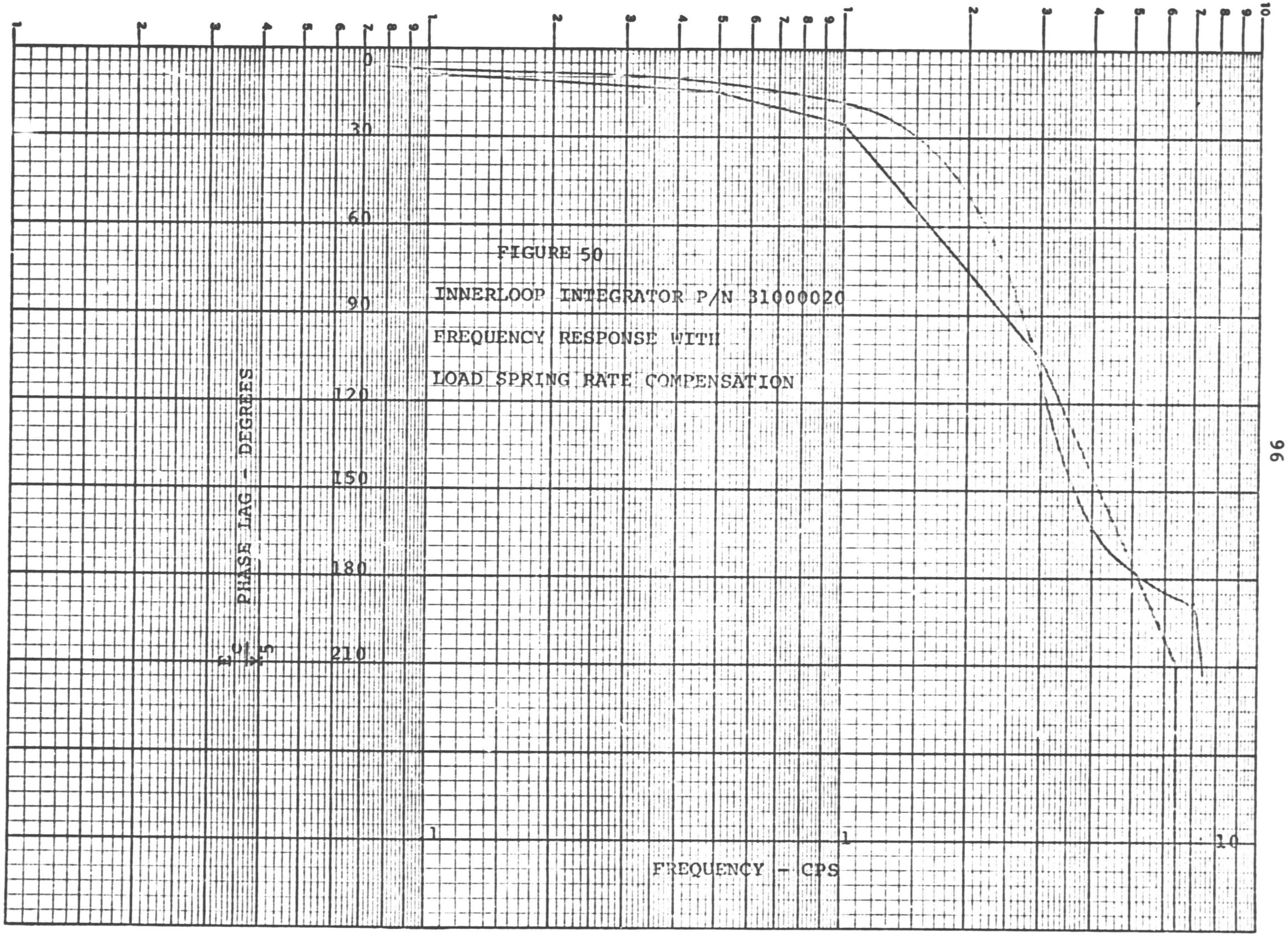



FIGURE 50

INNERLOOP INTEGRATOR P/N 81000020

FREQUENCY RESPONSE WITH

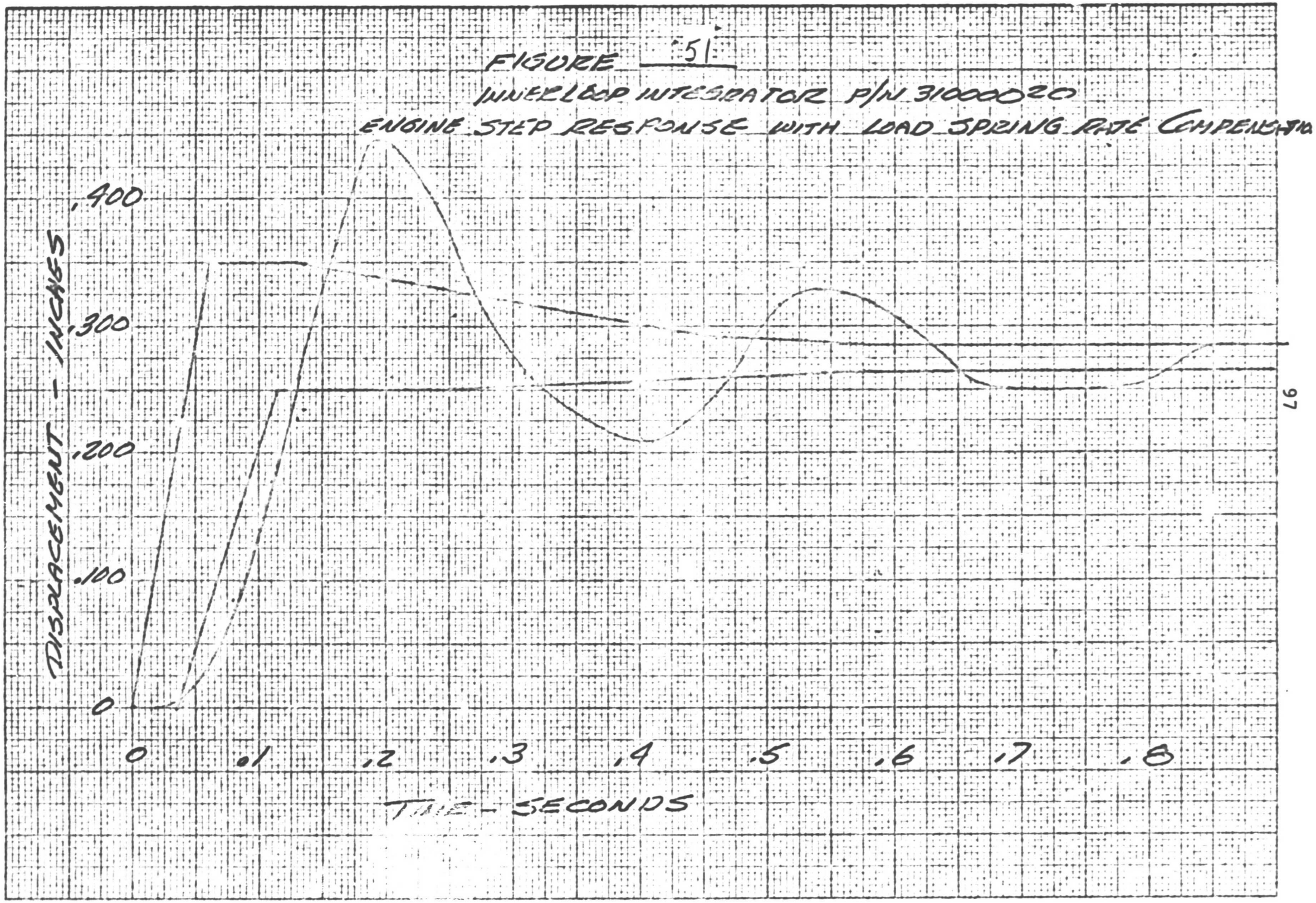
LOAD SPRING RATE COMPENSATION

K•E 7½ X 10 IN. • ALBANENE® KEUFFEL & ESSER CO.

FIGURE 51

INNER LOOP INTEGRATOR P/N 3100020

ENGINE STEP RESPONSE WITH LOAD SPRING RATE COMPENSATION



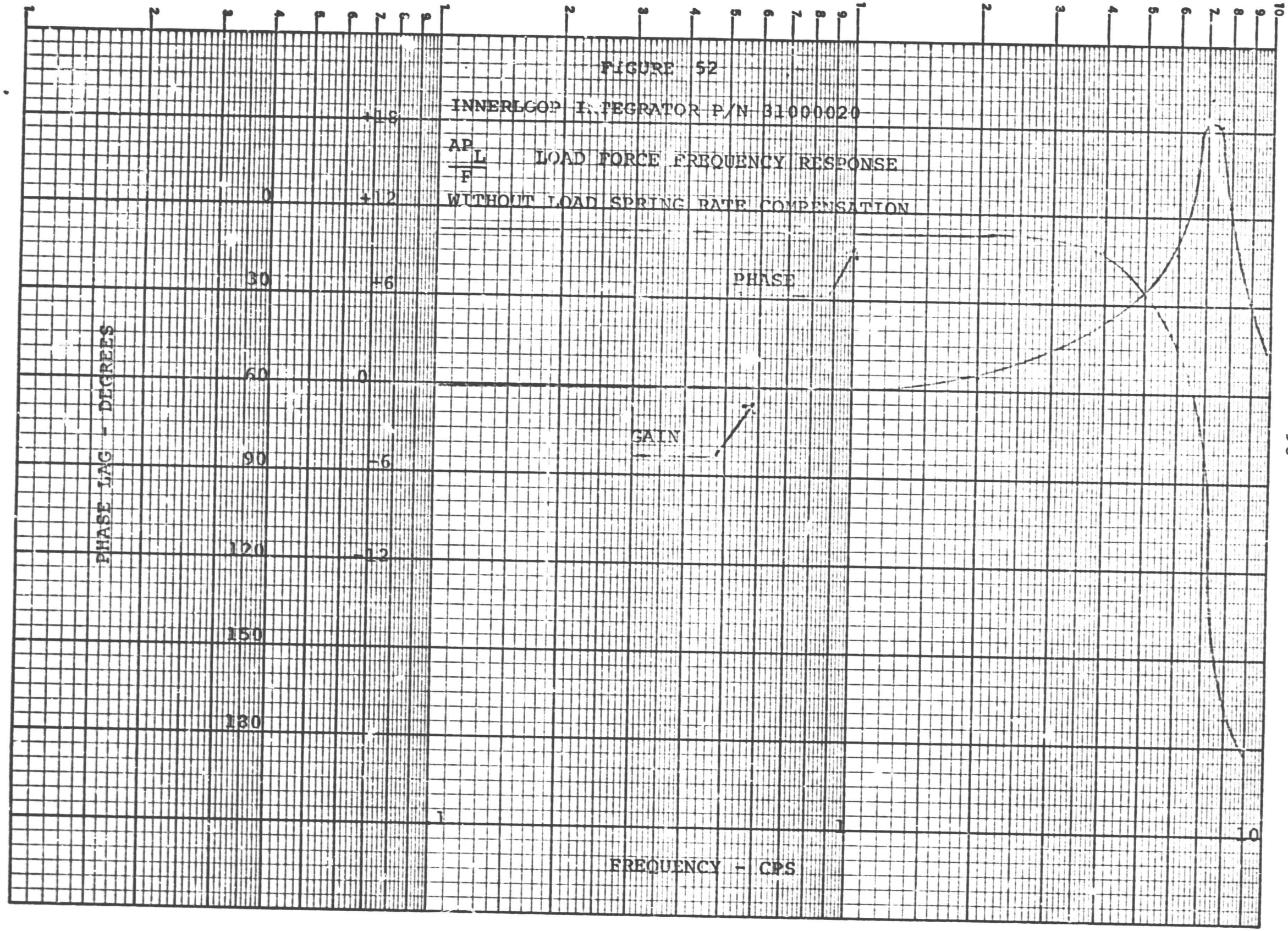
K•E 3 CYCLES X 60 DIVISIONS KEUFFEL & ESSER CO. MADE IN U.S.A.

FIGURE 52

INNERLOOP INTEGRATOR P/N 81000020

$\frac{\Delta P}{F} \frac{L}{}$ LOAD FORCE FREQUENCY RESPONSE

WITHOUT LOAD SPRING RATE COMPENSATION

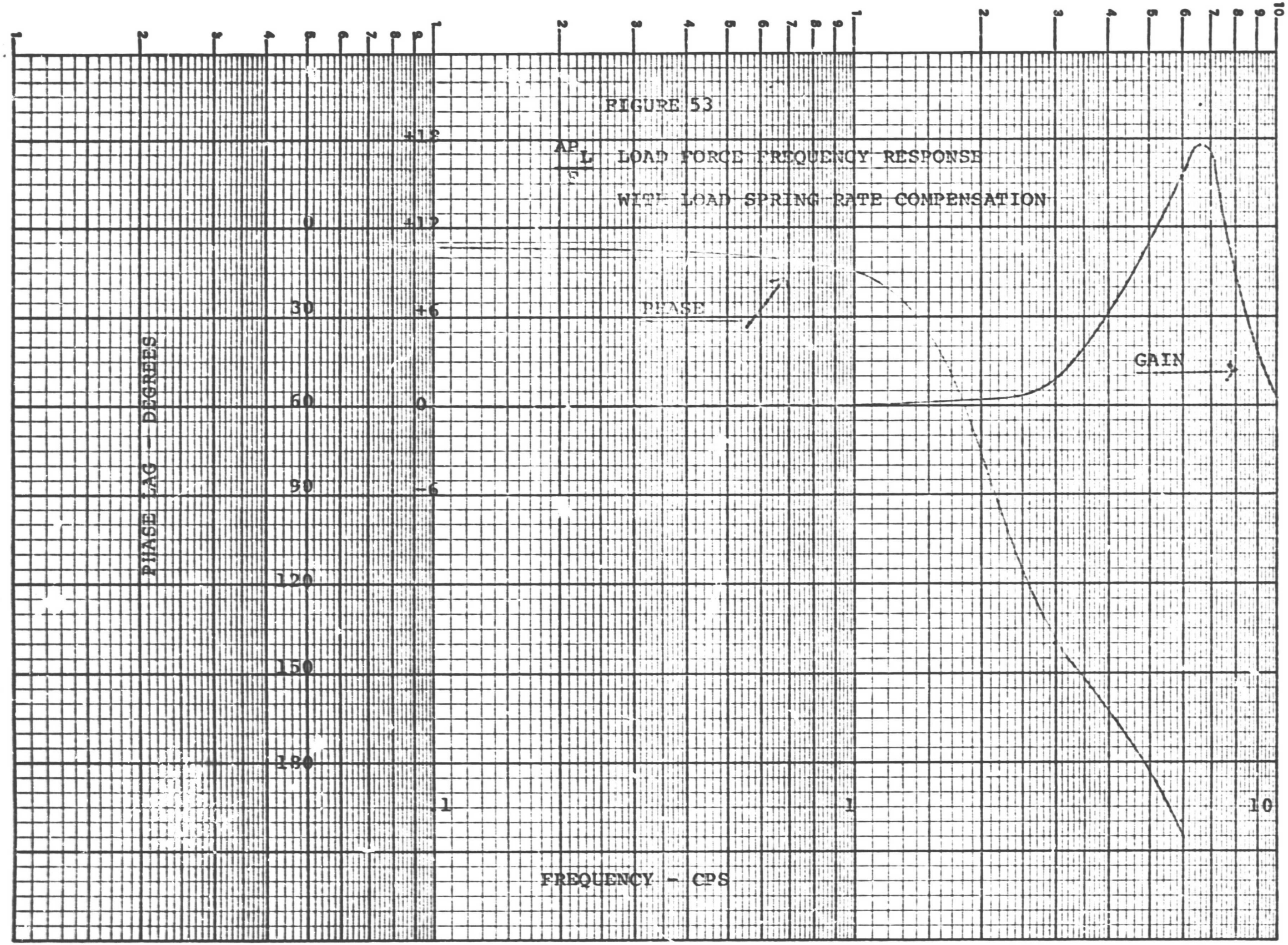


K&E LOGARITHMIC 5 53
5 CYCLES X 60 DIVISIONS MADE IN U.S.A.
KEUFFEL & ESSER CO.

FIGURE 53

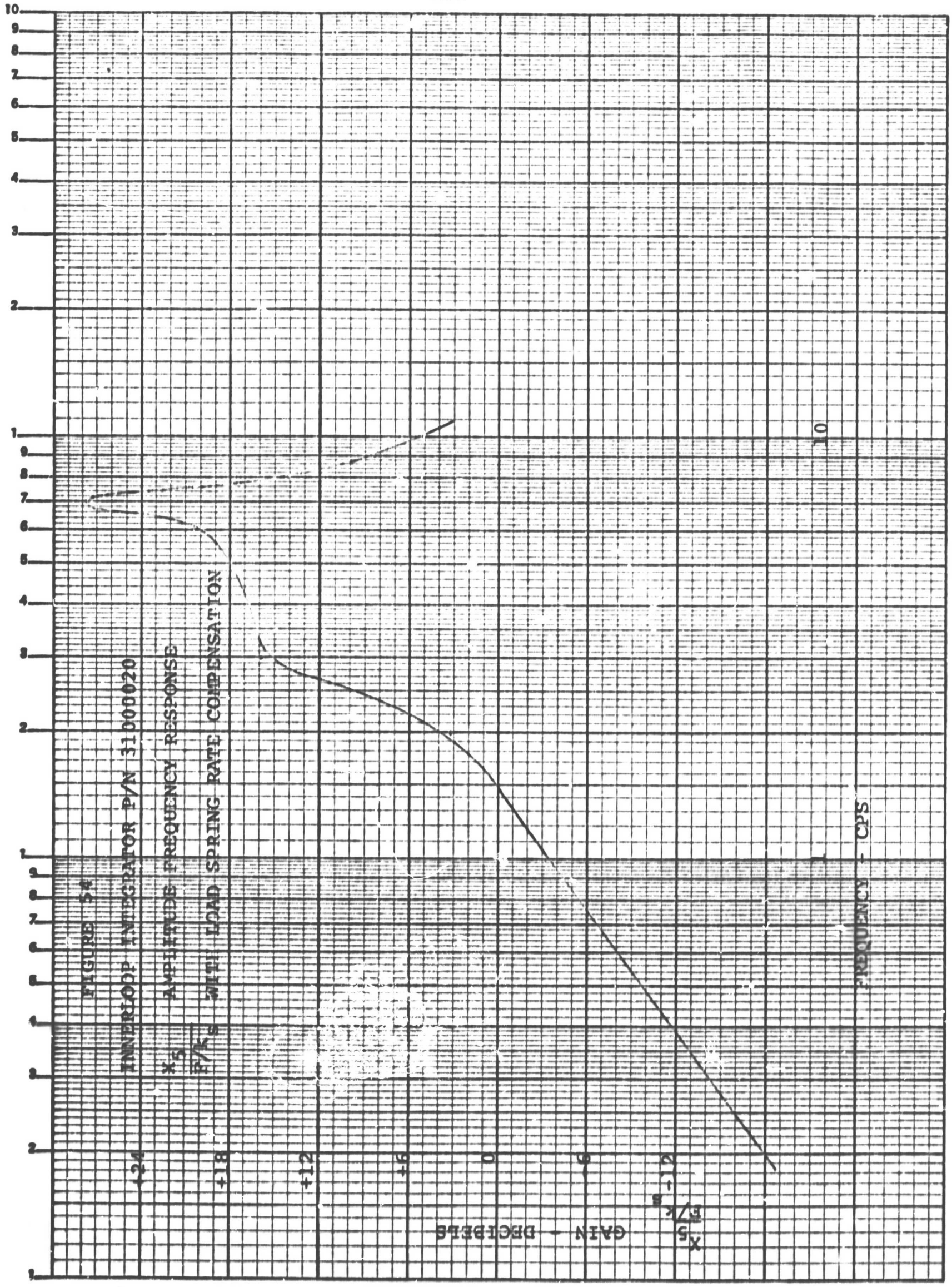
$\frac{AP_L}{F}$ LOAD FORCE FREQUENCY RESPONSE

WITH LOAD SPRING RATE COMPENSATION






HR 73900000

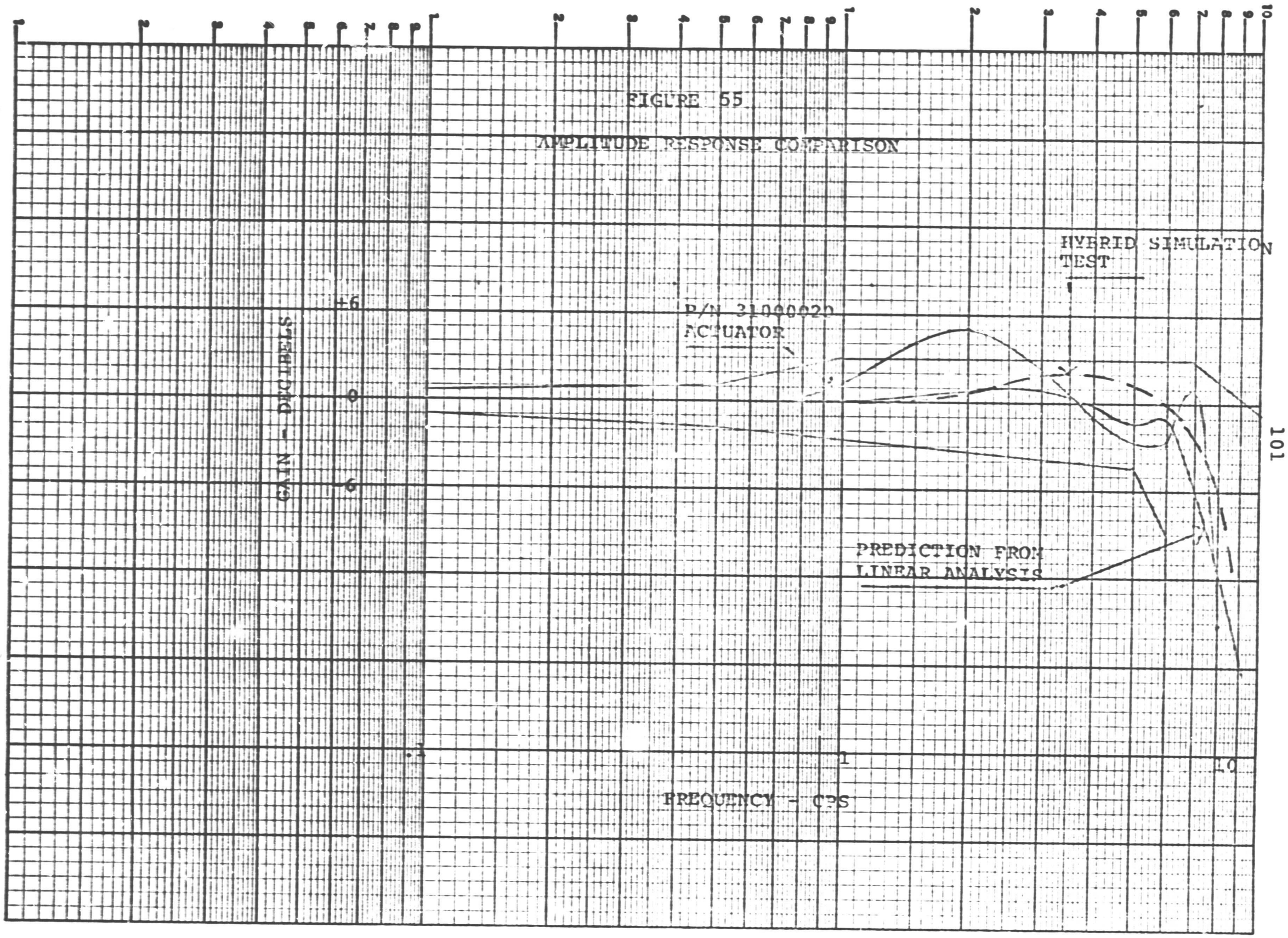

FIGURE 54
INNERLOOP INTEGRATOR P/N 3100020
$\frac{X_5}{F/K_s}$ AMPLITUDE FREQUENCY RESPONSE
WITH LOAD SPRING RATE COMPENSATION
GAIN - DECIBELS
+24
+18
+12
+6
0
-6
-12
$\frac{X_5}{F/K_s}$
FREQUENCY - CPS
10
1
2
4
6
8
KEUFFEL & ESSER CO.

HR 73900000

KEUFFEL & ESSER CO.

FIGURE 55

AMPLITUDE RESPONSE COMPARISON

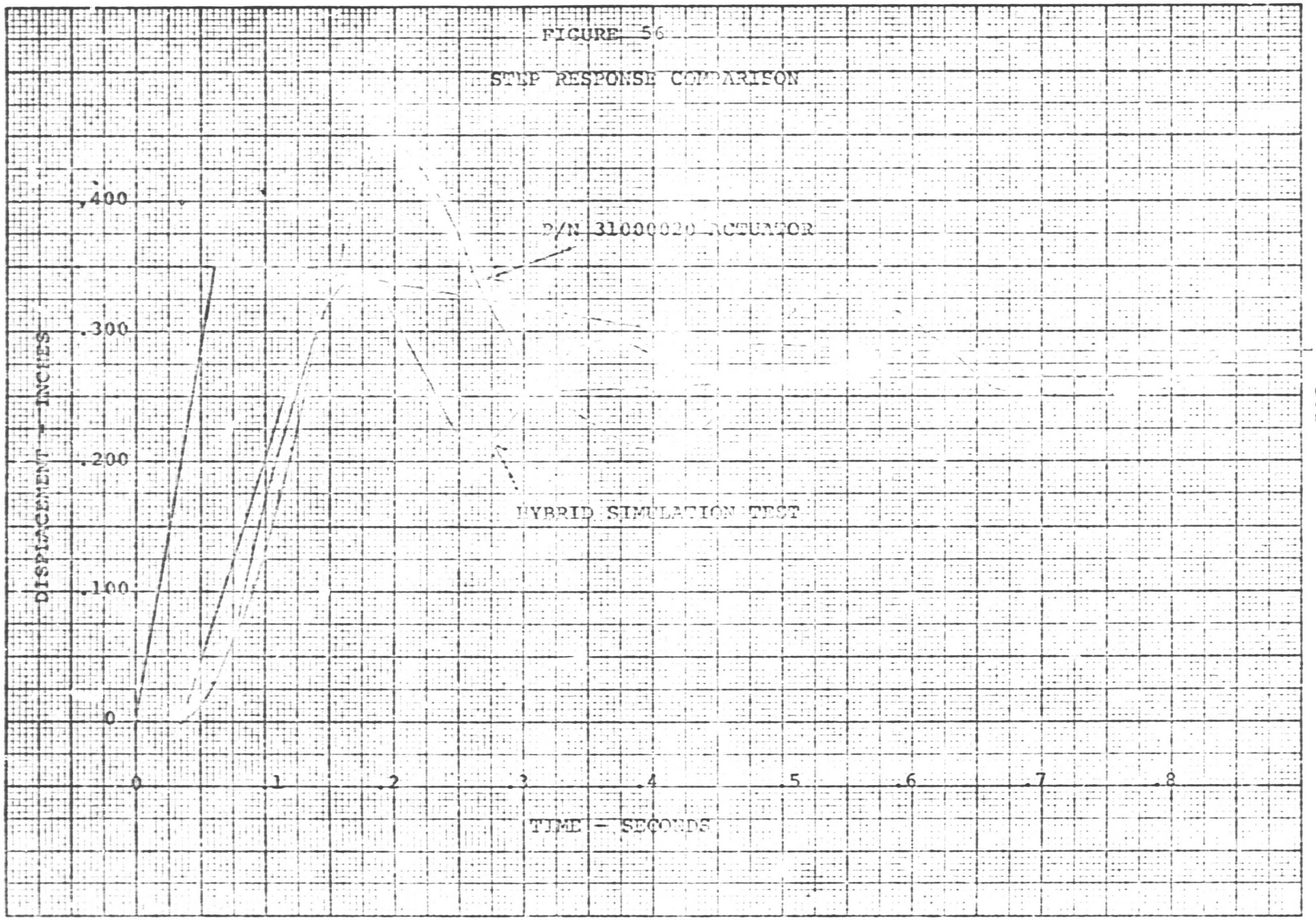


KEUFFEL & ESSER CO.

FIGURE 56

STEP RESPONSE COMPARISON

P/N 31000020 ACTUATOR




HR 73900000



REPRODUCIBILITY OF THE ORIGINAL PAGE IS POOR.

# 6.0 CONCLUSIONS AND RECOMMENDATIONS

The test results presented in section 5.2 show that the Inner Loop Integrator actuator does not deflect under static load and further that the use of positive pressure feedback provides compensation for structural deflection. Even though the frequency response characteristic did not exhibit the desired amount of damping, this program has demonstrated the feasibility of this concept for application to flight type actuators.

HR&M is convinced that the observed low amplitude limit cycles and less than optimum load damping are not inherent to the system, and that additional testing would establish the cause of these phenomena. On the basis of the testing that was accomplished, a number of small changes are recommended to improve performance:

1) Replace rod end bearings on actuator 31000020.
2) Install a bleed valve at the load pressure capsule to remove trapped air during operation.
3) Increase negative pressure feedback gain by redesigning springs.
4) Redesign first stage of servovalve to reduce flow saturation effects.

More extensive improvements on the present configuration do not seem warranted. This actuator was not designed as a mechanical feedback unit hence, rod and bearing tolerances limit the resolution and linearity achievable.

Further development of this concept should be directed toward stiffening a pneumatic action system. Analysis of the load force response tests points up an important constraint on this application, low frequency force inputs are negated by the action of the integrator piston and do not cause significant displacements. However, as the frequency of the input force approaches the load resonance frequency, the efficacy of the system decreases. Hence, a low pressure pneumatic system, inherently exhibiting a low natural frequency if the load inertia is high, would be able to reject dynamic load disturbances only over a very narrow band width. A high pressure system buys improved performance at the cost of increased operational hazards. Further study of these considerations is the logical next step in this development program.